Cognitive Radar: Theory and Simulations

COGNITIVE RADAR: THEORY AND SIMULATIONS

BY

YANBO XUE, B.Sc., M.A.Sc.

A THESIS

SUBMITTED TO THE DEPARTMENT OF ELECTRICAL & COMPUTER ENGINEERING

AND THE SCHOOL OF GRADUATE STUDIES

OF MCMASTER UNIVERSITY

IN PARTIAL FULFILMENT OF THE REQUIREMENTS

FOR THE DEGREE OF

DOCTOR OF PHILOSOPHY

Doctor of Philosophy (2010)   McMaster University

(Electrical & Computer Engineering)   Hamilton, Ontario, Canada

TITLE: Cognitive Radar: Theory and Simulations

AUTHOR: Yanbo Xue

                     B.Sc. (Automation Engineering)

                     Northeastern University at Qinhuangdao, China

                     M.A.Sc. (Control Theory & Control Engineering)

                     Northeastern University, China

SUPERVISOR: Dr. Simon Haykin, Distinguished University Professor

NUMBER OF PAGES: xx, 185

To my wife and my parents

Abstract

For over six decades, the theory and design of radar systems have been dominated by probability theory and statistics, information theory, signal processing and control. However, the similar encoding-decoding property that exists between the visual brain and radar has been sadly overlooked in all radar systems. This thesis lays down the foundation of a new generation of radar systems, namely *cognitive radar*, that was described in a 2006 seminal paper by Haykin. Four essential elements of cognitive radar are Bayesian filtering in the receiver, dynamic programming in the transmitter, memory, and global feedback to facilitate computational intelligence. All these elements excluding the memory compose a well known property of mammalian cortex, the perception-action cycle. As such, the cognitive radar that has only this cycle is named as the *basic cognitive radar* (BCR). For tracking applications, this thesis presents the underlying theory of BCR, with emphasis being placed on the cubature Kalman filter to approximate the Bayesian filter in the receiver, dynamic optimization for transmit-waveform selection in the transmitter, and global feedback embodying the transmitter, the radar environment, and the receiver all under one overall feedback loop.

Built on the knowledge learnt from the BCR, this thesis expands the basic perception-action cycle to encompass three more properties of human cognition, that is, memory,

attention, and intelligence. Specifically, the provision for memory includes the three essential elements, i.e., the *perceptual memory*, *executive memory*, and *coordinating perception-action memory* that couples the first two memories. Provision of the three memories adds an advanced version of cognitive radar, namely the *nested cognitive radar* (NCR) in light of the nesting of three memories in the perception-action cycle.

In this thesis, extensive computer simulations are also conducted to demonstrate the ability of this new radar concept over a conventional radar structure. Three important scenarios of tracking applications are considered, they are (a), linear target tracking; (b), falling object tracking; and (c), high-dimensional target tracking with continuous-discrete model. All simulation results confirm that cognitive radar outperforms the conventional radar systems significantly.

In conducting the simulations, an interesting phenomenon is also observed, which is named the *chattering effect*. The underlying physics and mathematical model of this effect are discussed. For the purpose of studying the behaviour of cognitive radar in disturbance, demonstrative experiments are further conducted. Simulation results indicate the superiority of NCR over BCR and the conventional radar in low, moderate and even strong disturbance.

Acknowledgements

Completing an important cause requires mass efforts. This dissertation would not have been possible had it not been for the encouragements and supports by many people I am indebted to.

♡ In the first place, I would like to thank my supervisor Dr. Simon Haykin, who has provided me the possibility to work on a research topic that is indeed on the cutting edge of the new generation radar system spanning over multiple disciplines. His devotion, focus and vision have inspired and guided me along this journey. He is and always will be a model for me.

♡ I would also like to express my gratitude to two other professors in my committee, Dr. Thia Kirubarajan and Dr. Tom Hurd. Their comments and feedback have been assisting me throughout my research duration. I am grateful to Dr. Tim Davidson for all his valuable comments to my research.

♡ My thanks also extend to Cheryl Gies, Lola Brooks, Helen Jachana, Terry Greenlay, Cosmin Caroiu and Alexa Huang for helping me during my stay at the ECE.

♡ Thanks to my collaborators Ienkaran Arasaratnam and Amin Zia for working

List of Abbreviations

ATC: air traffic control

BCR: basic cognitive radar

CD-CKF: continuous-discrete cubature Kalman filter

CDS: cognitive dynamic systems

CKF: cubature Kalman filter

CR: cognitive radar

CRLB: Cramér-Rao lower bound

CTR: cognitive tracking radar

DP: dynamic programming

EA-RMSE: ensemble-averaged RMSE

EKF: extended Kalman filter

ESN: echo state network

FFT: fast Fourier transform

FIM: Fisher information matrix

FWF: fixed waveform

GHA: generalized Hebbian algorithm

KF: Kalman filter

KKT: Karush-Kuhn-Tucker

LFM: linear frequency modulation

MLP: multilayer perceptron

MTT: multiple-target tracking

NCR: nested cognitive radar

PCRB: posterior Cramér-Rao lower bound

PF: particle filter

RBF: radial basis function

RMSE: root mean-squared error

SNR: signal-to-noise ratio

SP: single-point

TPD: two-point differencing

UKF: unscented Kalman filter

VLSI: very-large-scale integration

VSC: variable structure control

VSF: variable structure filter

VSS: variable structure system

List of Notations

b: The chirp rate of the LFM pulse

c: Speed of the electromagnetic wave propagation

$\mathbb{E}[\cdot]$:   Statistical expectation operator

f_c: Carrier frequency

f_D: Doppler shift associated with target radial motion

$\mathbf{f}(\cdot)$:   System function modeling the state transition

$g(\cdot)$:   Cost function

$\mathbf{h}(\cdot)$:   Measurement function modeling the observer

$\mathcal{H}$:   Hypothesis

$\mathbb{H}$:   Entropy

$\mathbb{I}$:   Mutual information

$\mathbf{I}_k$:   Information vector, consisting of the measurements history

and waveform history till time k

$\mathcal{J}$:   Cost-to-go function

$\mathbf{J}$:   Fisher information matrix

L: Dynamic-programming horizon-depth

$n(t)$:   Gaussian noise at the radar receiver input,

with $\tilde{n}(t)$ denoting its complex envelope

$\mathcal{N}(\mathbf{x}; \boldsymbol{\mu}, \boldsymbol{\Sigma})$: Gaussian distribution of $\mathbf{x}$ with mean $\boldsymbol{\mu}$ and covariance $\boldsymbol{\Sigma}$

N_g: The waveform-parameter grid size

N_x: The state-space dimension

N_z: The measurement-space dimension

$\mathcal{P}_k$: The waveform library at time k

$r(t)$: Received signal at the receiver input from the target

$\mathrm{Re}\{\cdot\}$: The real part of a complex value

$\mathbf{R}_k(\boldsymbol{\theta}_{k-1})$: Measurement-noise covariance matrix at discrete time k as a function of the transmit waveform parameters $\boldsymbol{\theta}_{k-1}$

$\tilde{s}(t)$: Complex envelope of the transmitted pulse

$s_R(t)$: Received signal reflected from the target

$s_T(t)$: Transmitted radar signal

$\mathrm{Tr}(\cdot)$: Operator extracting the trace of a matrix

$\mathbf{x}_k$: The state vector at time k

$\mathbf{z}_k$: The measurement vector at time k

$\mathbf{Z}_k$: The measurements history

ρ: Range of the target, with $\dot{\rho}$ denoting the range rate

τ: Delay between the transmitted and received signal reflected by the target

μ: Policy function mapping the information vector into an action

λ: Duration of the Gaussian envelope for LFM chirp

$\boldsymbol{\theta}_k$: The transmit waveform parameters at time k

$\boldsymbol{\Theta}_k$: The waveform history at time k

η_ρ: The returned pulse SNR for target at range ρ

Contents

List of Tables

List of Figures

Chapter 1

Introduction

Stones from other hills may serve to polish the jade of this one.

An ancient Chinese proverb

1.1 The Reason for Cognition in Radar Systems

The term *radar*, as an electromagnetic device for target signature acquisition, was coined by the U.S. Navy in 1940 as an acronym for *RAdio Detection And Ranging*. For over 60 years, the theory and design of radar systems have been dominated by probability theory and statistics, information theory, signal processing, and control, whose combined contributions have enabled us to make the radar more *adaptive* and *powerful* [1]. Needless to say, using these tools coupled with dramatic advances in computing and very-large-scale integration (VLSI), we now have a wide array of highly sophisticated radar systems, extending from air traffic control (ATC) radar to phased array radar, each and every one of which has impacted the civilian as well as the military world in its own way. Thanks to many radar researchers and

1
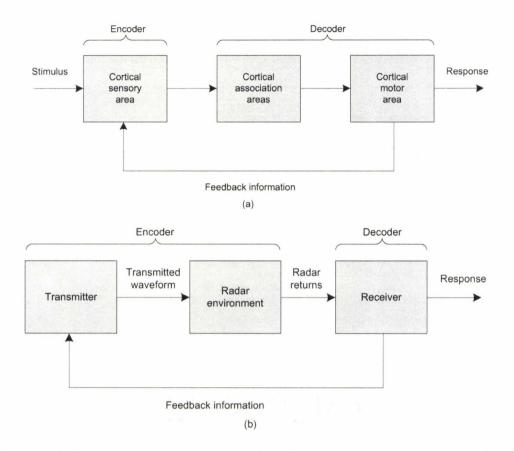
Figure 1.1: (a) Block-diagram representation of processing stages in perceptual tasks; (b) Block-diagram representation of processing stages in radar, where the "radar environment" is meant to encompass unknown targets embedded in the environment.

engineers, the functional design of a radar system in completing tasks such as range identification, direction estimation, speed measurement, and target classification, etc, has now become much easier [2, 3, 4].

However, throughout those years the analogy that exists between the visual brain and radar has been sadly overlooked in all the radar systems, dated back to the very first radio detector invented by Christian Hülsmeyer in 1904 [5]. Figure 1.1 depicts this analogy in its most vivid way, where Figure 1.1(a) is adapted from [6]. What

is truly remarkable is how close encoding-decoding, a distinct property of human cognition in the visual brain, is to that in radar [7]. The point that we are trying to emphasize here is that if we are to build up our knowledge about the fundamentals of cognitive radar, there is much that we can learn from the mammalian brain.

In saying so, we are not belittling the development we have made in the theory and design of traditional radar systems, for example the invention of microwave magnetron by Randall and Boot in 1940 [8], the modulating algorithms for pulse compression in 1960 [9], and the intensive development of phased array theory in the 1960s [10], to name a few. Rather, we are emphasizing that, through the use of cognition, we are indeed able to build a new generation of radar systems, which will be more powerful than ever before. To achieve this goal, we need to broaden our kit of tools by adding cognitive information processing (including learning theory), the practical impact of which is summarized as follows:

> *Cognitive information processing is a transformative software technology that will significantly impact the theory and design of radar systems, new and old.*

To elaborate on this, imagine a radar that interfaces with the environment, the feedback link from the receiver to the transmitter is actually missing if we compare its current structure, shown in Figure 1.2, with the one shown in Figure 1.1. In Figure 1.2, we plot the block diagram of a monostatic radar by adapting from [3].

An intuitive question we may ask is: *Why is it important to build the linkage between the receiver and the transmitter?* To answer this question, we need to pursue our answers in neuroscience. Let us first take the echo-location system of a bat as an example [11]: While preying on insects like moth, the bat emits an ultrasound
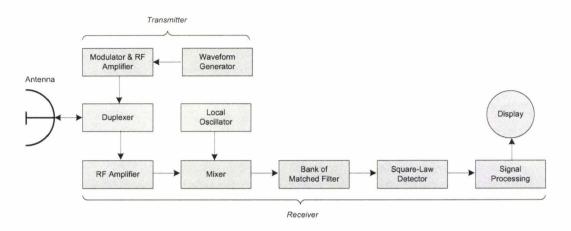
Figure 1.2: Block diagram of a monostatic radar, where the transmitter and receiver are co-located.

signal from his mouth to determine the position, speed and even kind of the targets. We call this ultrasound signal *the sonar*. This process of thought to knowing the outside world is scientifically defined as *cognition*. Cognition represents a faculty for processing of information, applying knowledge, and changing preferences. In a classic book written by Pylyshyn [12], the foundation of cognitive science is laid down in a psychological context.

Another equally compelling motivation for cognition is the visual brain. In most basic terms, the visual brain is characterized by two important functions, perception of the environment (the outside world) in one part of the brain and action to control the environment in a separate part of the brain [13]. The net result of these two functions, working together in a coordinated fashion, is the perception-action cycle; this basic cycle is indeed the brain's counterpart to the information-processing cycle in a cognitive radar that was described in [14].

To summarize our initiatives of introducing cognition into the current radar systems, we may list the following points:

4

- The ever-increasing power of computers makes it possible to select a wide range of radar signals that were seen before as a physical limitation,

- The development of nonlinear tracking algorithms and waveform control techniques were treated separately, and combining them offers a great potential,

- The research of cognitive science has undergone almost four decades, starting from Pylyshyn's early work to Fuster's in-depth descriptions of the cognition, and we are now in a phase of transferring cognitive science into *cognitive engineering* [1], and most importantly,

- The global feedback from the receiver to the transmitter is an enabler of computational intelligence.

1.2 Literature Review

In this section, we review the literature preceding the birth of Haykin's paradigm of *cognitive radar* (CR). Needless to say, it is impractical to make this review complete and comprehensive. Nevertheless, we expect that this list of the related research can pave the way for interested researchers to conduct future research.

As a cross-disciplinary research topic, the background of cognitive radar spans over radar signal processing, information theory, control theory and neuroscience. Actually, for over four decades, most of the research efforts devoted to this area share the same motivation: to increase the flexibility of the radar waveform and enhance the performance of radar detection and tracking. But few researchers have tried to

---

[1]We define "cognitive engineering" as the research that can utilize the theoretical achievements obtained from cognitive science in a system engineering's manner.

address this issue in an *outside-of-the-box* manner.

Because of the incapabilities in waveform generation techniques for both hardware and software, the earlier work has been focusing on the design of ambiguity function attributed to the standard range-Doppler ambiguity function description of Woodward [15]. Right after the publication of Woodward's classic book on ambiguity function, many excellent improvements have been made on the properties of various waveform classes and their ambiguity functions. To be more specific, ambiguity function enables us to represent the time-frequency autocorrelation functions of the radar waveform on the delay-Doppler domain, with the peak centered at the origin. It is amazing that even half a century after the introduction of the ambiguity function, many researches including this thesis still utilize some crucial properties that this function has to study the waveform property. For some exemplary ambiguity functions, we may refer to [16] (Chapter 10, vol 3). Overall, bearing the importance of ambiguity function in mind, we must stress that the early work strictly depended on the radar task. As such, the waveform was designed in an off-line fashion.

To the best of our knowledge, the earliest research that has considered the adaptivity of the waveform transmission was due to Delong and Hofstetter [17, 18]. Their 1967 and 1969 papers studied the adjustable pulse amplitudes and adjustable pulse phases with limited dynamic range, respectively. By maximizing signal-to-interference as the performance matric, they constructed a nonlinear programming problem and then solved it using the Karush-Kuhn-Tucker (KKT) theorem [19]. Their theoretical study was aimed at optimal waveform design. However, the sequence of successively *better* signals obtained provides considerable improvement in performance a sub-optimal sense. The Delong-Hofstetter algorithm has been proven equivalent to

6

perfect clutter suppression in an environment highly dominated by clutter [20].

It is noteworthy to point out that these early attempts were derived directly from the fact that a radar is first of all a sensor. With the advance of digital computer and signal processing technology, the functions that a radar can perform are both diversified and specialized. For example, two of the main functions are *detection* and *tracking*. For a detection radar, we need to test two hypotheses for the cell under study, $\mathcal{H}_0$ (the target is absent) and $\mathcal{H}_1$ (the target is present); for the tracking problem, the radar is designed to estimate the state of a moving target. The design of optimal waveform is then task-dependent: for detection task, the optimal radar waveform should be able to put as much transmitted energy as possible into the largest mode of the target to maximize the output signal-to-noise ratio (SNR); and for estimation task, the optimal radar waveform should allocate the energy as efficiently as possible among the different modes of the target to maximize the mutual information between the received signal and the target signature.

Two mainstream schools of waveform design appeared around the 60's and late 80's: the control-theoretic approach and the information-theoretic approach, respectively.

- **Control-Theoretic Approach:** The earliest literature on optimal waveform design via control-theoretic approach was due to Athans [21]. Two tricks employed by Athans in [21] are still very much valid, which are:

  - The Kalman-Bucy theory is used to formulate an optimization algorithm with *states* being the elements of the covariance matrices, *control* being the radar waveform, and *cost* being a function of the covariance matrix.

  - Under the physical constraints of total energy and peak amplitude, the

time-dependent optimal waveform must alternate between its peak-power and zero-power levels.

Even though research after Athans followed this idea to some extent, the first sound foundation under the control-theoretic approach can be found in [22]. With the advent of digital waveform generators that are capable of generating almost any form of radar signals, the waveform design should be considered as an integral part of the overall tracking system. A radar equipped with different waveforms has a different resolution and thus, leads to a different measurement error. Mathematically, we denote by $\boldsymbol{\theta}$ the radar waveform and $\mathbf{z}$ as the measurement, the covariance matrix for the measurements noise can be represented as a function of $\boldsymbol{\theta}$, i.e., $\mathbf{R}(\boldsymbol{\theta})$. From the systems engineering viewpoint, the waveform design problem is to find the optimal tracking filter and waveform parameters that give us a minimum covariance of the target state in an on-line fashion. It is noteworthy to point out that this work is based on the linear tracking problem and a clutter-free environment. Thus, the theory is derived in the context of Kalman filter. Kershaw and Evans extended their research in a later paper [23] to study the data association algorithm in a cluttered environment. Following this line of thinking and also thanks to the development of nonlinear filtering, *e.g.* the extended Kalman filter (EKF) [24], the unscented Kalman filter (UKF) [25], and particle filter (PF) [26], in recent years, many other researchers have extended Kershaw and Evans's work to encompass the tracking of maneuvering targets in both clutter-free and cluttered environments [27, 28].

- **Information-Theoretic Approach:** The pioneer work done by Woodward

and Davis [15, 29, 30] was the earliest investigation of possible application of information theory to radar system. Bell was the first person to consider the use of information theory in radar waveform design [31, 32]. Bell assumed a random extended target. Recent work done by Leshem *et. al.* [33] has extended Bell's work to incorporate multiple extended targets using multiuser information theory [34]. Those elegant theories of radar waveform design nevertheless have to be greatly discounted for their lack of enough flexibility when it comes to generate desired waveform in practical systems. On the other hand, with the requirement of multiple functional radar systems, a waveform that can fulfill or smoothly switch between these tasks will assist a radar to outperform its competitors. Since we know that a large SNR margin that is beyond the SNR detection threshold does not make more sense for battlefield, a waveform that can carry more information about the target based on the satisfaction of its SNR detecting threshold will be more useful. Obviously, a radar that can gain more information about the target is better than a detection-only radar.

Based on the above-mentioned facts, we have done some preliminary study to efficiently synthesize waveforms with the aim of providing a trade-off between estimation performance for a Gaussian ensemble of targets and detection performance for a specific target [35]. In particular, this method synthesizes (finite length) waveforms that achieve an inherent trade-off between the (Gaussian) mutual information and the SNR for a particular target. Moreover, this method can accommodate a variety of constraints on the transmitted spectrum. However, the optimal waveform design algorithm assumes the presence of radar scene analyzer that informs the design algorithms of the impulse response of a

specified target and power spectral density of the Gaussian ensemble. In practice, these terms may not be known precisely. A similar technique can also be found in [36].

In line with the research efforts made by the radar community, the psychological and computational study of the human brain that branches to neural network, artificial intelligence and cognitive science was also making progress in their individual ways. As an actual fact, researchers' desire to understand the underlying mechanism of human brain has never stopped. An ancient Chinese proverb says: *you never know the shape of a mountain as long as you are in it.* It is similarly impossible to study our own human nature. The most optimistic result that we could obtain is the functional simulations. In building the *unified theories of cognition*, Newell [37] admitted that the list of areas that we need to cover may be infinite, to name a few: problem solving, decision making, routine action, memory, learning, perception, language, emotion, dreaming, daydreaming, etc. For a dynamic system like the human brain, time plays a key role in its input-output behaviour. This system is built up of a hierarchy of multiple systems. The subsystems are linked together to produce the human behaviour at the system level. Echoing the division of frequency band in radar community, Newell divided the time scale of human action into four bands [37].

1. The *biological band*, at the bottom level, operates in a range from microseconds to milliseconds. It is composed of neurons that transmit pulses at a high speed. An aggregation of tens of thousands of neurons makes the neural circuit. It is this level that has engaged many researchers to propose different forms of neural network structures in a way to emulate brain's behaviour. Some famous neural networks including the perceptron [38], multilayer perceptron (MLP) [39], radial

basis function (RBF) network [40, 41], support vector machine (SVM) [42], echo-state network (ESN) [43, 44], etc. For detailed description and illustrative experiments, the reader may refer to [7].

2. The *cognitive band* operates in the range from hundreds of milliseconds to seconds. This band is regarded as the apparatus that interfaces the neural circuits with general cognition. The cornerstone book, namely, *Computation and Cognition*, written by Pylyshyn is mostly concerned with this band [12]. Specifically, the science of studying the cognitive band forms the common ground of *cognitive science*. Fuster's book on *Cortex and Mind: Unifying Cognition* [13] is the first one to explain the essential transactions underlying cognition of different networks in hierarchies. His viewpoint of *perception-action cycle* underlies the foundational blocks of our current understanding of the human brain. To our knowledge, Fuster's work could be regarded as the best interpretation of cognition in the literature.

3. The *rational band*, at the knowledge level, operates from minutes to hours depending on the specific task.

4. The *social band*, at the highest level, operates from days to months and even years. It provides the platform for human beings to communicate with each other in a way to form the order or law in the society.

The rational band and social band are very much beyond the scope of system engineering. Readers may refer to [37] for more information.

Having conducted an overview of related works on the radar community and cognitive science, we have attempted to show how concepts from these two disciplines

converge, thus giving birth to a new generation of radar system, namely *cognitive radar*. To this end, two solid steps have been taken:

1. In [14], the idea of *Cognitive Radar* was described for the first time. Four essential points were emphasized in a conceptual manner: Bayesian filtering in the receiver, dynamic programming in the transmitter, memory, and global feedback to facilitate computational intelligence. Three important conclusions are made in [14]:

   (a) For a radar to be cognitive, the radar transmitter has to learn from continuous interactions with the environment. The radar must be intelligent enough to make use of the information extracted by the receiver. This indicates that existing radar systems do not incorporate intelligence.

   (b) Feedback is a new component that must be embedded in the current radar systems to facilitate computational intelligence.

   (c) Information preservation, indicated even in Shannon's paper in an implicit way [45], is crucial to the receiver's performance, which indirectly affects the performance of the transmitter. In this context, the Bayesian approach is the paradigm of choice.

2. In [46], the underlying theory of cognitive radar for tracking applications was presented for the first time ever, with emphasis being placed on the cubature Kalman filter to approximate the Bayesian filter in the receiver, approximate dynamic programming for transmit-waveform selection in the transmitter, and global feedback embodying the transmitter, the radar environment, and the

receiver all under one overall feedback loop. We name this system the *cognitive tracking radar* (CTR). Simulation results presented therein substantiate practical validity of the superior performance of a CTR over a traditional radar.

1.3   Scope of the Thesis

After discussing the related literature, we are now ready to describe the problem this thesis has tackled. Here we may remind ourselves that a radar system, should it be cognitive or non-cognitive, covers a wide domain of research topics that may go beyond any individual researcher's work. This thesis focuses on the fundamental theory and demonstrative experiments of a scrutinized cognitive radar building on the pioneering paper on cognitive radar [14]. The following components are underscored:

- Cubature Kalman filter (CKF) is claimed to be the best known approximation to the optimal Bayesian filter under the Gaussian assumption. We start from the linear tracking using classic Kalman filter to nonlinear tracking using Cubature Kalman filter. The continuous-discrete model is also studied to encompass practical radar systems, based on which the recently developed continuous-discrete cubature Kalman filter (CD-CKF) is used as the optimal Bayesian filter under the Gaussian assumption.

- Dynamic programming is chosen to be the algorithm for selecting the waveform. Its special case, namely dynamic optimization, is studied in an effort to provide a computationally efficient solution to the transmitter.

- Mean-squared error (MSE) is used in the formulation of the feedback-information metric that connects the receiver to the transmitter through a feedback link.

13

- Beside the perception function, three other components, namely memory, at-
  tention and intelligence, are included to compose a memory-assisted cognitive
  radar system. Neural networks are used to build the memory elements.

1.4   Contributions

As the first doctoral dissertation on cognitive radar, this thesis paves the way to-
ward the study of an emerging discipline: *cognitive dynamic systems* (CDS) [47]. A
new member of cognitive radar is proposed, namely the *nested cognitive radar*. The
contributions of our research are summarized as follows:

- The fundamental theory of cognitive radar is refined to reflect the recent devel-
  opment of optimal Bayesian filter theory. Realizing the impact that CKF may
  have on the tracking performance, this thesis selects the CKF as the tracking
  filter and shows that CKF is the method of choice in optimal filtering. For prac-
  tical systems that has continuous system-equation and discrete measurement-
  equation. The continuous-discrete cubature Kalman filter (CD-CKF) algorithm
  is selected as the tracking filter.

- Approximate dynamic programming theory is employed to tackle the *imperfect
  state-information problem*. The computational cost is also analyzed for the
  dynamic programming problem with a horizon depth of L. The special case of
  $L = 1$ is named dynamic optimization. Approximation techniques are studied
  to address this problem. The computational complexity for the general case of
  dynamic programming is also analyzed.

- Adopted from architecture of visual cortex, the nested structure for cognitive

radar is constructed, where perceptual memory, executive memory and coordinating perception-action memory are designed in bottom-up and top-down manners. The memories are composed of three independent multilayer perceptrons networks. Back-propagation algorithm is used to train the networks off-line and generalized Hebbian algorithm is used to tune the memories on-line.

- To validate the new structures, comprehensive computer simulations are conducted for three cases: linear target tracking, object falling in space, and high-dimensional continuous-discrete model target tracking.

- In-depth analysis of the simulation results reveals two underlying physical phenomena of cognitive radar: First, to provide a good performance for state-error reduction, the measurements will offer a variety of deviations. We call this phenomenon the *chattering effect*. Mathematical model of the chattering in an $\mathcal{L}_p$ sense is also proposed; Second, to study the behaviour of cognitive radar in external disturbance, we simulate the scenario that a linear travelling target encounters a disturbance for a short duration.

1.5 Organization of the Thesis

The rest of the thesis is organized as follows:

- Chapter 2 describes the fundamental theory of cognitive radar enabled with the basic perception-action cycle. Two important components include the optimal Bayesian filtering in the receiver and the optimal waveform selection in the transmitter. Specifically, the dynamic optimization algorithm is derived in this chapter as a special case of dynamic programming.

15

- Chapter 3 develops a cognitive radar system with enhanced intelligence. Four components of the new systems include perception for information categorization, memory, attention, and intelligence. We name this new cognitive radar system the *nested cognitive radar* in that three memories, i.e. perceptual memory, executive memory, and coordinating perception-action memory, are embedded within the basic perception-action cycle. Both the system aspect and algorithmic aspect of this system are discussed.

- Chapter 4 evaluates the performance of the cognitive radar for three different applications. They are: (i) linear target tracking, (ii) object falling in space, and (iii) high-dimensional continuous-discrete model target tracking.

- Chapter 5 discusses the two underlying physical phenomena in cognitive radar, they are the chattering effect and behaviours in multi-mode disturbance. Mathematical definition that explains the chattering effect is also provided. Simulations are also conducted to observe the behaviours of cognitive radar in low, moderate and high disturbances.

- Chapter 6 summarizes the thesis and suggests three topics to continue the research in the future. First, a new lower bound needs to be proposed in a cognitive radar system. Second, continued research about the chattering effect is also expected to discover the reason behind the impressive performance enhancement in cognitive radar. Lastly, more in-depth study of the behaviour of a cognitive radar in presence of external disturbance may reveal the potential of cognition in dealing with a complicated scenario.

Chapter 2

Basic Cognitive Radar

A bird is an instrument working according to a mathematical law. It lies within the power of man to make this instrument with all its motions.

Leonardo Da Vinci (1452-1519)

In [14], the idea of *cognitive radar* was described for the first time in a seminal paper. Motivation for this new idea was the echo-location system of a bat [11]. Another equally compelling motivation for cognitive radar is the visual brain. In most basic terms, the visual brain is characterized by two important functions, perception of the environment (the outside world) in one part of the brain and action in the environment in a separate part of the brain [13]. The net result of these two functions, working together in a coordinated fashion, is the perception-action cycle. This basic cycle is indeed the brain's counterpart to the information-processing cycle in a cognitive radar that was described in [14]. Another way to see the close relationship between cognitive radar and the visual brain is to examine the coding-decoding function. Here again, it is rather striking to find that this basic property of cognition in

17

the brain and its counterpart in cognitive radar are ever so closely analogous [7].

With optimal performance as the goal, the ideal way to build a cognitive radar is to look to the optimal Bayesian filter [48] as the central functional block in the receiver for perception of the environment, and Bellman's dynamic programming [49] as the central functional block in the transmitter for action to control the environment. Naturally, there has to be feedback from the receiver to the transmitter to make it possible for the receiver to send relevant information about the environment to the transmitter. In so doing, global feedback embodies the two parts of the radar system and the environment under a single overall loop operating in an *on-line* manner, and with it the radar becomes computationally intelligent. Here again, if we are to examine the visual brain, we will find that, unlike perception and action, there is no single functional block that takes care of intelligence; rather, this important function is distributed through feedback across many parts of the brain.

From this introduction, we see that the cognitive radar system mentioned here manifests a basic characteristic, i.e., *basic perception-action cycle*. In consideration of the development of cognitive radars with enhanced sophistication and information processing power in Chapter 3 and possibly in the future, we name this the *basic cognitive radar* (BCR) under the following points:

- Inclusion of global feedback from the receiver to the transmitter,

- Exclusion of memory, and

- Exclusion of attention.

We may now describe the baseband model of the signal transmission link.

2.1   Model of Radar Measurements in Baseband

A commonly used method to control selection of the transmit-waveform is to equip the transmitter with a digitally implementable waveform generator that embodies a prescribed library of waveforms. To elaborate, when we speak of a baseband model, we mean a band of frequencies determined by the waveform-generator's spectral content. For designing the waveform generator, we have opted for linear frequency modulation (LFM) combined with Gaussian pulse for amplitude modulation. With f_c denoting the carrier frequency of the transmitted radar signal, $s_T(t)$, we may now use complex baseband theory to express it as follows:

$$s_T(t) = \sqrt{2}\mathrm{Re}\left\{\sqrt{E_T}\tilde{s}(t)\exp\left(j2\pi f_c t\right)\right\}, \tag{2.1}$$

where E_T is the transmitted signal energy, $\mathrm{Re}\{\cdot\}$ denotes real part of a complex value, and $\tilde{s}(t)$ is the complex envelope of $s_T(t)$; for complex baseband theory, see [50].

The radar echo reflected from the target received at the receiver input is correspondingly defined by

$$r(t) = s_R(t) + n(t), \tag{2.2}$$

where $s_R(t)$ is the signal component of $r(t)$ and $n(t)$ is the additive white Gaussian noise, both of which are centered on the carrier frequency f_c. Invoking complex baseband theory, we may define $s_R(t)$ as follows:

$$s_R(t) = \sqrt{2}\mathrm{Re}\left\{\sqrt{E_R}\tilde{s}(t-\tau)\exp(j2\pi(f_c t + f_D t))\right\}, \tag{2.3}$$

where E_R is the received signal energy; $\tau = 2\rho/c$ is the delay of the received signal

with ρ denoting the range of the target, and c denoting the speed of electromagnetic wave propagation (i.e. the speed of light); f_D is the Doppler shift defined by $2f_c\dot\rho/c$ with $\dot\rho$ denoting the range rate of the target, assuming that the target is moving toward the radar. Finally, $\tilde n(t)$ denotes the complex envelope of the noise $n(t)$ at the receiver input. Throughout the paper, it is assumed that the transmitted radar signal is narrowband, which means the complex envelopes $\tilde s(t)$ and $\tilde n(t)$ in the baseband model occupy a frequency band small in comparison to the carrier frequency f_c.

The idea behind baseband modeling, exemplified by the complex envelopes $\tilde s(t)$ and $\tilde n(t)$, is that both of these components are low-pass in their spectral characteristics, whereas the band-pass transmitted signal $s_T(t)$ and received signal $r(t)$ are more difficult to handle. Most importantly, baseband modeling dispenses with the carrier frequency f_c and there is no loss of information in basing the radar signal analysis on complex envelopes.

2.1.1 Bank of Matched Filters and Envelope Detectors

At the front end of the receiver, typically, we have a bank of matched filters, shown in Figure 2.1. The impulse response of a matched filter is defined by the conjugate of the complex transmitted signal envelope $\tilde s(t)$, shifted in time as well as frequency by scaled versions of desired time- and frequency-resolutions, respectively. Recognizing that a matched filter is basically equivalent to a correlator, it follows that the bank of matched filters acts as a time-frequency correlator of the complex transmitted signal envelope with itself. In the absence of receiver noise, the squared magnitude of this correlation constitutes the ambiguity function [15]. Every matched filter in the filter bank is therefore followed by a square-law envelope detector. The resulting

real-valued two-dimensional output of each envelope detector, involving time delay and Doppler shift, defines an inter-pulse vector denoted by $\mathbf{z}_k$, where the subscript k denotes discrete time. This vector performs the role of *measurement vector* in the state-space model of the radar target, discussed next.
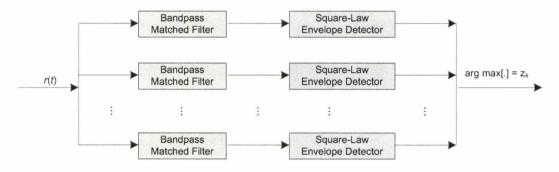
Figure 2.1: Bank of matched filters

2.1.2 State-Space Model of the Target

A: Discrete Model

There are two equations in the discrete state-space model of a radar target:

System equation, which describes evolution of the target's state across time in accordance with the nonlinear equation:

$$\mathbf{x}_k = \mathbf{f}(\mathbf{x}_{k-1}) + \mathbf{v}_k, \tag{2.4}$$

where $\mathbf{x}_k \in \mathbb{R}^{N_x}$ denotes the *state* of the radar target at discrete time k, and $\mathbf{v}_k$ denotes the additive system noise accounting for environmental uncertainty about the target.

Measurement equation, which describes dependence of the measurement vector $\mathbf{z}_k \in \mathbb{R}^{N_z}$ on the state $\mathbf{x}_k$, the waveform vector $\boldsymbol{\theta}_{k-1}$, and the measurement noise $\mathbf{w}_k$, as shown by [51]

$$\mathbf{z}_k = \mathbf{h}_k(\mathbf{x}_k, \boldsymbol{\theta}_{k-1}, \mathbf{w}_k). \tag{2.5}$$

Assuming that the measurement noise $\mathbf{w}_k$ is an additive white Gaussian process dependent on the waveform vector $\boldsymbol{\theta}_{k-1}$, Eq. (2.5) can be further simplified as

$$\mathbf{z}_k = \mathbf{h}(\mathbf{x}_k) + \mathbf{w}_k(\boldsymbol{\theta}_{k-1}), \tag{2.6}$$

where $\mathbf{w}_k(\boldsymbol{\theta}_{k-1})$ denotes the measurement noise that acts as the *driving force*. In the rest of this thesis, we will simplify the notation of measurement noise as $\mathbf{w}_k$. It is in the dependence of this noise on the waveform-parameter vector $\boldsymbol{\theta}_{k-1}$ that the transmitter influences accuracy of the state estimation in the receiver.

B: Hybrid Model

For many tracking problems, dynamics of the target are described by a continuous-time system equation. Therefore, Eq. (2.4) is not applicable any more. Consider the system equation being described by [52]:

$$d\mathbf{x}(t) = \mathbf{f}(\mathbf{x}(t), t)dt + \sqrt{\mathbf{Q}}d\boldsymbol{\beta}(t), \tag{2.7}$$

where $\mathbf{x}(t) \in \mathbb{R}^{N_x}$ denotes state of the system at time t; $\boldsymbol{\beta}(t) \in \mathbb{R}^{N_x}$ denotes the standard Brownian motion with increment $d\boldsymbol{\beta}(t)$ that is independent of $\mathbf{x}(t)$ and it plays the same role as system noise as in Eq. (2.4); $\mathbf{f} : \mathbb{R}^{N_x} \times \mathbb{R} \rightarrow \mathbb{R}^{N_x}$ is a known nonlinear function with appropriate regularity properties; and $\mathbf{Q} \in \mathbb{R}^{N_x \times N_x}$ is called

the diffusion matrix. State of the system can be inferred through noisy measurements sampled at time $t_k = kT$ using the same measurement equation as (2.6). It is also assumed that the initial conditions and noise processes are statistically independent.

To discretize the stochastic differential equation (2.7) in an efficient manner, we may use the Itô-Taylor expansion. Itô-Taylor expansion of higher order is theoretically more accurate than that of lower order [53]. Applying the Itô-Taylor expansion of order 1.5, chosen because of its most effective approximation capability, to the stochastic differential equation over the time interval $(t, t + \delta)$, we have

$$\mathbf{x}(t+\delta) = \underbrace{\mathbf{x}(t) + \delta\mathbf{f}(\mathbf{x}(t),t) + \frac{1}{2}\sigma^2(\mathbb{L}_0\mathbf{f}(\mathbf{x}(t),t))}_{\mathbf{f}_d(\mathbf{x}_t,t)} + \sqrt{\mathbf{Q}}\boldsymbol{\omega} + (\mathbb{L}\mathbf{f}(\mathbf{x}(t),t))\boldsymbol{\psi}, \quad (2.8)$$

where we have the following notations:

- $\mathbb{L}_0$ and $\mathbb{L}_j (j = 1, 2, ..., N_x)$ are two differential operators, defined by

$$\mathbb{L}_0 = \frac{\partial}{\partial t} + \sum_{i=1}^{N_x} \mathbf{f}_i \frac{\partial}{\partial \mathbf{x}_i} + \frac{1}{2} \sum_{j,p,q=1}^{N_x} \sqrt{(\mathbf{Q}_{p,j})}\sqrt{\mathbf{Q}_{q,j}}\frac{\partial^2}{\partial \mathbf{x}_p \partial \mathbf{x}_q} \qquad (2.9)$$

$$\mathbb{L}_j = \sum_{i=1}^{N_x} \sqrt{\mathbf{Q}_{i,j}}\frac{\partial}{\partial \mathbf{x}_i}; \qquad (2.10)$$

- $\mathbb{L}\mathbf{f}$ denotes a square matrix with its (i, j)-th entry being $\mathbb{L}_j\mathbf{f}_i$, $(i, j = 1, 2, ..., N_x)$;

- $\mathbf{f}_d(\mathbf{x}_t, t)$ is the discretized noise-free system equation;

- Pair of correlated N_x-dimensional Gaussian random variables $(\boldsymbol{\omega}, \boldsymbol{\psi})$ can be generated from a pair of independent N_x-dimensional standard Gaussian random

variables $(\mathbf{u}_1, \mathbf{u}_2)$ as follows:

$$\boldsymbol{\omega} = \sqrt{\delta}\mathbf{u}_1 \tag{2.11}$$

$$\boldsymbol{\psi} = \frac{1}{2}\delta^{3/2}(\mathbf{u}_1 + \frac{\mathbf{u}_2}{\sqrt{3}}), \tag{2.12}$$

using which, three covariance matrices can be obtained as follows:

$$\mathbb{E}\left[\boldsymbol{\omega}\boldsymbol{\omega}^T\right] = \delta\mathbf{I}_{N_x} \tag{2.13}$$

$$\mathbb{E}\left[\boldsymbol{\omega}\boldsymbol{\psi}^T\right] = \frac{1}{2}\delta^2\mathbf{I}_{N_x} \tag{2.14}$$

$$\mathbb{E}\left[\boldsymbol{\psi}\boldsymbol{\psi}^T\right] = \frac{1}{3}\delta^3\mathbf{I}_{N_x}. \tag{2.15}$$

Examination of the system noise in Eqs. (2.4)/(2.7) and measurement noise in Eq. (2.6) reveals an important physical fact in modeling the radar target, that is

The evolution of the target's state is governed by the target's dynamics itself, independent of the radar system. The radar interacts with the target only when the measurement system is switched on.

Application of the state-space model described in Eqs. (2.4)/(2.7) and (2.6) hinges on the following four basic assumptions:

- First, the nonlinear vectorial functions $\mathbf{f}(\cdot)$ and $\mathbf{h}(\cdot)$ in Eqs. (2.4) and (2.6) are both smooth and otherwise arbitrary.

- Second, the system noise $\mathbf{v}_k$ and measurement noise $\mathbf{w}_k$ are zero-mean Gaussian distributed and statistically independent of each other.

- Third, the covariance matrix of system noise is known.

24

- Fourth, the state is independent of measurement noise.

Examining Eqs. (2.4) and (2.6), we immediately see that the state $\mathbf{x}_k$ is *hidden* from the observer, and the challenge for the receiver is to exploit dependence of the measurement vector on the state to compute an estimate of the state and do so in a sequential and on-line manner.

With this objective in mind, we need to determine statistical characteristics of the measurement noise $\mathbf{w}_k$. To this end, we first recognize that the measurement noise covariance is dependent on the parameter $\boldsymbol{\theta}_{k-1}$ of the waveform generator in the transmitter [22], hence the notation $\mathbf{R}_k(\boldsymbol{\theta}_{k-1})$ for this covariance, here we define $\boldsymbol{\theta}_{k-1} = [\lambda, b]$ with λ and b denoting the duration of Gaussian pulse and chirp rate, respectively. Moreover, the inverse of the *Fisher information matrix* (FIM) is the *Cramér-Rao lower bound* (CRLB) on the state estimation error covariance matrix for unbiased estimator [16]. Denoting the Fisher information matrix by $\mathbf{J}$, we may consider the inverse matrix $\mathbf{J}^{-1}$ as a suitable characterization for optimal waveform selection, and thus write

$$\mathbf{R}_k(\boldsymbol{\theta}_{k-1}) = \boldsymbol{\Gamma}\mathbf{J}^{-1}(\boldsymbol{\theta}_{k-1})\boldsymbol{\Gamma}, \tag{2.16}$$

where $\boldsymbol{\Gamma}$ is a symmetric matrix defined by

$$\boldsymbol{\Gamma} \triangleq \operatorname{diag}\left[\frac{c}{2}, \frac{c}{4\pi f_c}\right]. \tag{2.17}$$

For convenience of presentation, it is desirable to separate the contribution of the waveform parameter vector in the Fisher information matrix from the received signal

25

energy-to-noise spectral density ratio (i.e. the SNR) defined by

$$\eta = \frac{2E_R}{N_0}, \tag{2.18}$$

where N_0 is spectral density of the complex noise envelope $\tilde{n}(t)$. To this end, we write

$$\mathbf{J}(\boldsymbol{\theta}_{k-1}) = \eta \mathbf{U}(\boldsymbol{\theta}_{k-1}). \tag{2.19}$$

Accordingly, we may rewrite Eq. (2.16) in the desired form [23]

$$\mathbf{R}_k(\boldsymbol{\theta}_{k-1}) = \frac{1}{\eta}\boldsymbol{\Gamma}\mathbf{U}^{-1}(\boldsymbol{\theta}_{k-1})\boldsymbol{\Gamma}, \tag{2.20}$$

with the matrix $\mathbf{U}(\boldsymbol{\theta}_{k-1})$ being merely a scaled version of the Fisher information matrix $\mathbf{J}(\boldsymbol{\theta}_{k-1})$. This new matrix is a symmetric matrix whose three elements are described as mean-square values of the following errors:

- the Doppler estimation error,

- the cross Doppler-delay estimation error, and

- the delay estimation error.

In [22], it is shown that for the transmit waveform, combining linear frequency modulation (LFM) with Gaussian amplitude modulation, the measurement noise covariance matrix is given by

$$\mathbf{R}_k(\boldsymbol{\theta}_{k-1}) = \begin{bmatrix} \dfrac{c^2\lambda^2}{2\eta} & -\dfrac{c^2 b \lambda^2}{2\pi f_c \eta} \\[3mm] -\dfrac{c^2 b \lambda^2}{2\pi f_c \eta} & \dfrac{c^2}{(2\pi f_c)^2 \eta}\left(\dfrac{1}{2\lambda^2} + 2b^2\lambda^2\right) \end{bmatrix}, \tag{2.21}$$

where, as before, b denotes the chirp rate of the LFM pulse and λ denotes the duration of the Gaussian pulse for the LFM pulse. Gathering these two parameters, we have the transmitted waveform parameter vector $\boldsymbol{\theta} = [\lambda, b]$.

It is important to note however that this formula for $\mathbf{R}_k(\boldsymbol{\theta}_{k-1})$ is valid so long as the assumption that the energy per transmitted waveform remains constant from one cycle to the next. Otherwise, we would have to expand the waveform parameter vector $\boldsymbol{\theta}_{k-1}$ by adding a new variable η_{k-1}.

Having the state-space model of the target, we are now ready to describe the perception-action cycle in its most basic form.

2.2   Basic Perception-Action Cycle

In a cognitive radar, perception of the environment in the receiver leads to an action taken by the transmitter on the environment in accordance with the basic perception-action cycle of Figure 2.2. It is through the continuation of this cycle across time that the system acquires its ability to adapt to changes in the environment by making successive internal changes of its own through lessons learned from continuing interactions with the environment.

The integration of functions involved in the perception-action cycle across time is a distinctive characteristic of cognition in that time plays three key roles [13]:

1. Time separates incoming sensory signals (stimuli) so as to guide the overall system behaviour.

2. Time separates sensory signals responsible for perception in the receiver from actions taken in the transmitter.
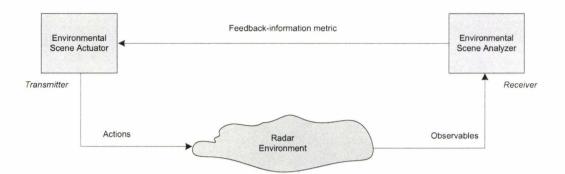
Figure 2.2: The perception-action cycle in its most basic form

3. Time separates the occurrence of sensory feedback from further action.

The implication of these three points is profound:

Temporal organization of the system behaviour requires the integration across time of the following:

- percepts with other percepts;

- actions with other actions; and

- percepts with actions.

Simply put, the integration of functions in the perception-action cycle, irrespective of its structure, is a defining property of cognitive radar systems. Hereafter, we refer to this property as the *cognitive functional integration-across-time property*.

2.3 Optimal Bayesian Filtering of Environmental Perception

For a cognitive radar to perceive the environment in which it operates, the radar must be equipped with an appropriate set of sensors to learn from the environment. To be

specific, antennas are placed at the front end of the radar receiver so as to couple it electromagnetically to the environment. By the same token, another set of antennas is placed at the output of the radar transmitter so as to couple it electromagnetically to the environment in its own way.

The sensors in the receiver feed a functional block called the *environmental scene analyzer*; its function is to perform perception, defined as follows:

Definition 2.1 (Perception). *Perception is the sensory analysis of the incoming stimuli aimed at learning the underlying physical attributes that characterize the environment.* □

Exact composition of the scene-analyzer is naturally dependent on the application of interest. For example, in a cognitive radar designed for target tracking, the environmental scene analyzer consists of a sequential state estimator, the function of which is to estimate the state of the target across time in a sequential manner.

As we may know that the optimal Bayesian filter is the ideal tool for tracking the target's state in the radar receiver. Optimal Bayesian filtering is a general probabilistic approach to estimate the posterior density of the state over time by using new measurements. The optimal Bayesian filtering consists of the following two steps:

- Propagation of the *old* posterior density at the current time without incorporating the current measurements. This step is also called the *time update*.

- Using Bayes's rule to combine the *a priori* prediction and the current measurements. This step is also called the *measurement update*.

Typically, the two steps are executed one after another. The time update step

advances the state estimate followed by the measurement update step upon the availability of a new observation. The measurement update then becomes the starting point for next update step. Under the linearity and Gaussianity assumptions, the Kalman filter (KF) is equivalent to the optimal Bayesian filter [54]. However, if we are faced with a discrete-time nonlinear filtering problem as expressed by Eqs. (2.4) and (2.6), KF is not applicable. We need to approximate the optimal Bayesian filter.

One well-known approximation to the Bayesian filter is the extended Kalman filter (EKF) [24]. EKF is based on the linear approximation of dynamics obtained from the first-order Taylor series approximation of the system and measurement equations. Mean vector and covariance matrix are the statistics propagated by the algorithm. The computational complexity of a real-time EKF algorithm is of the order of N_x^3 for estimating state vectors of dimension N_x. The accuracy of the estimation is adequate for *mild* nonlinearities and Gaussian noise [55].

Another popular algorithm is the unscented Kalman filter (UKF) [25]. UKF is based on the idea that the approximation of a probability distribution is easier than the approximation of a nonlinear function . It uses a deterministic sampling method called unscented transform to choose a minimal set of sample points around the mean. The chosen sample points, which are also known as sigma points, are propagated through the nonlinear functions in order to update the mean and covariance of the estimate. UKF provides a significant improvement compared to EKF in the presence of sever nonlinearities and Gaussian noise.

However, if the assumption of Gaussianity is violated, we can employ the particle filter (PF) [26]. Complete probability density conditioned on the measurements is the statistics propagated by the PF algorithm. To predict statistics from one

measurement to the next, Monte Carlo integration using importance sampling is employed. Also, to correct the statistics at measurement time, Monte Carlo sampling of the conditional density using both importance sampling and resampling is employed. However, it is computationally demanding especially for high-dimensional problems [55].

It is computationally infeasible to directly derive the Bayesian filter for a discrete-time nonlinear state-space model as expressed by Eqs. (2.4) and (2.6), hence the practical need for its approximation. The aforementioned filters, EKF, UKF, and PF, are all approximations of optimal Bayesian filter. Recently, another nonlinear filter, namely the cubature Kalman filter (CKF) [56], was developed as the closest known approximation to the Bayesian filter that could be designed in a nonlinear setting under the key assumption: The predictive density of the joint state-measurement random variable is Gaussian. The CKF algorithm is summarized in Appendix A for the purpose of implementation and discussion in the rest of the thesis.

By the same token, for a continuous-discrete system, the system equation (2.8) describes a process with infinite steps of time update. Following the Itô-Taylor expansion, we need to predict m consecutive steps until the new observation is available, where $m = \frac{T}{\delta}$. Thereafter, we need a Bayesian filtering algorithm with m-step predictions and one-step update. We also know that it is impractical to implement the optimal Bayesian filter due to the integrals that need to be evaluated when computing the posteriors. Again, we approximate it using the cubature rules [57]. Following this way of thinking, another new filter was recently described in [58] and named the continuous-discrete cubature Kalman filter (CD-CKF). Similarly, for the same purpose of algorithmic implementation, CD-CKF is summarized in Appendix B. Needless

to say, the variants of EKF and UKF for a continuous-discrete system, namely CD-EKF [52] and CD-UKF [59], are both applicable but proven to be inferior to CD-CKF [58].

In the rest of this chapter, we will base our discussion on the CKF for a discrete-time nonlinear system and the CD-CKF for a continuous-discrete nonlinear system.

2.4 Dynamic Optimization for Waveform Selection

Previously we remarked that the measurement covariance in the measurement equation (2.6) depends on the transmitted waveform parameter vector $\boldsymbol{\theta} = [\lambda, b]$, which applies to LFM with Gaussian amplitude modulation. Hence, if the waveform parameters are selected optimally, any *action* taken by the transmitter will be regarded as an optimal *reaction* to the environment perceived by the receiver. We call this the *action-reaction cycle*, equivalent to the perception-action cycle in an inverse sense. Interestingly, this statement interprets a basic common sense: For any action applied to the system, there will be correspondingly a reaction made by the system. With this point in mind, we may now address the algorithmic formulation for waveform selection in the transmitter. We name this the *dynamic optimization* algorithm, considering that it is a special case of dynamic programming in case of only one step into the future. In effect, dynamic optimization assumes the role of a controller in a nonlinear feedback system that tunes the transmit-waveform parameters so as to tame the behaviour of the receiver in an effort to minimize the tracking errors in some statistical sense.

It is assumed that $\mathbf{z}_0$ is the initial condition for the perception-action cycle, and the cognition is wired to start from this initial observable. The transmitter then

operates on the cost-to-go function (computed from the receiver output) to produce a waveform parameter vector $\boldsymbol{\theta}_0$ on which radar waveform will be transmitted at next cycle $k = 1$, which correspondingly leads to a new observable $\mathbf{z}_1$. This cycle runs recursively for $k = 2, 3, ...$ Unfolding the perception-action cycle, we have $\mathbf{z}_0 \to \boldsymbol{\theta}_0 \to \cdots \to \mathbf{z}_k \to \boldsymbol{\theta}_k$.

However, if we were to follow the aforementioned *action-reaction cycle*, the initial condition is the waveform parameter $\boldsymbol{\theta}_0$, rather than the observable $\mathbf{z}_0$. The cognition is switched on upon the receipt of a new observable $\mathbf{z}_k$ for $k = 1, 2, ...$ The transmitter then operates on the cost-to-go function to produce a waveform parameter vector $\boldsymbol{\theta}_k$ on which radar waveform will be transmitted at next cycle $k+1$. Similarly, unfolding the action-reaction cycle yields $\boldsymbol{\theta}_0 \to \mathbf{z}_1 \to \cdots \to \boldsymbol{\theta}_{k-1} \to \mathbf{z}_k$.

To avoid confusion, the rest of the thesis will assume that cognitive radar system starts from an initial observable $\mathbf{z}_0$. Before proceeding further, two other important remarks also deserve particular attention:

- First, when a cognitive tracking radar is viewed as a feedback control system, the basic perception-action cycle is also regarded as a *measurement-waveform selection cycle*, that is, $\mathbf{z}_k \to \boldsymbol{\theta}_k$, where k denotes the current cycle. In other words, the measurement $\mathbf{z}_k$ made by the receiver at cycle k leads to waveform selection $\boldsymbol{\theta}_k$ to be transmitted at the next cycle, i.e., $k + 1$.

- Second, the state of the target is *hidden* from the receiver, which, in turn, poses a practical problem in the following sense: The formulation of Bellman's dynamic programming, a general case of our dynamic optimization algorithm, not only demands that the environment to be Markovian but also the controller has perfect knowledge of the state. In reality, however, the transmitter of a radar

tracker has an *imperfect* estimate of the state reported to it by the receiver. Accordingly, we are faced with an *imperfect state-information problem*. To resolve this problem, we follow [51] by introducing a new information state vector defined by

$$\mathbf{I}_k \triangleq (\mathbf{Z}_k, \boldsymbol{\Theta}_{k-1}), \quad \text{with } \mathbf{I}_0 = \mathbf{z}_0, \quad k = 1, 2, ..., \tag{2.22}$$

where

$$\mathbf{Z}_k = [\mathbf{z}_0, \mathbf{z}_1, ..., \mathbf{z}_k] \tag{2.23}$$

$$\boldsymbol{\Theta}_k = [\boldsymbol{\theta}_{0+}, \boldsymbol{\theta}_1, ..., \boldsymbol{\theta}_k]. \tag{2.24}$$

Here the notion $\boldsymbol{\theta}_{0+}$ denotes the fact that the initial point of waveform parameter vector always comes after the initial point of observables.

From these three equations, we readily obtain the recursion

$$\mathbf{I}_k = (\mathbf{I}_{k-1}, \mathbf{z}_k, \boldsymbol{\theta}_{k-1}), \quad k = 1, 2, ... \tag{2.25}$$

which may be viewed as the state evolution of a new dynamic system with perfect-state information, and therefore applicable to dynamic optimization. According to Eq. (2.25), we may say:

- $\mathbf{I}_{k-1}$ is the old value of the information state vector;

- $\boldsymbol{\theta}_{k-1}$ is the waveform parameter vector computed at time $k - 1$, and on which the transmitter acts at time k; this also implies the fact that $\boldsymbol{\theta}_k$ is unknown at time k;

- the current measurement $\mathbf{z}_k$ is viewed as a *random disturbance* resulting from the control decision $\boldsymbol{\theta}_{k-1}$; and

- note that the terminology adopted in Eq. (2.25) is consistent with the system equation (2.4).

At any discrete time k, the dynamic optimization algorithm seeks to find the best waveform parameters by minimizing a cost-to-go function, defined as the tracking *expected* mean-square error (MSE):

$$g(\mathbf{x}_k, \boldsymbol{\theta}_k) = \mathbb{E}_{\mathbf{x}_{k+1}, \mathbf{z}_{k+1} | \mathbf{I}_k, \boldsymbol{\theta}_k} \left[(\mathbf{x}_{k+1} - \hat{\mathbf{x}}_{k+1|k+1})^T (\mathbf{x}_{k+1} - \hat{\mathbf{x}}_{k+1|k+1}) \right], \qquad (2.26)$$

where $\hat{\mathbf{x}}_{k+1|k+1}(\mathbf{I}_k, \boldsymbol{\theta}_k, \mathbf{x}_{k+1}, \mathbf{z}_{k+1})$ is the posterior *expected* state estimation given the selected parameter vector $\boldsymbol{\theta}_k$.

2.4.1 Directed-Information Flow

Along with the distributed information in cognitive radar system, time also stamps itself in three components of the system, which are the target, the receiver and the transmitter. This relationship is depicted by the diagram of radar pulse timing in Figure 2.3. If we backtrack to Section 2.2 where we have summarized three key roles that time plays in cognitive radar, an important physical observation about cognitive radar system emerges as follows:

The total time, namely *cycle time* τ_{cycle}, needed for the directed-information to flow across the cognitive radar system is composed of three parts, expressed as

$$\tau_{\text{cycle}} = \tau_{\text{target}} + \tau_{\text{receiver}} + \tau_{\text{transmitter}}, \qquad (2.27)$$

35

where

1. τ_{target}: time for the radar signal to reach to the target and bounce back;

2. τ_{receiver}: time for the radar echo to be processed in the receiver; and

3. $\tau_{\text{transmitter}}$: time for the transmitter to perform its action in the environment.
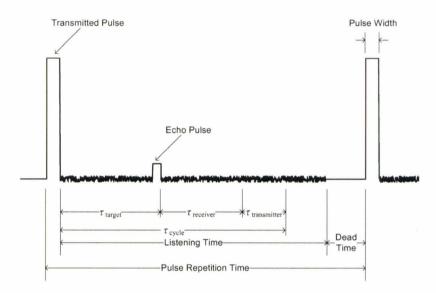
Figure 2.3: Diagram of radar pulse timing

Referring also to Figure 2.3, a necessary property needs to be satisfied for a cognitive radar system to work:

$$\tau_{\text{cycle}} < \text{Pulse Repetition Time}.$$

With this discussion of radar pulse relationship in mind, and to simplify the mathematical formulation throughout the thesis, we assume that the cycle time is considered only once as a delay during transition from one cycle to another.

Now, to elaborate more about the behaviour of the cognitive tracking radar system, we may look to the directed-information flow across the system, depicted in Figure 2.4, where the information flow across the system is classified into two paths:

Figure 2.4: Information flow in cognitive tracking radar

Feedforward transmission path for joint control-estimation in the receiver. In this path, the transmitter has already selected the waveform parameter vector $\boldsymbol{\theta}_{k-1}$, on which radar waveform $\tilde{\mathbf{s}}_{k-1}$ acts on the radar environment. The receiver then builds on previous knowledge of the radar waveform and current observable $\mathbf{z}_k$ available at time k to locally optimize the state estimation, obtaining $\{\mathbf{x}_{k|k}, \mathbf{P}_{k|k}\}$. A one-step prediction is performed to obtain $\{\hat{\mathbf{x}}_{k+1|k}, \mathbf{P}_{k+1|k}\}$ by evolving $\hat{\mathbf{x}}_{k|k-1}$ and $\mathbf{P}_{k|k-1}$ one cycle ahead. From CKF, it is easy to conclude that $\mathbf{P}_{k+1|k}$ is independent of the waveform parameter vector $\boldsymbol{\theta}_k$ since $\boldsymbol{\theta}_k$ is unknown at this stage. The pair $\{\hat{\mathbf{x}}_{k+1|k}, \mathbf{P}_{k+1|k}\}$ is then fedback to the transmitter as a feedback-information metric.

Feedback transmission path for updating the waveform selection in the transmitter. Given the feedback-information metric $\{\hat{\mathbf{x}}_{k+1|k}, \mathbf{P}_{k+1|k}\}$ computed at time k and for any unknown waveform parameter $\boldsymbol{\theta}_k$, the *expected* state-error covariance $\mathbf{P}_{k+1|k+1}$ can be calculated by evolving $\mathbf{P}_{k|k}$ one cycle ahead. The dependence of $\mathbf{P}_{k+1|k+1}$ on $\boldsymbol{\theta}_k$ can be justified by first evolving $\mathbf{P}_{\mathbf{zz},k|k-1}$ to $\mathbf{P}_{\mathbf{zz},k+1|k}$ and then

substituting it into $\mathbf{P}_{k+1|k+1}$. Now, the requirement is to formulate a cost-to-go function based on the pair $\{\mathbf{P}_{k+1|k+1}, \boldsymbol{\theta}_k\}$ and then find the policy μ_k that selects $\boldsymbol{\theta}_k$ for the next signal transmission at time $k+1$. To simplify the presentation, we will use $\mathbf{P}_{k+1|k+1}(\boldsymbol{\theta}_k)$ to denote the dependence of the expected error covariance on unknown waveform parameter vector in the rest of the thesis.

Note that in Figure 2.4 we plot the signal-flow by looking one-step into the future. As discussed in the perception-action cycle, the computation starts with the initial condition $\mathbf{z}_0$ and proceeds by computing $\boldsymbol{\theta}_0$, which then leads to new observable $\mathbf{z}_1$, and so on. The dynamic optimization algorithm is therefore expressed as:

$$\boldsymbol{\theta}_k^* = \arg \min_{\boldsymbol{\theta}_k \in \mathcal{P}_k} \left[\mathrm{Tr}(\mathbf{P}_{k+1|k+1}) \right] \tag{2.28}$$

where $\mathcal{P}_k$ is the waveform library at time k.

When there is provision of a horizon looking more steps into the future, we will have a general optimization problem. It can be tackled by a dynamic programming approach derived in Appendix C.

2.4.2 Analysis and Synthesis of Waveform Library

As described by Eq. (2.28), dynamic optimization relies closely on waveform library in conducting the policy evolution. By a similar argument, the waveform agility of cognitive radar will be greatly degraded if the waveform library is not efficiently designed. In this thesis, we design the waveform library using a very straightforward strategy, including two steps:

Analysis: To start the first step, the waveform parameter vector is divided into grid points. The coordinates of each point on the grid correspond to one subset in

the space, which is spanned by the waveform parameter vector. Let us take the two-dimensional waveform parameter vector $\boldsymbol{\theta} = [\lambda, b]$ as an example, where λ and b are chirp rate and pulse duration of the envelope, respectively. If each element of this vector has a maximum and a minimum determined by the transmitter, we then have a grid of waveform library as follows:

$$\mathcal{P} = \{\lambda \in [\lambda_{min} : \Delta\lambda : \lambda_{max}], b \in [b_{min} : \Delta b : b_{max}]\},$$

where $\Delta\lambda$ and Δb denote the step-size of chirp rate and envelope duration, respectively.

To implement this step, the expected error covariance matrix $\mathbf{P}_{k+1|k+1}$ is calculated with respect to each unknown $\boldsymbol{\theta}_k$ in the waveform library, expressed as

$$\mathbf{P}_{k+1|k+1} = \mathbf{P}_{k+1|k} - \mathbf{G}_{k+1}\mathbf{P}_{\mathbf{zz},k+1|k}\mathbf{G}_{k+1}^T, \tag{2.29}$$

for each subset $\boldsymbol{\theta}_k \in \mathcal{P}_k$, where the Kalman gain is

$$\mathbf{G}_{k+1} \doteq \mathbf{P}_{\mathbf{xz},k+1|k}\mathbf{P}_{\mathbf{zz},k+1|k}^{-1} \tag{2.30}$$

with

$$\begin{aligned}
\mathbf{P}_{\mathbf{xz},k+1|k} &= \int_{\mathbb{R}^{N_x}} \mathbf{x}_{k+1}\mathbf{h}^T(\mathbf{x}_{k+1})\mathcal{N}(\mathbf{x}_{k+1}; \hat{\mathbf{x}}_{k+1|k}, \mathbf{P}_{k+1|k})d\mathbf{x}_k - \hat{\mathbf{x}}_{k+1|k}\hat{\mathbf{z}}_{k+1|k}^T, \\
\mathbf{P}_{\mathbf{zz},k+1|k} &= \int_{\mathbb{R}^{N_x}} \mathbf{h}(\mathbf{x}_{k+1})\mathbf{h}^T(\mathbf{x}_{k+1})\mathcal{N}(\mathbf{x}_{k+1}; \hat{\mathbf{x}}_{k+1|k}, \mathbf{P}_{k+1|k})d\mathbf{x}_k \\
&\quad - \hat{\mathbf{z}}_{k+1|k}\hat{\mathbf{z}}_{k+1|k}^T + \mathbf{R}_{k+1}(\boldsymbol{\theta}_k).
\end{aligned}$$

Synthesis: Having obtained the expected error covariance matrix $\mathbf{P}_{k+1|k+1}$ for

every $\boldsymbol{\theta}_k$ in the waveform library, it is not difficult to calculate the cost pertaining to each grid point. The task of this second step is to search over the waveform grid, in order to locate the grid point that produces a minimum of cost. This method is called *grid-searching*. When the radar waveform $\boldsymbol{\theta}_k^*$ that can produce a minimal cost is discovered, it completes the *synthesis* of radar signal from the waveform library.

In what follows, we apply approximation to the cost function.

2.4.3   Approximation of the Cost Function $g(\cdot)$:

Inclusion of the state $\mathbf{x}_{k+1}$ under the expectation defined in Eq. (2.26) speaks for itself. As for the observable $\mathbf{z}_{k+1}$, its inclusion under the expectation is justified on the following ground: In CKF, the estimate $\hat{\mathbf{x}}_{k+1|k+1}$ depends on $\mathbf{z}_{k+1}$, which itself depends nonlinearly on $\mathbf{x}_{k+1}$. Consequently, it is difficult to evaluate this expectation. We may therefore approximate the cost $g(\mathbf{x}_k, \boldsymbol{\theta}_k)$ as shown by

$$g(\mathbf{x}_k, \boldsymbol{\theta}_k) \approx \mathrm{Tr}(\mathbf{P}_{k+1|k+1}), \tag{2.31}$$

where $\mathrm{Tr}(\cdot)$ is an operator that extracts the trace of the enclosed covariance $\mathbf{P}_{k+1|k+1}$; see Appendix D for detailed derivation of this approximate formula.

In words, the dynamic optimization algorithm encompasses the feedback transmission path, extending from the cost-to-go function computed at the receiver output at the previous cycle to the waveform selection by the transmitter for the next cycle. Most importantly, the whole computation is feasible in an on-line manner by virtue of setting the horizon depth $L = 1$.

40

2.5 Summary

This chapter presents the underlying theory of basic cognitive radar for tracking application. The following ideas are exploited:

1. Use of the cubature Kalman filter in the receiver for perception of the radar environment; this new filter is the best known approximation to the optimal Bayesian filter under the Gaussian assumption, an assumption that is justified for tracking targets in space.

2. Formulation of the dynamic optimization algorithm for action to control the waveform selection in the transmitter. This novel algorithm derives its information-processing power in two important ways:

   • First, it is based on the notion of *imperfect-state information*, which gets around the fact that our dynamic optimization algorithm requires perfect knowledge of the state, whereas in a real-world of environment the state is hidden from the radar.

   • Second, clever use is made of the cubature rule of third degree in the approximation of certain integrals involved in deriving the dynamic optimization algorithm.

Chapter 3

Cognitive Radar with Nested Memory

Copper mirrors the clothes and hat; history mirrors the rise and fall of a nation; people mirrors the success and failure.

Emperor Taizong of Tang Dynasty (599-649)

So far, we have laid down the foundation of cognitive radar that is confined to the basic perception-action cycle. In this chapter, we will develop a new structure of cognitive radar by introducing three other important processes into the basic perception-action cycle, i.e., memory, attention, and intelligence. Before proceeding to do that, we need to remind ourselves two crucial aspects of a radar system: (i) the system aspects which describe the functional ingredients, and (ii) the algorithmic aspects which describe the algorithm design. In this chapter, we will first describe the system aspect followed by the algorithmic design.

3.1   Important Facts about Cortex and Mind

As we stated in Chapter 2, the global feedback between the receiver and the transmitter acts as the tunnel for information delivery in basic cognitive radar system. It is fair to say that global feedback facilitates computational intelligence in the perception-action cycle of cognitive radar. Therefore, global feedback is *necessary* for a radar to be cognitive. However, with global feedback alone, we are not anywhere close to the visual brain. Reflecting on the perspectives on cognitive science in studying the brain cortex, we conclude that the basic cognitive radar discussed in Chapter 2 is merely a junior member of the cognitive radar family.

In order to develop a radar system with full cognition, four basic facts deserve attention:

- The first fact that has been overlooked is that the mammalian cortexes are layered networks and are organized in a *hierarchical* manner. They have input layers, output layers and hidden layers between them. The three layers cooperatively accomplish the three basic functions of the brain: *convergence*, *divergence*, and *recurrence*.

- The second fact is that information flows in the cortex are in two directions: *bottom-up*, and *top-down*. On the one hand, cognitive networks in the brain are auto-associated networks. When new inputs are presented to the network, new associations are established by expanding pre-existing networks. This procedure is called the bottom-up process. It describes how information is stored in the memory. On the other hand, to select the sensory stimuli and distinguish them from the outside world, the information will flow from the higher associative

cortex to the lower one. This procedure is called the top-down control.

- The third fact is that all the five cognitive functions, i.e., perception, attention, memory, intelligence and language [1], share the same biological architecture. At different temporal and functional levels and also relying on the external stimuli, this architecture may exhibit different cognitive behaviour.

- The last fact, which is also the most important one, is that the mammalian cortex as it currently stands is the result of a continuing evolution process for millions of years [60]. The cortex has become heavier and larger during this process and has reached its peak in complexity and ability in human being in an effort to enable cognition.[2]

Having summarized the important facts that we can learn from the cortex, we now identify a new cognitive radar with more sophistication and information-processing power [61, 62], namely the *nested cognitive radar*. The nested cognitive radar distinguishes itself from the basic cognitive radar in the "nesting" of three memories within the perception-action cycle as depicted in Figure 3.1. The three memories are:

- *perceptual memory* in the receiver,

- *executive memory* in the transmitter, and

- *coordinating perception-action memory* that reciprocally couples the first two memories.

---

[1]Language will not be covered in this thesis considering its uniqueness to human cognition.

[2]To be more accurate, complexity contributes to the intelligence level more than the volume of the brain does.

The net result is improved information processing power over the basic cognitive radar by virtue of now having, in addition to the basic perception-action cycle, the following: memory, attention and enhanced intelligence .

The nested cognitive radar is well-suited for monostatic radar, where the transmitter and receiver are co-located. On the other hand, the basic cognitive radar, memoryless but equipped with global feedback, is perhaps more suitable for bistatic radar where the transmitter and receiver are separately located.

Now, let us describe the first important ingredient in Figure 3.1, *memory*.
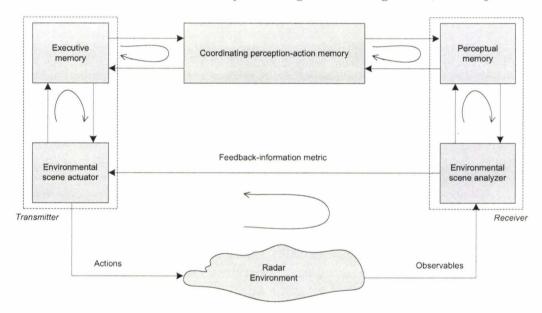
Figure 3.1: Nested perception-action cycle of cognitive radar

3.2   Memory for Information Storage

Before proceeding to discuss the important role of memory in cognitive radar, it is instructive that we make a distinction between knowledge and memory:

Definition 3.1 (Knowledge). *Knowledge is a memory of certain facts and rela-tionships that exist between them, none of which changes with time.* □

In other words, knowledge is *static* in its contents.

Definition 3.2 (Memory). *Memory is dynamic in that its contents continually change over the course of time in accordance with changes in the environment.* □

Stated in another way: The contents of the memory are subject to time con-straints, whereas knowledge is timeless and therefore, free of time constraints.

With a cognitive radar consisting of a transmitter and a receiver, it is logical to split the memory into two parts, one residing in the receiver and the other residing in the transmitter. These two parts of memory are respectively called *perceptual memory* and *executive memory*.

3.2.1   Perceptual Memory

As the name implies, perceptual memory is an integral part of how, in an overall sense, the receiver perceives the environment. To be more specific, perceptual memory provides the ability for the receiver to interpret the incoming stimuli so as to recognize their distinctive features and categorize the features accordingly. We may thus offer the following definition:

Definition 3.3 (Perceptual Memory). *Perceptual memory is the experiential knowledge that is gained by the receiver through a process of learning from the en-vironment, such that the contents of the memory continually change with time in accordance with changes in the environment; the experiential knowledge so gained through learning becomes an inextricable part of the perceptual memory.* □

To satisfy the cognitive functional integration-across-time property, we require that the perceptual memory be reciprocally coupled to the environmental scene analyzer. This reciprocal coupling implies the use of two links:

- *Feedforward link* from a compartment within the environmental scene analyzer to the perceptual memory, which is intended to make it possible for the memory to update its contents in light of the new stimuli.

- *Feedback link* from the perceptual memory to the environmental scene analyzer, the purpose of which is to enable the analyzer to retrieve information stored in memory; the retrieved information is naturally relevant to the particular categorical interpretation of the environment that is the focus of the attentional mechanism.

In effect, the perceptual memory adds sophistication in the form of *bottom-up and top-down learning* to the perception-action cycle, making it much more powerful.

3.2.2   Executive Memory

Just as perceptual memory relates to perception of the environment in the receiver, executive memory relates to the corresponding transmitter's action on the environment. To be more precise, contents of the executive memory are acquired through the transmitter's actions in response to information about the environment that is passed onto it by the receiver via feedback. Hence, the need for the feedback link included in Figure 3.1; we may thus offer the following definition:

Definition 3.4 (Executive Memory). *Executive memory is the experiential knowledge gained by the transmitter through the lessons learned from the actions taken to*

control the environment, with contents of the memory changing with time in accordance with how the receiver perceives the environment; here again, the knowledge so gained through experience becomes an inextricable part of the executive memory.   □

Executive memory plays a key role of its own by making it possible for any new action taken by the transmitter on the environment to benefit from the experiential knowledge gained from previous actions.

Here again, in order to satisfy the *cognitive functional integration across-time property*, the executive memory needs to be reciprocally coupled to the environmental scene actuator, as depicted in Figure 3.1.

The need for this second reciprocal coupling in a cognitive radar is justified as follows:

1. The *forward link* from the environmental scene actuator to the executive memory, which enables the memory to update its contents in light of new feedback information passed onto the actuator by the environmental scene analyzer.

2. The *feedback link* from the executive memory to the environmental scene actuator, which enables the actuator to retrieve information stored in the memory, with the retrieved information being relevant to the particular category of decision-making that is the focus of attention.

3.2.3 Coordinating Perception-Action Memory

Thus far, we have justified the needs for perceptual memory in the receiver and executive memory in the transmitter. Naturally, we cannot expect these two memories to function independently from each other. To be more precise, these two memories

have to be also reciprocally coupled, as indicated in Figure 3.1. The transmitter and receiver of the cognitive radar are thereby enabled to operate in a *synchronous (coherent) manner* all the time that the system is in the operation mode.

To be more precise, *reciprocal coupling of the executive memory to the perceptual memory* is required to address the issue of having to fully account for the cognitive functional integration across-time property. In so doing, the two memories are enabled to interact with each other so as to select the best action that can be taken by the transmitter to control the environment in light of the feedback information passed onto it by the receiver. As depicted in Figure 3.1, the cross-coupling between the perceptual memory and executive memory is made through the new memory: *coordinating perception-action memory*, whose function is to coordinate sensory perception in the receiver with the corresponding action in the transmitter in an orderly and timely manner.

Recognizing that the three memories, namely, perceptual memory, executive memory, and coordinating perception-action memory, are nested within the expanded perception-action cycle of Figure 3.1, this figure is referred to as the *nested perception-action cycle*. Correspondingly, the second member of the family of cognitive radars based on Figure 3.1 is referred to as the *nested cognitive radar*.

Next, we proceed to discuss another important ingredients of the nested cognitive radar, *attention*.

3.3   Attention for Resource Allocation

As a psychological term, *attention* was first defined in late nineteenth century by William James as follows [63]:

It (Attention) is the taking possession by the mind, in clear and vivid form, of one out of what seem several simultaneously possible objects or trains of thought. Focalization, concentration, of consciousness are of its essence. It implies withdrawal from some things in order to deal effectively with others.

For cognitive radars, the definition suggests the following facts:

- Attention is distributed among all the components of cognitive radar.

- Attentional control is the *selective allocation of processing resources*. To facilitate this function in cognitive radar, the perception and action mechanisms should have both *excitatory* and *inhibitory* components, which are elaborated in the following:

  - The excitation function operates on a singular neural network in the memory. Response of the activated neural network (referred to as working memory later in this section) to one incoming stimulus will be continuously strengthened to another similar subsequent stimulus. This states the excitation-transfer theory [64]. To ensure the excitation-transfer process in cognitive radar, two conditions are necessary. First, the subsequent stimulus occurs before the complete decay of the excitation from the previous stimulus. Second, the neural network can not reach the excitatory threshold before it is exposed to the incoming stimulus.

  - The inhibition function operates on multiple neural networks in the memory. In completing a complex task, cognitive radar goes through a series of alternating states, such as, distraction, attention, and focus. When

50

one state dominates, other neural networks excluding the engaging neural network need to be inhibited from getting to the dominated state.

These two components together guarantee a fundamental property of the attentional control in cognitive radar: *cooperative duality of excitation and inhibition* [13].

As a matter of fact, this *cooperative duality* makes the two critical functions of attention possible:

- enhanced activation of one functional network; and

- suppression of other functional networks.
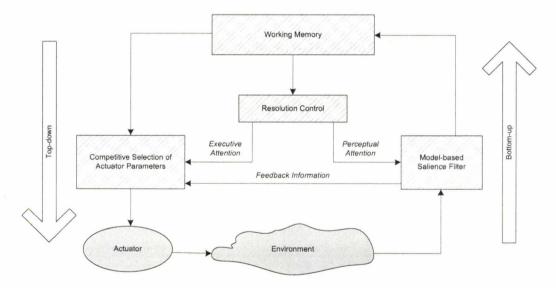
Figure 3.2: Functional components of attention

For nested cognitive radar, attention connects all the functional components in top-down and bottom-up manners, as shown in Figure 3.2. Following the insightful

51

model suggested by Knudsen in [65], we name the four key components contributing to the function of attention as *working memory* [66], *resolution control*, *competitive selection of actuator parameters*, and *model-based salience filter of the environment*, where the working memory links to the sensibility control in a top-down manner and the filter accesses the working memory in a bottom-up manner. It is noteworthy to point out that , similar to the classification of memory, there are two categories of attentions depicted in Figure 3.2, namely the *perceptual attention* and the *executive attention*. Collaborations between them play a key role in completing the overall function of attention in a cognitive radar system:

- In one part of the cognitive radar system, in response to information gained from the environment, the resolution controller needs to retrieve the best system model from the working memory, specifically the *active perceptual memory*. The behaviour involved in this process is the core of *perceptual attention*.

- In the other part of the system, when the information about the radar scene is fedback to the actuator, it prompts the resolution controller to retrieve the optimal waveform library from the working memory, specifically the *active executive memory*. What we stress here is that waveform library is dependant on working memory. The behaviour involved in the retrieval process is the core of *executive attention*.

In a fundamental sense, the purpose of attention is to *selectively allocate* the available information-processing resources to realize the execution of a goal-directed action by the transmitter to control the environment in response to feedback information about the environment extracted by the receiver. We may therefore think of attention as a mechanism for *selective resource allocation*, which, from a practical

perspective, makes a great deal of sense for the following reason: The computational (i.e., information-processing) resources of a cognitive radar are naturally limited.

We may therefore offer the following definition:

Definition 3.5 (Attention). *Attention is a mechanism that protects both the perceptual-processing power of the receiver and the decision-making power of the transmitter from the information-overload problem through selective allocation of computational resources.* □

In the context of a cognitive radar, the term "information overload" refers to the difficulty experienced by the system when the receiver's task of sensing the environment and the transmitter's task of decision-making are compromised by having to handle too much information.

Before we introduce the two categories of attention, it is necessary to describe one component in Figure 3.2, *working memory*.

3.3.1 Working Memory

In cognitive psychology, working memory is referred to as the temporary memory of incoming stimuli in the process of executing cognitive operations [13]. Recalling the three aforementioned memories, working memory is not a new form of memory. Rather, it is a formation or selection of neural networks for the short term. Therefore, working memory is an *active memory* activated by the focus of attention in process of incoming stimuli analysis and prospective action selection. In other words, working memory plays the role of extracting contents from *long-term memory* and forming active neural networks with the purpose of guiding attentional control of the radar receiver and transmitter. Relating to the top-down attention, the working memory

can generally improve the quality of the information being processed via the resolution control, besides the functionality of information storage and manipulation.

With this discussion in mind, the working memory is defined as follows:

Definition 3.6 (Working Memory). *Working memory is composed of the attentional activation of neural resources of a large cognitive network of perceptual memory, executive memory, and coordinating perception-action memory.* □

Here, we remind ourselves that a cognitive radar should be able to perform multiple functions under a variety of environmental conditions. This requires that all three memory components, including perceptual memory, executive memory, and coordinating perception-action memory, should consist of a bank of neural networks, each of which is trained under a different environmental configuration oriented at a specific task.

3.3.2   Perceptual Attention

In the receiver, the above-described objective of protecting it from information-overload is realized by having the environmental scene analyzer *focus its attention* on a particular category of features that *best match* the underlying attributes of the incoming stimuli. This matching is achieved through *bottom-up filtering* of possible categories in the scene analyzer. The matching through filtering, in turn, leads to *top-down expectation* performed by the perceptual memory. The forward bottom-up feature matching and category recognition followed by the top-down feedback is continual on a cyclic basis, leading to focused attention and further scene analysis. In effect, what we are describing here is the circular manifestation of a localized

"perception-action cycle" within the receiver as depicted on the right-hand side of Figure 3.1.

Moreover, referring to Figure 3.1, we see a link from the receiver to the transmitter, labeled the *feedback-information metric*. Basically, this metric serves the purpose of a *cost-to-go function* conditional on the measurements at the receiver input, and which is to be minimized by the transmitter. To further protect the cognitive radar from the information-overload problem, this metric should be formulated with the following objective in mind:

> *Relevant information about the environment is preserved in the metric in the most effective way possible.*

This statement sums up the essence of the *principle of information preservation*. It is the design of this feedback link that reflects the intelligence level of a cognitive radar. We will further discuss this link in Section 3.4.

3.3.3   Executive Attention

The processing of actions in the transmitter requires the selective allocation of computational resources, just as it is with perceptual processing in the receiver. In other words, just as there is perceptual attention, we also have executive attention. Basically, what we are saying here is that there is indeed another "perception-action cycle" localized within the transmitter, as depicted on the left-hand side of Figure 3.1.

To validate this latter statement, let us begin with feedback information about the environment sent to the environmental scene actuator by the environmental scene

analyzer at some point in time, in accordance with Figure 3.1. This feedback information prompts the transmitter to act in the environment. That particular action is selected from a *prescribed library* of possible actions exemplified by linear-frequency modulated waveforms, for example, through the use of a *dynamic optimization algorithm* or *approximate dynamic programming*, the purpose of which is to minimize the feedback-information metric in some statistical sense. In any event, the action so taken moves forward in a bottom-up manner, which, in turn, leads to a top-down expectation performed by the executive memory. This latter move results from matching the action taken against the experiential knowledge on directed goals and possible consequences that reside in the executive memory. The continued circular bottom-up processing followed by top-down processing leads to the transmitter's own localized perception-action cycle.

There are two localized perception-action cycles to account for, which result from the reciprocal coupling built in between the executive memory and perceptual memory, as depicted at the top of Figure 3.1. The purpose of this last pair of cross-couplings, manifesting themselves through feedforward from the executive memory to the perceptual memory followed by feedback in the opposite direction, is to prompt these two memories to interact with each other so as to select the best action to control the environment.

To sum up, we say that a cognitive radar is endowed with

- *first*, attention in the executive domain, just like attention in the perceptual domain, is generated and guided through the selective allocation of computational resources available to the transmitter;

- *second*, cyclic interactions between the executive memory and perceptual memory lead to the coordination of sensory perception of the environment in the receiver with action taken on the environment in the transmitter in an orderly and timely manner; and

- *finally*, feedback control, in both local and global forms, is responsible for self-organized realization of attentional mechanisms in a distributed manner throughout the system; yet, this realization is achieved without having a separate structure or group of structures dedicated exclusively to attention as a separate function within the radar system.

3.4 Intelligence for Information Synchronization

Earlier in the chapter, we identified perception, memory, attention and intelligence as the four defining properties of cognitive radar. Among these four properties, intelligence stands out as the most complex property and the hardest to define. We say so because the other three properties, perception, memory and attention, in their own individual ways and varying degrees, make contributions to intelligence, hence the difficulty in defining it. In the Penguin Dictionary of Psychology, Reber makes the following point on the lack of consensus, concerning the definition of intelligence [67]:

> *"Few concepts in psychology have received more devoted attention and few have resisted clarification so thoroughly."*

Indeed, there is no universal agreement upon the definition and theory of intelligence [68]. It is easier to identify the existence of intelligence than to measure it. In

dictionary, intelligence is defined as *(1) the ability to learn new situation by proper behaviour adjustments; or (2) the ability to perceive the interrelationships of presented facts so as to guide action toward a desired goal* [69], which states the complexity of intelligence.

As a matter of fact, attempts of bringing artificial intelligence into radar systems have never stopped. One of the earliest work was due to Baldygo *et. al.* [70], where artificial intelligence was interpreted as the combined use of algorithms and heuristics. Different from the idea we have in this thesis, it will be more accurate to gather the early work on artificial intelligence under the umbrella of knowledge-based (KB) radar [71, 72].

Now we may go on to offer the following definition in the context of cognitive radar:

Definition 3.7 (Intelligence). *Intelligence is the ability of a cognitive radar to continually adjust itself through an adaptive process by responding to new changes in the environment and, thereby, create new forms of action and behaviour.* □

An important point to note in this statement is the following fact:

Cognition implies adaptation to a nonstationary environment.

To understand the essence of intelligence, we may look to the nested perception-action cycle of Figure 3.1, where we see that feedback control for interactions between the perceptual and executive parts of the system manifests itself both globally and locally. To this end, we may also go on to make the following statement [14]:

The abundant use of feedback distributed across the entire radar system is responsible for computational intelligence.

As it is with attention, this statement stresses the fact that there is no separate structure or group of structures dedicated to intelligence as a separate function within the radar system.

3.4.1   Efficiency of Processing Information

For intelligence to stand for the processing of cognitive information toward the achievement of behavioural goals, the degree of intelligence is indeed the efficiency with which that information is being processed [13]. The key question, however, is the following:

How do we measure the efficiency of processing information?

As noted earlier, the objective of a cognitive radar is to minimize the feedback-information metric sent to the environmental scene actuator by the environmental scene analyzer in some statistical sense. On this basis, we may therefore respond to the question as follows:

Through the use of dynamic optimization or approximate dynamic programming, the cognitive radar becomes increasingly more intelligent as the feedback information metric is progressively minimized, cycle after cycle.

In saying so however, we should not overlook the issue of overall computational complexity of the system, which, desirably, should be maintained at the minimum level possible.

3.4.2 Coordinated Cognitive Information Processing in a Self-Organized Manner

Looking at the nested perception-action cycle of Figure 3.1, we see that we have a sophisticated feedback control system with four visible local feedback loops positioned alongside two global feedback loops. As such, there is no external clock to coordinate the cognitive information processing performed by the radar system. Rather, the system coordinates itself in a self-organized and orderly manner in accordance with different facets of the cognitive functional integration across time property. The time needed for the completion of one cognitive information-processing cycle is determined by how long it takes for each one of all the feedback loops, local as well as global, to accomplish its own preassigned task.

3.4.3 Feedback-Information Metric

Keeping the above discussion in mind, we conclude that, for a cognitive radar equipped with memory and attention, intelligence is determined by the selection of *(i) system structure, (ii) filtering algorithm, (iii) performance measures used in the waveform design algorithm, and (iv) synchronization of all entries (i), (ii) and (iii).* Considering that we have already designed the system structure and cubature Kalman filter is the best known filtering algorithm for our application, we conclude that at this stage the selection of performance measure is probably the most important aspect in designing the cognitive radar system.

As we know, the general form of the waveform design can be expressed as the

following optimization problem:

$$\min_{\boldsymbol{\theta}_k \in \mathcal{P}_k} \quad \text{objective function} \tag{3.1}$$

$$\text{subject to} \quad \text{constraints} \tag{3.2}$$

where $\mathcal{P}_k$ is the waveform library at time k.

In formulating the objective function of cognitive radar system, the selection of feedback-information metric appears as another important research topic that deserves some efforts. Considering that the attention of this thesis has been focused on the fundamental theory and structural design (including the perception-action cycle, memory components, and attention), we only employ an objective function based on the mean-squared error (MSE) of the state [46].

3.5 Practical Benefits of Abundant Use of Distributed Feedback

A distinctive feature of the nested cognitive radar, compared to its most basic counterpart, is the abundant use of local as well as global feedback loops throughout the radar system. The two global feedback loops include the environment. On the other hand, the four visible local feedback loops in the system are reciprocal in nature but exclude the environment.

Most importantly, these feedback loops empower the nested cognitive radar with the following practical advantages over the basic cognitive radar:

1. The intelligence capability of the radar is significantly enhanced.
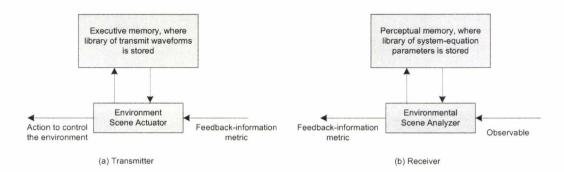
Figure 3.3: Illustrating: (a) Selection of transmitted LFM waveform for use in the transmitter; (b) Selection of system-equation parameters for use in the receiver.

2. The bottom-up and top-down linkages that reciprocally couple the receiver to the perceptual memory enable the receiver to select that particular set of system-equation parameters stored in the perceptual memory, which best matches the characterizing features of the current observables processed in the receiver; see Figure 3.3(b).

3. The bottom-up and top-down linkages that reciprocally couple the transmitter to the executive memory enable the transmitter to select that particular linear-frequency modulated (LFM) waveform stored in the executive memory, which optimally minimizes the feedback information metric passed onto this transmitter by the receiver; see Figure 3.3(a).

4. Last but by no means least, thanks to the use of local feedback loops positioned alongside global feedback loops makes it possible for the coordinated fulfillment of the cognitive information processing being performed by the radar system in a self-organized and orderly manner in accordance with the different facets of the cognitive functional integration across time property of the radar.

With system description of the nested cognitive radar just presented, we are now

ready to describe the algorithmic design of the system.

3.6 Algorithmic Design of the Nested Cognitive Radar

As an extension to basic cognitive radar described in Chapter 2, the nested cognitive radar also has both an environmental scene analyzer and an environment scene actuator, algorithmically implemented by cubature Kalman filter (or continuous-discrete cubature Kalman filter) and dynamic optimization, respectively. Considering that the scene analyzer and actuator have been described in Chapter 2, rest of this section will be devoted to the algorithm design of other components.

3.6.1 Design of the Memories

As claimed earlier in this chapter, memories are the most essential components in the nested cognitive radar. The function of memory is to map the sets of input data onto a set of appropriate outputs. A neural network is generally considered as a straightforward structure to construct the memories in cognitive radar. This chapter looks to a popular neural network structure known as the *multilayer perceptron* (MLP) [73]. Figures 3.4 shows the demonstrative structure of an MLP with two hidden layers, where all the neurons include a nonlinear activation function that is *differentiable*. To generalize our description in the rest of this section, we assume the MLP is *fully connected*, which means each neuron in any layer is connected to all the neurons in the previous layer.
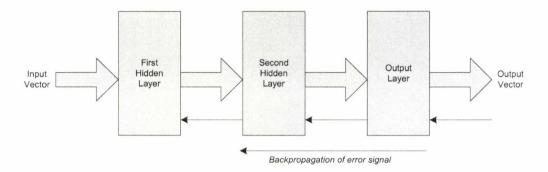
Figure 3.4: Demonstrative structure of an MLP with two hidden layers.

Design of the Perceptual and Executive Memories

In order to structurally design the perceptual and executive memories described earlier in Sections 3.2.1 and 3.2.3, we use the multilayer perceptron (MLP) network [73]. Referring to Figure 3.5(a), the design of perceptual memory proceeds as follows:

- A multilayer perceptron (MLP) network with one hidden layer is constructed. Its input vector is the observables obtained in the receiver from the radar environment and its output vector is the system-equation parameters.

- The observables obtained in the receiver are first preprocessed and then, fed to the first hidden layer of the MLP. The preprocessing includes two steps: (i) mean removal, and (ii) covariance equalization.

- Next, the features contained in the preprocessed observables are encoded layer-by-layer into the perceptual memory. This step completes the *bottom-up* phase.

- Relevant information stored in the perceptual memory on system-equation parameters is retrieved to provide the environmental scene analyzer with parameters that can best characterize the environment including the target. This finishes the *top-down* phase of the algorithmic design.

64
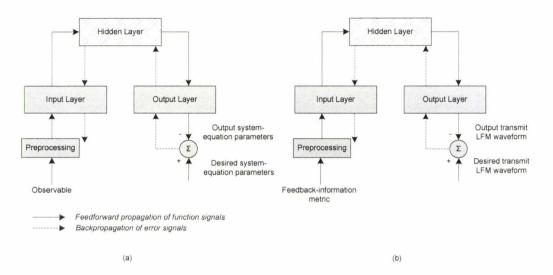
Figure 3.5: Design of the memories using MLPs. (a) Perceptual memory; (b) Executive memory.

Similarly, the executive memory depicted in Figure 3.5(b) is designed as follows:

- Another multilayer perceptron (MLP) with one hidden layer is constructed, with feedback-information metric obtained from the receiver as the input and the transmit linear-frequency modulated waveform as the output.

- Before the feedback-information metric is fed to the input layer, it is also pre-processed in the two-step way, i.e., the removal of mean and equalization of covariance.

- For the bottom-up phase, the preprocessed feedback-information metric obtained from the receiver is fed to the input of the hidden layer of the executive memory. Again, the features extracted from the feedback-information metric are encoded in the executive memory in a layer-by-layer manner.

- For the top-down phase, the LFM waveform stored in the executive memory is

retrieved to control the radar environment with an optimal action.

Design of the Coordinating Perception-Action Memory

As the name speaks for itself, the coordinating perception-action memory reciprocally couples the perceptual and executive memories. The structure of this memory should also reflect the reciprocal coupling. To coordinate the sensory perception in the receiver with the corresponding action in the transmitter, we design a third MLP network depicted in Figure 3.6 as follows:

- The third multilayer perceptron network with one hidden layer is constructed.

- The output of the *hidden layer of the perceptual memory* is connected to the input layer of the coordinating perception-action memory.

- The output of the *hidden layer of the executive memory* is used as a teacher for the off-line training of the coordinating perception-action memory.
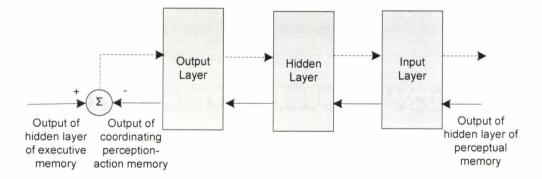
Figure 3.6: Design of the coordinating perception-action memory using MLP.

Back-Propagation Algorithm for Off-line Training

The structural designs of three memories shown in Figures 3.5 and 3.6 highlight two basic signal flows in the MLPs, i.e., the *function signals* denoted by solid arrows, and the *error signals* denoted by dashed arrows. The function signals represent the stimuli that come into the input layer and propagate forward through the network. The error signals are calculated at the output layer of the network and propagate backward through the network. By making use of these two kinds of signals, we can obtain a supervised training algorithm to train the MLPs. This training algorithm is called the *back-propagation algorithm* [74, 75].
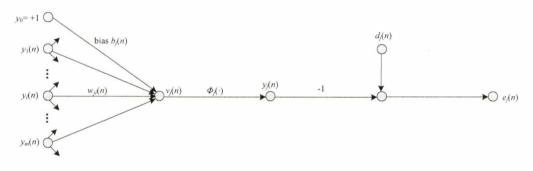
Figure 3.7: Signal-flow graph of output neuron j.

To derive the back-propagation algorithm, let us consider the signal-flow graph of output neuron j shown in Figure 3.7 (reproduced from [73]), where the error signal is calculated by

$$e_j(n) = d_j(n) - y_j(n) \tag{3.3}$$

with $d_j(n)$ and $y_j(n)$ as the desired value and output value, respectively. Note that $d_j(n)$ is obtained from the training data and $y_j(n)$ is the output of the activation

function of neuron j, given by

$$y_j(n) = \phi_j(\nu_j(n)). \tag{3.4}$$

Here $\phi_j(\cdot)$ is the activation function assumed to be nonlinear and $\nu_j(n)$ is the signal produced before input to the activation function, expressed as

$$\nu_j(n) = \sum_{i=0}^{m} w_{ji} y_i(n), \tag{3.5}$$

where $w_{ji}(n)$ is the synaptic weight from neuron i in previous layer to neuron j in current layer.

If we follow a manner similar to the least-mean square algorithm, we may make corrections to the synaptic weights based on the minimization of the *total instantaneous error energy* of the whole MLP network, expressed as

$$\mathcal{E}(n) = \frac{1}{2} \sum_j e_j^2(n). \tag{3.6}$$

Using the idea of gradient descent, the correction to the weight $w_{ji}(n)$, i.e., $\Delta w_{ji}(n)$, is proportional to the partial derivative of $\mathcal{E}(n)$ with respect to $w_{ji}(n)$, that is

$$\Delta w_{ji}(n) = -\eta \frac{\partial \mathcal{E}(n)}{\partial w_{ji}(n)}, \tag{3.7}$$

where η is the learning-rate parameter. Since the idea of gradient descent is to reduce the value of the energy, we include the minus sign in this regard.

To expand (3.7), we may apply the chain rule of calculus and yield

$$\frac{\partial \mathcal{E}(n)}{\partial w_{ji}(n)} = \frac{\partial \mathcal{E}(n)}{\partial e_j(n)} \frac{\partial e_j(n)}{\partial y_j(n)} \frac{\partial y_j(n)}{\partial \nu_j(n)} \frac{\partial \nu_j(n)}{\partial w_{ji}(n)}. \tag{3.8}$$

Substituting (3.6), (3.3), (3.5) into (3.8) yields

$$\frac{\partial \mathcal{E}(n)}{\partial w_{ji}(n)} = -e_j(n)\phi_j'(\nu_j(n))y_i(n). \tag{3.9}$$

From Eqs. (3.7) and (3.9), we calculate the weight correction as

$$\Delta w_{ji}(n) = \eta \underbrace{e_j(n)\phi_j'(\nu_j(n))}_{\text{local gradient}} y_i(n) \tag{3.10}$$

We now summarize the two phases of training the memories built on MLPs as follows:

1. The feedforward phase is shown by solid arrows in Figures 3.5 and 3.6. At this stage, the weights of the network are fixed and the input signals are propagated through the network, layer by layer, until they reach the output. Thus, in this phase, changes are confined to the activation potentials and outputs of neurons in the network.

2. The backward phase is shown by dashed arrows in Figures 3.5 and 3.6. In this phase, error signals are produced by comparing the outputs of the network with the desired responses, using Eq. (3.3) for all neurons. The resulting error signals are propagated through the network, again layer by layer. But this time, the propagation is performed in the backward direction. In this second phase,

successive adjustments are made to the weights of the network using Eq. (3.10).

Generalized Hebbian Algorithm for On-line Tuning

The back-propagation algorithm discussed in the section above is a perfect candidate for off-line supervised training, which is also a necessary step for building existing knowledge into the memories. However, for the nested cognitive radar, we also need an approach to absorb the new information obtained from the environmental scene analyzer into the perceptual and executive memories, when they are switched on-line. Unfortunately, neural networks trained using the back-propagation algorithm experience the following problems:

- First, we may only find local minima in the off-line training. Therefore, an optimal solution is not guaranteed.

- Second, the back-propagation algorithm is generally slow and prohibitive for on-line training of a neural network with a large number of neurons.

- Last and most importantly, the on-line training requires an *unsupervised* learning procedure in the nested cognitive radar system.

Hebb's learning is one famous theory of adjusting weights in a cost-effective manner. Hebbian theory was named in honour of Hebb, a famous neuropsychologist. In his 1949's book *The Organization of Behaviour: A Neuropsychological Theory* [76], he described a basic mechanism of adjusting the synaptic weights based on the presynaptic cell's *repeated* and *persistent* stimulation of the postsynaptic cell. This basic principle can be expressed as $w_{ji}(k) = x_i(k)x_j(k)$, where $w_{ji}(k)$ is the weight from neuron i to neuron j, $x_i(k)$ is the input for neuron i at discrete time k. However, it

can be shown that Hebb's rule is unstable for any neuron model. Therefore, some other learning algorithm is needed.

One of the most successful unsupervised learning algorithms is the generalized Hebbian algorithm proposed by Sanger [77]. For a feedforward neural network, the set of weights connecting m source nodes and l output nodes is denoted by $\{w_{ji}(k)\}$ with $i = 1, 2, ..., m$ and $j = 1, 2, ..., l$. The learning rule of GHA is a combination of Oja's rule and Gram-Schmidt process, given by

$$\Delta w_{ji}(k) = \eta \left(y_j(k)x_i(k) - y_j(k) \sum_{n=1}^{j} w_{ni}(k)y_n(k) \right), \tag{3.11}$$

where η is the learning rate parameter. Here the output $y_j(k)$ at time k is given as follows:

$$y_j(k) = \sum_{i=1}^{m} w_{ji}(k)x_i(k), \quad j = 1, 2, ..., l. \tag{3.12}$$

It is noteworthy that the most important parameter of the GHA is the learning parameter, which governs the learning speed of unsupervised learning. We have found that a reasonable value for the learning parameter is 10e-3.

Recalling the four bands theory discussed in Chapter 1, we may say that the off-line learning builds knowledge at the *rational band* and even *social band*. The on-line learning will operate at the *biological band* or *cognitive band*. These two facts mean that a successful on-line learning algorithm for memory building in the NCR should provide relatively *mild* tuning to the neural network. We have found that $\eta = 1e - 3$ is a reasonable learning parameter of GHA.

With the designing procedures of three memories in mind, we now summarize the parameters used for each memory, shown in Table 3.1, where PM, EM, and CM

denote the perceptual memory, executive memory, and coordinating perception-action memory, respectively.

Memory	Input Layer	Hidden Layer	GHA	Epochs
PM	20	10	1e-3	50
EM	20	10	1e-3	50
CM	10	4	1e-3	50

Table 3.1: Parameters used in the memory design

3.6.2 Design of Working Memory

To design the working memory, it is necessary to revisit the three memories designed in Section 3.6.1. Therein, each memory component is implemented by an individual MLP network, considering that tracking radar is our main concern throughout the thesis. In other words, attention has already been focused on the tracking task. It is therefore valid to conclude, a working memory is the aggregation of the activated neural networks selected by attention. As a matter of fact, the selective neural processing performed by attention exactly reflects the existence of a working memory.

However, to implement a cognitive radar system that is capable of multiple functions under a diversity of environmental conditions, the three memory components should be expanded in the following way:

- **Expanding the Perceptual Memory**: Referring to Figure 3.8, the perceptual memory is expanded using a bank of MLPs. The observables obtained in the receiver from the radar environment are connected to each MLP as an input vector. The output vector is the system-equation parameters.

72
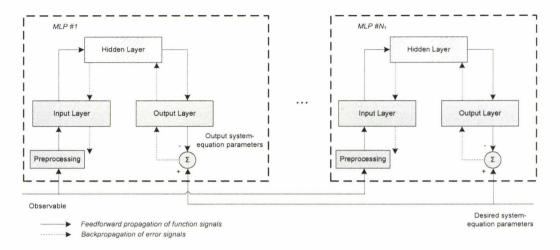
Figure 3.8: Design of expanded perceptual memory using bank of MLPs
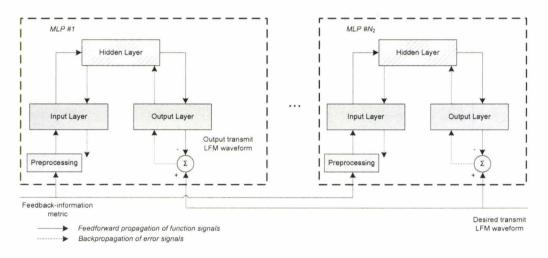
Figure 3.9: Design of expanded executive memory using bank of MLPs

- **Expanding the Executive Memory**: Similarly, the executive memory is expanded using another bank of MLPs, depicted in Figure 3.9, with feedback-information metric obtained from the receiver as the input and the transmit LFM waveform as the output.

73

- **Expanding the Coordinating Perception-Action Memory**: The third bank of MLPs is used to expand the coordinating perception-action memory, shown by Figure 3.10. Output of the hidden layer of each MLP in the expanded perceptual memory is connected to the input layer of each MLP in the expanded coordinating perception-action memory. Output of the hidden layer of each MLP in the executive memory is used as a teaching to train the MLP networks in the expanded coordinating perception-action memory.
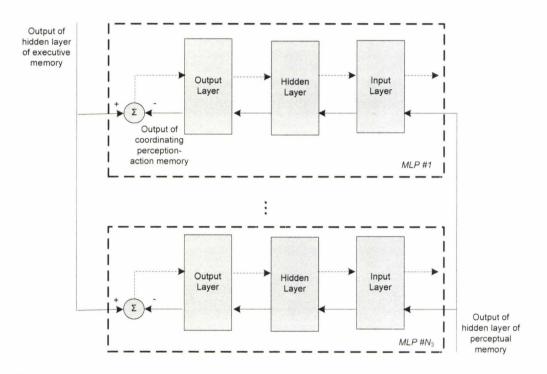
Figure 3.10: Design of expanded coordinating perception-action memory using bank of MLPs

As for the bottom-up attention, some emergent behaviours may have happened in the environment, i.e., the appearance of a new target or sudden change of target dynamics, can prompt competition in the working memory and/or possibly influence

the composition of working memory. The issue of designing the bottom-up attention is now transposed into the on-line tuning of the selected MLP or switching to another MLP that can represent the environment more accurately. The on-line tuning can be accomplished using the generalized Hebbian algorithm described earlier in this Chapter.

3.6.3   Design of the Feedback-Information Metric

Take the continuous-discrete model described in Chapter 2 as an example and assume the CD-CKF is selected as the target tracking algorithm, if we are at time k, we may predict the measurement update at time $k+1$ before the real measurement is obtained, written as:

$$
\begin{aligned}
\hat{\mathbf{z}}_{k+1|k} &= \frac{1}{2n} \sum_{i=1}^{2n} Z_{i,k+1|k} \\
\mathbf{P}_{\mathbf{zz},k+1|k} &= \frac{1}{2n} \sum_{i=1}^{2n} Z_{i,k+1|k} Z_{i,k+1|k}^T - \hat{\mathbf{z}}_{k+1|k} \hat{\mathbf{z}}_{k+1|k}^T + \mathbf{R}_{k+1}(\boldsymbol{\theta}_k).
\end{aligned}
$$

where $Z_{i,k+1|k}$ is the i-th propagated cubature point originated from $X_{i,k+1|k}$. The cubature point $X_{i,k+1|k}$ is calculated using the m-step time update of the predicted state $\hat{\mathbf{x}}_{k+1|k}$.

An advantage of both CKF and CD-CKF is that we can update the state-error covariance without knowledge of the real measurement. Indeed, by evolving $\mathbf{P}_{k|k}$ one cycle ahead, we have the state-error covariance

$$
\mathbf{P}_{k+1|k+1} = \mathbf{P}_{k+1|k} - \mathbf{G}_{k+1} \mathbf{P}_{\mathbf{zz},k+1|k} \mathbf{G}_{k+1}^T,
$$

where the *Kalman gain* is

$$\mathbf{G}_{k+1} = \mathbf{P}_{\mathbf{xz},k+1|k}\mathbf{P}^{-1}_{\mathbf{zz},k+1|k}.$$

Utilizing the Cramér-Rao lower bound we obtained in Chapter 2, it is not difficult to prove that the waveform selection algorithm boils down to an optimization problem of finding the minimum of the objective $\mathrm{Tr}(\mathbf{P}_{k+1|k+1})$. Since $\mathbf{P}_{k+1|k+1}$ is a symmetric non-negative matrix, we express $\mathrm{Tr}(\mathbf{P}_{k+1|k+1})$ as

$$\mathrm{Tr}(\mathbf{P}_{k+1|k+1}) = \sum_i \lambda_i \tag{3.13}$$

where λ_i is the i-th eigenvalue of $\mathbf{P}_{k+1|k+1}$. Therefore, we have the following optimization problem

$$\min_{\boldsymbol{\theta}_k \in \mathcal{P}_k} \mathrm{Tr}\{\mathbf{P}_{k+1|k+1}\}. \tag{3.14}$$

To emphasize the claims made earlier on, this measure assumes that the cross-covariances of the states are negligible, i.e., the cross-covariance matrix is sparse with large values located at the diagonal entries.

3.7 Communications Among Subsystems of Cognitive Radar with Nested Memory

In an effort to understand how the components in a nested cognitive radar communicate among each other, we only need to describe one cycle of the nested cognitive radar. The communication starts from the observable obtained from the environment:

Step (1) : Observable received by the receiver is sent to the perceptual memory to retrieve system model of the target.

Step (2) : The retrieved system model is fedback to environmental scene analyzer to provide necessary information to the filtering algorithm. Meanwhile, the information stored in the hidden layer of perceptual memory, namely *Information A*, is collected for future use in **Step (6)**.

Step (3) : The feedback information calculated by the filtering algorithm in the receiver is transferred to radar transmitter.

Step (4) : In response to the receiver, the feedback information is sent to the executive memory to retrieve waveform library that suits the environment. Meanwhile, the information stored in the hidden layer of executive memory, namely *Information B*, is collected for future use in **Step (6)**.

Step (5) : The environmental scene actuator selects the best waveform from the retrieved waveform library using the dynamic optimization algorithm.

Step (6) : To start the coordinating phase, *Information A* collected in **Step (2)** is fed to the coordinating perception-action memory with the output as the integration of perception memory.

Step (7) : Finally, *Information B* collected in **Step (4)** is fed to the coordinating perception-action memory in an response to the selected action.

To illustrate the communication mechanism embodied in **Step (1)** through **Step (7)**, the reader is referred to Figure 3.11.
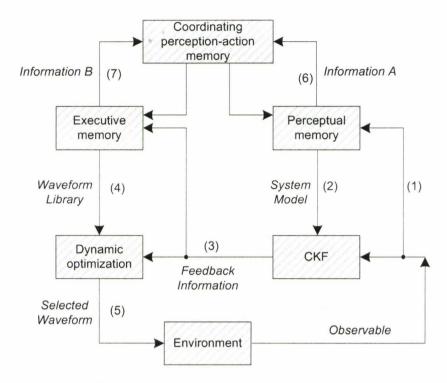
Figure 3.11: Cyclic communication flow-graph of the nested cognitive radar

To elaborate on the communications within the subsystems, we make the following comments:

- *Communications between scene analyzer and perceptual memory:* Irrespective of the application of interest, a cognitive radar's perception of the environment is continually influenced by the current data received by the system as well as cognitive information already stored in memory. In other words, every percept (i.e., snapshot of the perception process at some point in time) is made up of two components:

  1. The first component pertains to recognition and therefore retrieval of relevant information about the environment, which is stored in perceptual

memory for the purpose of representing past data.

2. The other component refers to categorization (classification) of a new set of data, which is correlated with the perceptual memory.

Processing of the first component is carried out in the perceptual memory, and that of the second component is carried out in the environmental scene analyzer. Most importantly, in both cases, the processing is executed in a self-organized manner.

- *Communications among scene analyzer, scene actuator, and executive memory:* Likewise, a cognitive radar's action onto the environment is continually influenced by the feedback information passed to the transmitter by the receiver as well as the waveform library already stored in memory. In other words, every execution (i.e., snapshot of the executive process at some point in time) is made up of two components:

  1. The first component pertains to recognition of feedback information and therefore retrieval of relevant waveform library about the environment, which is stored in executive memory for the purpose of representing past feedback information.

  2. The other component refers to categorization (classification) of a new set of data, which is correlated with the memory.

Processing of the first component is carried out in the executive memory, and that of the second component is carried out in the environmental scene actuator. Most importantly, in both cases, the processing is executed in a self-organized manner.

79

- *communications among perceptual memory, executive memory, and coordinating perception-action memory:* A cognitive radar's perceptual memory and executive memory are continually organized by the coordinating perception-action memory. In others words, the functional integration across time (i.e., coordination between perception at one point in time and action at next point in time) is made up two components:

  1. The first component pertains to integration of perception of the environment and therefore coordination of the executive memory.

  2. The other component refers to the tuning of the coordinating perception-action memory via the executive memory backward in response to the selected action for next transmission.

Processing of the first component is carried out from the perceptual memory to the coordinating perception-action memory, and that of the second component is carried out from the executive memory to the coordinating perception-action memory.

3.8   Summary

This chapter has expanded on what we already know about the basic cognitive radar discussed in Chapter 2 to encompass three more properties of human cognition: 1) memory, 2) attention, 3) enhanced intelligence in addition to the perception-action cycle. Specifically, the provision for memory includes the following essential elements:

1. *Perceptual memory*, whose contents continually change with time in accordance with changes in the environment; the knowledge so gained becomes an inextricable part of the perceptual memory.

2. *Executive memory*, the contents of which change with time in accordance with how the receiver perceives the environment; the knowledge so gained also becomes an inextricable part of the executive memory.

3. *Coordinating perception-action memory*, which involves reciprocal coupling of the perceptual memory and executive memory, with the result that the action taken on the environment by the transmitter and perception of the environment by the receiver are fully coordinated across time.

Unlike perception, action and memory, there are no specific locations for attention and intelligence. Rather, both of these two properties are distributed across the whole radar system. The net result of this distribution is two-fold:

1. *Attention*, which provides for the selective allocation of resources to the receiver and transmitter.

2. *Intelligence*, which is enhanced significantly by virtue of the fact that we now have two global feedback loops embodying the environment and four visible local feedback loops within the three memories.

The new radar structure is named *nested cognitive radar*. Simply put, in an attempt to equip radar with full cognition inspired by the visual brain and as realistic as possible, this chapter lays down the groundwork for a new generation of radar systems.

Chapter 4

Simulation Evaluations

No physician is really good before he has killed one or two patients.

A Hindu proverb

In the previous two chapters, we proposed a new generation of radar systems equipped with cognition. In this chapter, we consider three well-studied scenarios: *(a), linear target tracking; (b), falling object tracking in space; and (c), high-dimensional target tracking of continuous-discrete model.* The philosophy of employing these three scenarios relies on the characteristics of each simulation, summarized as follows:

- To demonstrate the power of cognition in its basic form, there is possibly no simpler problem than a linear target tracking. The Kalman filter (KF) is the most straightforward state estimator in such an environmental configuration. Feature of the first simulation study is *linearity*.

- Obviously, linearity represents only an extremely small portion of the tracking problem we may encounter. Nonlinear target tracking occupies a very important

position in the tracking literature because it is more practical for real applications. Also, thanks to the recent development of cubature Kalman filter (CKF) described in Appendix A, we select another extensively studied problem in the tracking community, namely the reentry problem. The distinguishing feature of the second simulation study is *nonlinearity*.

- Although nonlinearity can bring more practicality into our simulations, we expect to further challenge our cognitive radar system. To do so, the third scenario considers a high-dimensional target tracking with continuous-discrete model. Building on the the continuous-discrete cubature Kalman filter (CD-CKF) described in Appendix B, the third scenario can be regarded as the most complicated tracking problem to the best of our knowledge. This problem features *high-dimensionality* and *continuous-discrete model* of cognitive radar system.

In deciding upon the scenarios used in this chapter, we find that there is a common feature shared by them: All simulations study the tracking problem. Without loss of practical considerations, tracking is obviously one important function that a cognitive radar system performs. As such, it is equivalent to claim that *attention* has already been focused on a specific task, which also means it will be redundant to design a working memory that can switch between multiple neural networks.

In the discussion of feedback-information metric in Chapter 3, the mean-squared error (MSE) of the state was formulated as trace of the error covariance. Although it is possible to design the feedback-information metric using other methods, our simulation studies will be focused on the MSE-metric in an effort to maintain conciseness of the thesis.

4.1   Experimental Considerations

In Chapter 2, the analysis and synthesis of waveform library have been discussed. To expand on that, we use the *up-sweep* and *down-sweep* linear frequency modulated (LFM) chirp of Gaussian amplitude modulation to conduct simulations in this chapter. The parameters we can use to characterize this radar waveform are chirp rate $b \in [b_{min}, b_{max}]$ and pulse duration of the envelope $\lambda \in [\lambda_{min}, \lambda_{max}]$. Therefore, we have a two-dimensional waveform parameter vector $\boldsymbol{\theta} = [\lambda, b]$, based on which the grid can be expressed as:

$$\mathcal{P} = \{\lambda \in [\lambda_{min} : \Delta\lambda : \lambda_{max}], b \in [-b_{max} : \Delta b : -b_{min}] \cup [b_{min} : \Delta b : b_{max}]\},$$

where $\Delta\lambda$ and Δb denote the step-size of chirp rate and envelope duration, respectively.

All the computer experiments are conducted for three kinds of radar systems, the conventional radar system with fixed-waveform (FWF), the basic cognitive radar (BCR) developed in Chapter 2, and the nested cognitive radar (NCR) developed in Chapter 3. The testbed was developed using Matlab [78]. Throughout the chapter, we will use the ensemble-averaged root mean-squared error (EA-RMSE) as the metric to evaluate BCR and NCR, compared to FWF. The EA-RMSE is defined as

$$\text{EA-RMSE}_p(k) = \sqrt{\frac{1}{N}\sum_{n=1}^{N}\left((p_{1,k}^n - \hat{p}_{1,k}^n)^2 + (p_{2,k}^n - \hat{p}_{2,k}^n)^2 + (p_{3,k}^n - \hat{p}_{3,k}^n)^2\right)},$$

where $[p_{1,k}^n, p_{2,k}^n, p_{3,k}^n]$ and $[\hat{p}_{1,k}^n, \hat{p}_{2,k}^n, \hat{p}_{3,k}^n]$ are the coordinates of the true and estimated positions at time index k in the n-th Monte Carlo run. The simulation is run for N

Monte Carlo runs in total. In a similar manner, we may also define the EA-RMSE for the velocity as follows:

$$\text{EA-RMSE}_v(k) \;=\; \sqrt{\frac{1}{N}\sum_{n=1}^{N}\left((v_{1,k}^n - \hat{v}_{1,k}^n)^2 + (v_{2,k}^n - \hat{v}_{2,k}^n)^2 + (v_{3,k}^n - \hat{v}_{3,k}^n)^2\right)},$$

where $[v_{1,k}^n, v_{2,k}^n, v_{3,k}^n]$ and $[\hat{v}_{1,k}^n, \hat{v}_{2,k}^n, \hat{v}_{3,k}^n]$ are the true and estimated velocity components at time index k.

All the simulations are run on an Intel dual-core computer with 2.4 GHz processor. Every simulation is conducted for 50 Monte-Carlo runs. The physical memory of the computer is 3.0 GB.

4.2 Scenario A: Linear Target Tracking

In this first scenario, the linear target tracking problem is considered. An aircraft is assumed to move linearly in space. Unpredictable perturbations in the trajectory are modeled as additive white Gaussian noise processes. The purpose of using this model is to demonstrate the power of cognitive radar in a simple way.

4.2.1 State-Space Model

Let us define $\mathbf{x} = [\rho,\ \dot{\rho}]^T$ as the state of the target, where ρ and $\dot{\rho}$ denote the range and range-rate, respectively. We have the system equation as follows:

$$\mathbf{x}_k = \mathbf{F}_k \mathbf{x}_{k-1} + \mathbf{v}_k, \tag{4.1}$$

where $\mathbf{F}_k$ is the state transition matrix and $\mathbf{v}_k$ is assumed to be white Gaussian system noise with covariance $\mathbb{E}\{\mathbf{v}_k\mathbf{v}_k^T\} = \mathbf{Q}_k$.

The radar observations are delay and Doppler frequency, i.e. τ and f_D, respectively. The Doppler frequency f_D represents a *shift* in the carrier frequency f_c; this value is positive when the target is moving toward the radar, and negative when the target is moving away from the radar. The delay and Doppler frequency can be converted to range and range-rate using $\rho = \tau \times c/2$ and $\dot{\rho} = f_D \times c/(2f_c)$, where c is the speed of wave propagation and f_c is the carrier frequency. The measurement equation is given by:

$$\mathbf{z}_k = \mathbf{H}_k\mathbf{x}_k + \mathbf{w}_k(\boldsymbol{\theta}_{k-1}), \tag{4.2}$$

where $\mathbf{H}_k$ is the observation matrix that maps the true state space into the measurement space, $\mathbf{w}_k(\boldsymbol{\theta}_{k-1})$ is the measurement noise with zero-mean and covariance $\mathbb{E}\{\mathbf{w}_k(\boldsymbol{\theta}_{k-1})\mathbf{w}_k(\boldsymbol{\theta}_{k-1})^T\} = \mathbf{R}_k(\boldsymbol{\theta}_{k-1})$, which shows dependency of the measurement noise on radar waveform $\boldsymbol{\theta}_{k-1}$.

4.2.2 Experimental Configurations

Suppose an L-band radar of 2 GHz is employed. The radar is mounted at a height of 100 meters. Because the transmitter and the receiver are co-located, the received signal energy depends inversely on the fourth power of the target range ρ. For this reason, the returned pulse SNR, η_ρ, in Eq. (2.18) for the target observed at range ρ was modeled according to

$$\eta_\rho = \left(\frac{\breve{\rho}}{\rho}\right)^4,$$

where $\check{\rho}$ denotes the range at which 0 dB SNR was obtained. In our experiment, the 0 dB SNR ratio is defined at 20 km. The radar transmitter is assumed to be equipped with a library of *up-sweep* and *down-sweep* linear frequency modulated (LFM) waveforms of Gaussian amplitude modulation, defined on a discrete two-dimensional grid over parameter space

$$\mathcal{P} = \{\lambda \in [10e\text{-}6, 100e\text{-}6], b \in [-100e9, -10e9] \cup [10e9, 100e9]\} \tag{4.3}$$

with grid step-sizes $\Delta\lambda = 10e\text{-}6$ and $\Delta b = 10e9$. A target moves away from the radar from range $\rho_0 = 3$ km at a speed of $\dot{\rho}_0 = 200$ m/s.

The state transition matrix and measurement matrix are respectively defined as

$$\mathbf{F} = \begin{bmatrix} 1 & T \\ 0 & 1 \end{bmatrix} \tag{4.4}$$

and

$$\mathbf{H} = \begin{bmatrix} 1 & 0 \\ 0 & 1 \end{bmatrix}, \tag{4.5}$$

where T is the sampling duration, taken as 2.5 ms.

The system noise covariance is modeled as

$$\mathbf{Q} = \sigma_{\mathbf{v}}^2 \begin{bmatrix} T^4/4 & T^3/2 \\ T^3/2 & T^2 \end{bmatrix}, \tag{4.6}$$

where $\sigma_{\mathbf{v}}^2$ is the variance of piecewise constant white system noise [79].

Since we now have a linear filtering problem, the Kalman filter is employed in the receiver for state estimation of the target and grid-searching is used in the transmitter for action to control the environment. The filter is initialized with a state of large covariance: $[100, 1]^T$. Monte Carlo simulations are conducted to evaluate the performance of the nested cognitive radar versus the conventional radar with fixed waveform. To evaluate the validity of using memory, we also compare the performance of two members of the cognitive radar family, basic cognitive radar (BCR) and nested cognitive radar (NCR) equipped with perceptual memory, executive memory and coordinating perception-action memory.

4.2.3 Simulation Results

The root mean-squared error (RMSE) simulation results are shown in Figures. 4.1 and 4.2, where the conventional radar equipped with fixed-waveform (FWF), basic cognitive radar (BCR), and the nested cognitive radar (NCR) are depicted in dotted, dashed, and solid lines, respectively. Table 4.1 lists the ensemble-averaged RMSE (EA-RMSE) for FWF, BCR and NCR.

EA-RMSE	Range (meters)	Range-rate (meters/second)
FWF	0.3422	0.5231
BCR	0.1256	0.2723
NCR	0.0477	0.0415

Table 4.1: Ensemble-averaged RMSE for FWF, BCR and NCR: Scenario A

Examining the simulation results of Figures. 4.1 and 4.2, we see that an outstanding enhancement of the radar resolution for target tracking can be obtained using this new radar structure, compared with the basic cognitive radar that is confined to the

perception-action cycle, and even more so when memory is built into the cognitive radar system.

Next, to study how the cognition process evolves across time for both BCR and NCR, we have plotted the waveform selection for both the chirp rate and the duration of pulse envelope in Figure 4.3. We observe that the transition of the chirp rate is switched from maximum up-sweep to maximum down-sweep for the BCR, while the chirp rate quickly dwelled at the maximum up-sweep for the NCR. This explains the better performance of NCR over BCR. Both of the basic and nested cognitive radars will select the maximum duration of the pulse envelope starting from the beginning of the cognition process.

In investigating the reason for the enhancement of performance using cognitive radar, we notice an interesting phenomenon: the observables obtained by the receivers of cognitive radars have magnitudes higher than the conventional radar. We name this phenomenon the chattering effect. The chattering effects of range and range-rate are depicted in Figures 4.4 and 4.5, where Figures 4.4(a) and 4.5(a), Figures 4.4(b) and 4.5(b), and Figures 4.4(c) and 4.5(c) correspond to FWF, BCR and NCR, respectively. The superb performance of our cognitive radar has proved that chattering effect plays a positive role in increasing the resolution of a radar system. This effect will be studied in greater detail in Chapter 5.
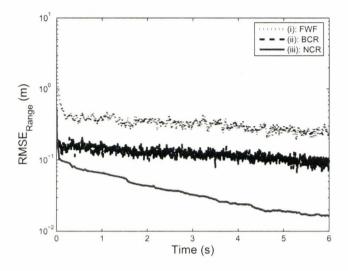
Figure 4.1: RMSE of target range (Scenario A). (i) conventional radar equipped with fixed waveform (dotted line), (ii) basic cognitive radar (dashed line), and (iii) nested cognitive radar (solid line).
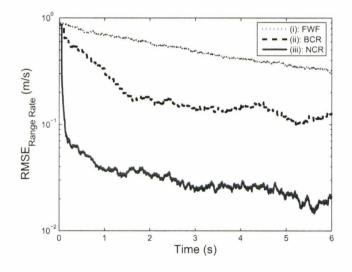
Figure 4.2: RMSE of target range-rate (Scenario A). (i) conventional radar equipped with fixed waveform (dotted line), (ii) basic cognitive radar (dashed line), and (iii) nested cognitive radar (solid line).
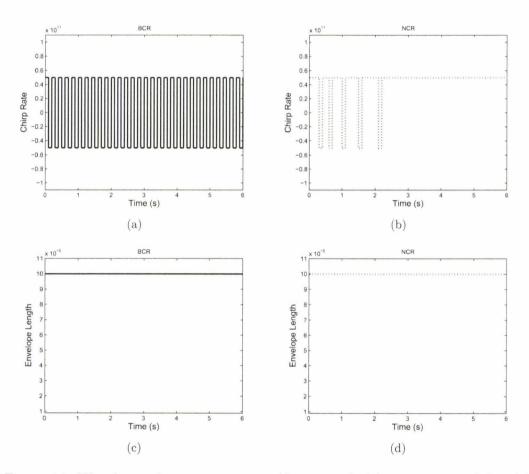
Figure 4.3: Waveform selection across time (Scenario A). (a) chirp rate for BCR, (b) chirp rate for NCR, (c) length of pulse envelope for BCR, (d) length of pulse envelope for NCR.
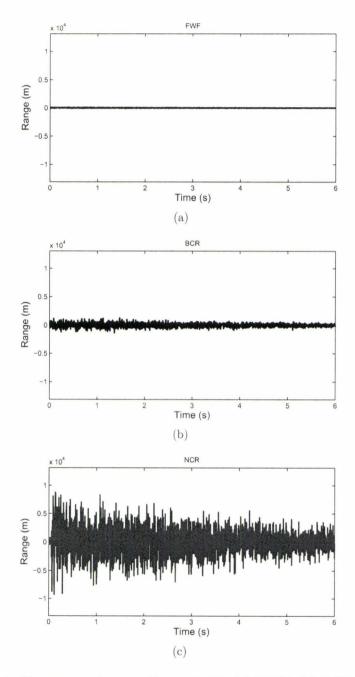
Figure 4.4: Chattering of range (Scenario A). (a) FWF, (b) BCR, (c) NCR.
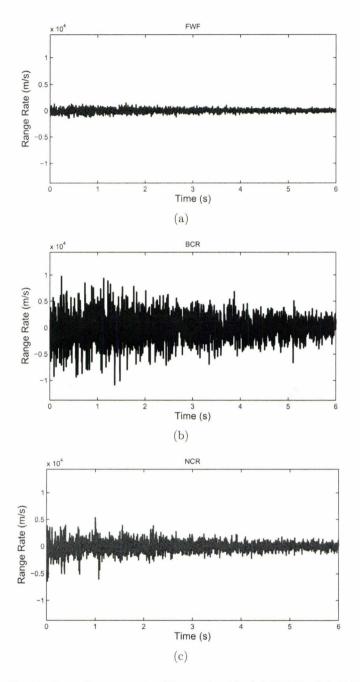
Figure 4.5: Chattering of range-rate (Scenario A). (a) FWF, (b) BCR, (c) NCR.

4.3   Scenario B: Tracking a Falling Object in Space

In this second scenario, we consider an extensively studied problem in the tracking community, that is, the reentry problem [80]. A ballistic target reenters the Earth's atmosphere after having travelled a long distance, its speed is high and the remaining time to ground impact is relatively short. The purpose of this scenario is to illustrate two features of our cognitive radars: (i) the enhancement of radar performance for *mildly* nonlinear target tracking, and (ii) the increased speed of reaction with the existence of cognition.

4.3.1   Problem Formulation

Geometry of the falling object is depicted in Figure 4.6. In the reentry phase, two types of forces are in effect: The most dominant is drag, which is a function of speed and has a substantial nonlinear variation in altitude; the second force is due to gravity, which accelerates the target toward the center of the earth. This tracking problem is highly difficult because the target's dynamics change rapidly. Under the influence of drag and gravity acting on the target, the following differential equation governs its motion [80]:

$$
\begin{aligned}
\dot{x}_1 &= -x_2 \\
\dot{x}_2 &= \underbrace{\frac{-\xi(x_1).g.x_2^2}{2x_3}}_{\text{drag}} + g \\
\dot{x}_3 &= 0,
\end{aligned}
\tag{4.7}
$$
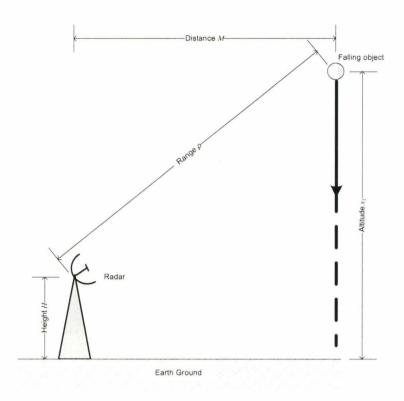
Figure 4.6: Geometry of the falling object scenario.

where x_1, x_2 and x_3 are the altitude, velocity, and ballistic coefficient that depends on the target's mass, shape, cross-sectional area, and air density, respectively. The term $\xi(x_1)$ is the air density and is modeled as an exponentially decaying function of x_1, given by

$$\xi(x_1) \;\; = \;\; \xi_0 \exp(-\gamma x_1),$$

with the proportionality constant $\xi_0 = 1.754$, $\gamma = 1.49e\text{-}4$, and the gravity $g = 9.8$ ms^{-2}.

To convert Eq. (4.7) to the state space, we define the state $\mathbf{x} = [x_1 \; x_2 \; x_3]^T$. The

system equation at continuous time t can now be expressed by

$$\dot{\mathbf{x}}_t = \mathbf{g}(\mathbf{x}_t),$$

Using the Euler approximation with a small integration step δ, we write

$$\mathbf{x}_k = \mathbf{x}_{k-1} + \delta\mathbf{g}(\mathbf{x}_{k-1})$$
$$= \mathbf{f}(\mathbf{x}_{k-1}). \tag{4.8}$$

In order to account for imperfections in the system model (*e.g.*, lift force, small variations in the ballistic coefficient, and spinning motion), we add zero-mean Gaussian system noise, thus obtaining the new system equation as it is in Eq. (2.4):

$$\mathbf{x}_k = \mathbf{f}(\mathbf{x}_{k-1}) + \mathbf{v}_k, \tag{4.9}$$

where we have

$$\mathbf{f}(\mathbf{x}_{k-1}) = \Phi\mathbf{x}_{k-1} - \mathbf{G}[D(\mathbf{x}_{k-1}) - \mathbf{g}] \tag{4.10}$$

with matrices

$$\Phi = \begin{bmatrix} 1 & -\delta & 0 \\ 0 & 1 & 0 \\ 0 & 0 & 1 \end{bmatrix}$$
$$\mathbf{G} = [0\ \delta\ 0]^T$$

and drag

$$D(\mathbf{x}_k) \;=\; \frac{\xi(x_{1,k})\mathbf{g}x_{2,k}^2}{2x_{3,k}}.$$

We assume that the system noise $\mathbf{v}_k$ is zero-mean Gaussian with covariance matrix

$$\mathbf{Q} \;=\; \begin{bmatrix} q_1\frac{\delta^3}{3} & q_1\frac{\delta^2}{2} & 0 \\[2mm] q_1\frac{\delta^2}{2} & q_1\delta & 0 \\[2mm] 0 & 0 & q_2\delta \end{bmatrix}.$$

The parameters q_1 and q_2 control the amount of system noise in target dynamics and ballistic coefficient, respectively. For our simulation, we consider that $q_1 = 0.01$, $q_2 = 0.01$ and $\delta = 0.1$ second.

4.3.2 Radar Configurations

We use LFM of Gaussian amplitude modulation with both up-sweep and down-sweep chirps, which composes the waveform library defined by

$$\mathcal{P} = \{\lambda \in [10e\text{-}6, 300e\text{-}6], b \in [-300e9, -10e9] \cup [10e9, 300e9]\} \tag{4.11}$$

with grid step-size $\Delta\lambda = 10e\text{-}6$ and $\Delta b = 10e9$. The bandwidth is set to be 5 MHz. The 0 dB SNR was set to 80 km. An X-band radar fixed at $(0,0)$ operates at a fixed carrier frequency of 10.4 GHz for a speed of electromagnetic-wave propagation $c = 3e8$ m/s in space.The fixed-waveform radar is equipped with down-sweep chirp rate and a pulse duration of $\lambda = 20$ μs. The sampling rate is set to $T_s = 100$ ms. The

97

radar is located at height $H = 30$ m with horizontal distance to the track $M = 30$ km. The measurements at discrete time k include the range ρ and the range-rate $\dot{\rho}$, given by

$$
\begin{aligned}
\rho_k &= \sqrt{M^2 + (x_{1,k} - H)^2} + w_{1,k} \\
\dot{\rho}_k &= \frac{x_{2,k}(x_{1,k} - H)}{\sqrt{M^2 + (x_{1,k} - H)^2}} + w_{2,k}
\end{aligned}
$$

where the measurement noise is $\mathbf{w}_k \sim \mathcal{N}(\mathbf{0}, \mathbf{R}_k)$.

Now that we have a discrete-time nonlinear filtering problem, the CKF is employed in the receiver for state estimation of the target. A detailed description of the CKF can be found in Appendix A. The true initial state of the target is defined as

$$
\mathbf{x}_0 = \begin{bmatrix} 61 \text{ km}, & 3048 \text{ m/s}, & 19161 \end{bmatrix}^T .
$$

The initial state estimate and its covariance are assumed to be

$$
\begin{aligned}
\hat{\mathbf{x}}_{0|0} &= \begin{bmatrix} 61.5 \text{ km}, & 3000 \text{ m/s}, & 19100 \end{bmatrix}^T \\
\mathbf{P}_{0|0} &= \operatorname{diag}\left(\begin{bmatrix} 1e6, & 1e4, & 1e4 \end{bmatrix} \right),
\end{aligned}
$$

respectively.

4.3.3   Simulation Results

Here, we show the simulation results for a radar with fixed waveform (FWF) and two cognitive radars, the basic cognitive radar (BCR) and nested cognitive radar

(NCR). Most of these results were first reported in [81]. Considering the curse-of-dimensionality problem that may arise from dynamic programming with a large horizon-length, we study two cases of dynamic programming:

- $L = 1$: a special case of dynamic programming, namely dynamic optimization, and

- $L = 2$: an example of dynamic programming, described in Appendix C.

To validate the performance of cognitive radars for the special case, i.e. $L = 1$, Figures 4.7, 4.8, and 4.9 respectively plot the root mean-squared error (RMSE) for the following three elements of the target's state: altitude, velocity, and ballistic coefficient, all three of which occupy the same time scale. Table 4.2 lists the ensemble-averaged RMSE (EA-RMSE) for FWF, BCR and NCR.

EA-RMSE	Altitude (meters)	Velocity (meters/second)	Ballistic coefficient
FWF	24.9421	16.4797	60.9974
BCR	2.4672	1.3322	60.9955
NCR	0.8799	0.6448	61.0330

Table 4.2: Ensemble-averaged RMSE for FWF, BCR and NCR: Scenario B

Similar to the first scenario, we have also plotted the waveform selection for both the chirp rate and duration of the pulse envelope in order to illustrate how the cognition process evolves across time in the cognitive radar, as shown by Figure 4.10. The transitions of waveform parameters across time appear to explain how the cognition performs in the cognitive radar, where the chirp rate of BCR switches more frequently than that of the NCR. The enhanced performance of the nested cognitive radar over its basic counterpart is possibly due to this behaviour.

Interestingly enough, the chattering effects are also observed in this scenario, which are plotted in Figure 4.11 for range and Figure 4.12 for range-rate. Figures 4.11(a) and 4.12(a), Figures 4.11(b) and 4.12(b), and Figures 4.11(c) and 4.12(c) correspond to FWF, BCR, and NCR, respectively. Specifically in Figure 4.12(c), a periodical chattering effect is observed at the initial stage. This is an interesting phenomenon that deserves some studies as a future research topic.

Examination of the RMSE results plotted in Figures 4.7 through 4.9, as well as the EA-RMSE results listed in Table 4.2, leads us to make the following important observations:

1. Figures 4.7 and 4.8 reveal that the basic cognitive radar outperforms the convectional radar with fixed transmit-waveform by an order of magnitude, and the nested cognitive radar even enhances the performance of its basic counterpart significantly.

2. In direct contrast to Figures 4.7 and 4.8, the RMSE plots presented in Figure 4.9 appear to reveal that insofar as the ballistic coefficient is concerned, the use of basic cognition with dynamic optimization does not improve estimation accuracy of the ballistic coefficient over the course of time. A higher fluctuation of the ballistic coefficient is even observed for the nested cognitive radar. The only explanation that we can offer here for the difference between Figures 4.7 and 4.8 on the one hand and Figure 4.9 on the other, is that the measurements are only limited to the range and range-rate. There, the estimated state of the ballistic coefficient is not directly affected by the measurements at hand.

For a good understanding of the dynamic programming algorithm with respect to different length of horizon, we also supply simulation results for $L = 2$, in comparison

to $L = 1$. The purpose of this simulation is to study if the performance of cognitive radar can be improved by increasing the length of horizon in dynamic programming. To make our demonstration illustrative, we use the same experimental configurations as before and select only the basic cognitive radar for comparison. Figures 4.13, 4.14, and 4.15 respectively plot the RMSE for the altitude, velocity and ballistic coefficient of the target. To see how the cognition has behaved in a cognitive radar, the waveform transition for both the chirp radar and length of pulse envelope is presented in Figure 4.16. The EA-RMSE for FWF and BCR ($L = 1, 2$) is summarized in Table 4.3.

EA-RMSE	Altitude (meters)	Velocity (meters/second)	Ballistic coefficient
FWF	24.7592	22.3393	60.9892
BCR($L = 1$)	6.1916	1.8249	60.9713
BCR($L = 2$)	2.5512	1.4505	60.9672

Table 4.3: Ensemble-averaged RMSE for FWF and BCR ($L = 1, 2$): Scenario B

The RMSE curves plotted in Figures 4.13 through 4.15 and the EA-RMSE values shown in Table 4.3 demonstrate the following important observations:

1. Figures 4.13 and 4.14 confirm that dynamic programming with a larger horizon-depth $L = 2$ performs better than dynamic programming with only one step of horizon length, i.e. dynamic optimization.

2. From Figure 4.15 we see that the ballistic coefficient exhibits a random fluctuation for dynamic programming with both $L = 1$ and $L = 2$. The reason for this is obvious: the measurements obtained by the receiver are unable to reflect any information about the ballistic coefficient.
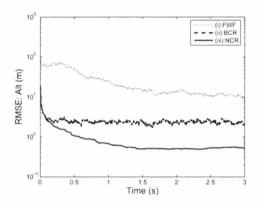
Figure 4.7: RMSE of target altitude (Scenario B). (i) conventional radar equipped with fixed waveform (dotted line), (ii) basic cognitive radar (dashed line), and (iii) nested cognitive radar (solid line).
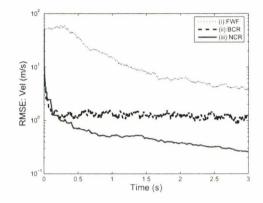
Figure 4.8: RMSE of target velocity (Scenario B). (i) conventional radar equipped with fixed waveform (dotted line), (ii) basic cognitive radar (dashed line), and (iii) nested cognitive radar (solid line).
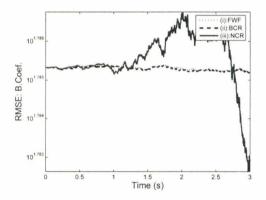
Figure 4.9: RMSE of ballistic coefficient (Scenario B). (i) conventional radar equipped with fixed waveform (dotted line), (ii) basic cognitive radar (dashed line), and (iii) nested cognitive radar (solid line).
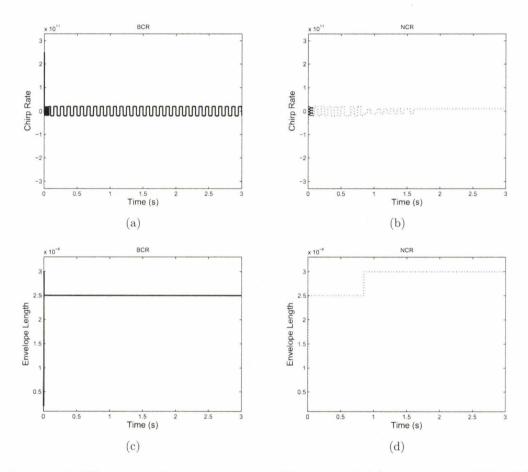
Figure 4.10: Waveform selection across time (Scenario B). (a) chirp rate for BCR, (b) chirp rate for NCR, (c) length of pulse envelope for BCR, (d) length of pulse envelope for NCR.

(a)

(b)

(c)
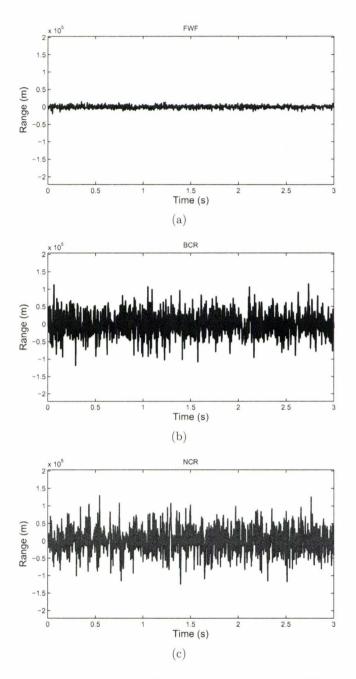
Figure 4.11: Chattering of range (Scenario B). (a) FWF, (b) BCR, (c) NCR.

(a)

(b)

(c)
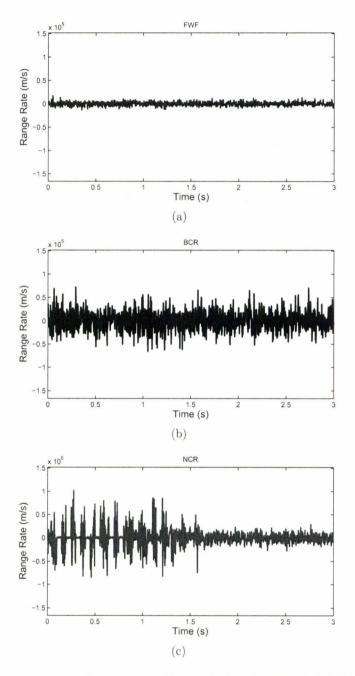
Figure 4.12: Chattering of range-rate (Scenario B). (a) FWF, (b) BCR, (c) NCR.
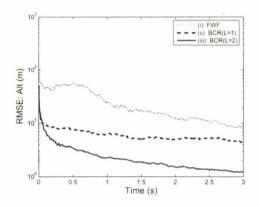
Figure 4.13: RMSE of target altitude (Scenario B). (i) conventional radar equipped with fixed waveform (dotted line), (ii) basic cognitive radar with $L = 1$ (dashed line), and (iii) basic cognitive radar with $L = 2$ (solid line).
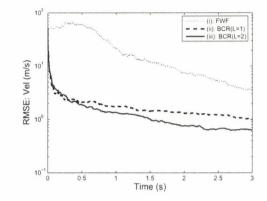
Figure 4.14: RMSE of target velocity (Scenario B). (i) conventional radar equipped with fixed waveform (dotted line), (ii) basic cognitive radar with $L = 1$ (dashed line), and (iii) basic cognitive radar with $L = 2$ (solid line).
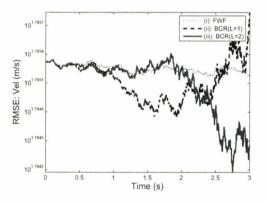
Figure 4.15: RMSE of ballistic coefficient (Scenario B). (i) conventional radar equipped with fixed waveform (dotted line), (ii) basic cognitive radar with $L = 1$ (dashed line), and (iii) basic cognitive radar with $L = 2$ (solid line).
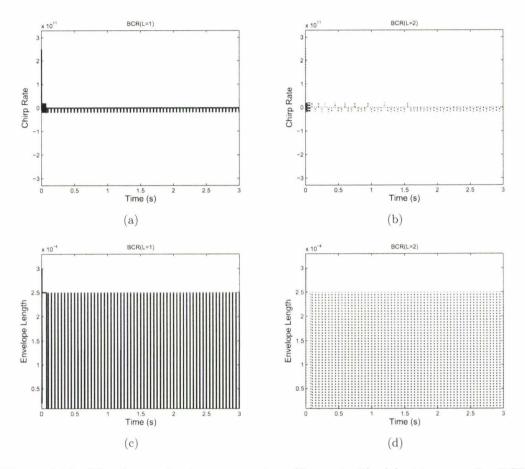
Figure 4.16: Waveform selection across time (Scenario B). (a) chirp rate for BCR with $L = 1$, (b) chirp rate for BCR with $L = 2$, (c) length of pulse envelope for BCR with $L = 1$, (d) length of pulse envelope for BCR with $L = 2$.

4.4   Scenario C: Target Tracking of High-Dimensional Continuous-Discrete Model

In this last case study, we consider a complicated scenario, the air-traffic-control problem, the objective of which is to track the trajectory of an aircraft that executes a maneuver at (nearly) constant speed and turn rate in the horizontal plane. We are interested in this problem because (i) air traffic control is important for both military and civilian applications, (ii) cognitive radar performs well for tracking problem with continuous system equation and discrete measurement equation, and (iii) most importantly the high-dimensional tracking problem will strongly confirm the need of cognition in tackling difficult target tracking problem.

4.4.1   State-Space Model

In the aviation language, this problem is commonly referred to as tracking of a target with (nearly) *coordinated turn* [79, 82]. In this scenario, the motion in the horizontal plane and the motion in the vertical plane are assumed to be decoupled. Hence, we can write the coordinated turn in the three-dimensional space, subject to fairly small noise modeled by independent Brownian motions, as shown by Eq. (2.7), where the seven-dimensional state of the aircraft $\mathbf{x} = [\epsilon\ \dot{\epsilon}\ \eta\ \dot{\eta}\ \zeta\ \dot{\zeta}\ \omega]^T$ with ϵ, η and ζ denoting positions and $\dot{\epsilon}, \dot{\eta}$ and $\dot{\zeta}$ denoting velocities in the x, y and z Cartesian coordinates, respectively; ω denotes the turn rate; the drift function

$$\mathbf{f}(\mathbf{x}) = \left[\ \dot{\epsilon},\ -\omega\dot{\eta},\ \dot{\eta},\ \omega\dot{\epsilon},\ \dot{\zeta},\ 0,\ 0\ \right]^T;$$

108

the noise term $\boldsymbol{\beta}(t) = [\beta_1(t), \beta_2(t), \cdots, \beta_7(t)]^T$ with $\beta_i(t), i = 1, 2 \ldots 7$, being all mutually independent standard Brownian motions, which account for unpredictable modeling errors; and finally the diffusion matrix is

$$\mathbf{Q} = \mathrm{diag}([0, \sigma_1^2, 0, \sigma_1^2, 0, \sigma_1^2, \sigma_2^2]).$$

For the problem at hand, the radar is located at the origin and equipped to measure the range, ρ, and azimuthal angle, θ, with a measurement sampling time T. Hence, we write the measurement equation

$$\begin{bmatrix} \rho_k \\ \theta_k \end{bmatrix} = \begin{bmatrix} \sqrt{\epsilon_k^2 + \eta_k^2 + \zeta_k^2} \\ \tan^{-1}\left(\frac{\eta_k}{\epsilon_k}\right) \end{bmatrix} + \mathbf{w}_k,$$

where the measurement noise is Gaussian $\mathbf{w}_k \sim \mathcal{N}(\mathbf{0}, \mathbf{R}_k)$ with $\mathbf{R}_k = \mathrm{diag}([\sigma_\rho^2, \sigma_\theta^2])$.

To simulate the target trajectory, we use $\sigma_1 = \sqrt{0.5}$; $\sigma_2 = \sqrt{5e\text{-}7}$; $\sigma_\rho = 50$ m; $\sigma_\theta = 0.001$ deg; and the initial state is

$$\mathbf{x}_0 = \begin{bmatrix} 10 \text{ km}, & 100 \text{ m/s}, & 10 \text{ km}, & 150 \text{ m/s}, & 5 \text{ km}, & 0 \text{ ms}^{-1}, & 20 \text{ deg/s} \end{bmatrix}^T.$$

With these parameters, the ideal trajectory of the target is plotted in Figure 4.17.

We use the notation $\mathbf{x}_k^j$ to denote $\mathbf{x}(t)$ at time $t = t_k + j\delta$, where $1 \le j \le m$ and $\delta = T/m$. Applying the Itô-Taylor expansion of order 1.5 to Eq. (2.7), we get the stochastic difference equation

$$\mathbf{x}_k^{(j+1)} = \mathbf{f}_d(\mathbf{x}_k^j) + \sqrt{\mathbf{Q}}\boldsymbol{\omega} + (\mathbb{L}\mathbf{f}(\mathbf{x}_k^j))\boldsymbol{\psi} \qquad (4.12)$$

where

$$\mathbf{f}_d(\mathbf{x}) = \begin{bmatrix} \epsilon + \delta\dot{\epsilon} - \delta^2\omega\dot{\eta}/2 \\[2mm] \dot{\epsilon} - \delta\omega\dot{\eta} - \delta^2\omega^2\dot{\epsilon}/2 \\[2mm] \eta + \delta\dot{\eta} + \delta^2\omega\dot{\epsilon}/2 \\[2mm] \dot{\eta} + \delta\omega\dot{\epsilon} - \delta^2\omega^2\dot{\eta}/2 \\[2mm] \zeta + \delta\dot{\zeta} \\[2mm] \dot{\zeta} \\[2mm] \omega \end{bmatrix}$$

and

$$\mathbb{L}\mathbf{f}(\mathbf{x}) = \begin{bmatrix} 0 & \sigma_1 & 0 & 0 & 0 & 0 & 0 \\[2mm] 0 & 0 & 0 & -\sigma_1\omega & 0 & 0 & -\sigma_2\dot{\eta} \\[2mm] 0 & 0 & 0 & \sigma_1 & 0 & 0 & 0 \\[2mm] 0 & \sigma_1\omega & 0 & 0 & 0 & 0 & -\sigma_2\dot{\epsilon} \\[2mm] 0 & 0 & 0 & 0 & 0 & \sigma_1 & 0 \\[2mm] 0 & 0 & 0 & 0 & 0 & 0 & 0 \\[2mm] 0 & 0 & 0 & 0 & 0 & 0 & 0 \end{bmatrix}.$$

To generate independent trajectories, we use $m = 1000$ time-steps/sampling interval.
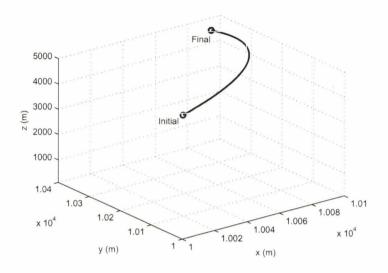
Figure 4.17: High-dimensional target trajectory of continuous-discrete model.

4.4.2 Radar Configurations

The experimental results presented in this section are based on simulating X-band radar with carrier frequency $f_c = 10.4$ GHz. We use LFM with both up-sweep and down-sweep chirps, which composes the waveform library given as follows:

$$\mathcal{P} = \{\lambda \in [10e\text{-}6, 100e\text{-}6], b \in [-100e9, -10e9] \cup [10e9, 100e9]\} \tag{4.13}$$

with grid step-sizes $\Delta\lambda = 10e\text{-}6$ and $\Delta b = 10e9$. The pulse is assumed to be Gaussian amplitude-modulated. The sampling frequency is set to $f_s = 400$ Hz and the update frequency of the cognitive algorithm is set to 20 Hz.

Now we have a continuous-discrete nonlinear filtering problem, the CD-CKF is selected in the receiver for perception of the environment. A detailed description of the CD-CKF can be found in Appendix B.

111

4.4.3 Simulation Results

We compare the performance of conventional radar with fixed waveform (FWF) to BCR and NCR by plotting the RMSE of the range and range-rate across the entire simulation duration in Figures 4.18 and 4.19, respectively. Here, to initialize the track, we can either use the single-point method (SP) [83] and the two-point differencing (TPD) method [79]. The SP method initializes the track by setting the position equal to the first measurement and the velocity as zero. The TPD method uses the first two measurements to estimate the states' statistics. For a comparison of the two methods, the reader may refer to [84]. In our simulation, we have adopted the TPD method for initialization. The EA-RMSE is also summarized in Table 4.4 for FWF, BCR and NCR. From Figures 4.18 and 4.19 and Table 4.4, a surprisingly good performance is obtained using cognitive radar, for either the basic version or the nested version. Furthermore, the nested cognitive radar even outperforms its basic counterpart.

The waveform selection procedure is depicted in Figure 4.20. Similar to Scenario B, the waveform transition is also observed for both the BCR and NCR. The chattering effects for range and range-rate are also plotted in Figures 4.21 and 4.22, where Figures 4.21(a) and 4.22(a), Figures 4.21(b) and 4.22(b), and Figures 4.21(c) and 4.22(c) correspond to FWF, BCR, and NCR, respectively.

EA-RMSE	Range (meters)	Range-rate (meters/second)
FWF	10.4195	12.0065
BCR	0.3725	2.9588
NCR	0.3122	1.8696

Table 4.4: Ensemble-averaged RMSE for FWF, BCR and NCR: Scenario C
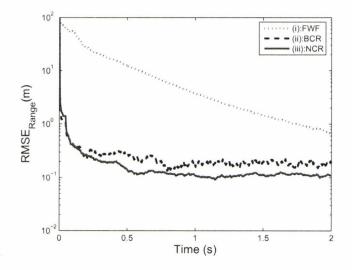
Figure 4.18: RMSE of target range (Scenario C). (i) conventional radar equipped with fixed waveform (dotted line), (ii) basic cognitive radar (dashed line), and (iii) nested cognitive radar (solid line).
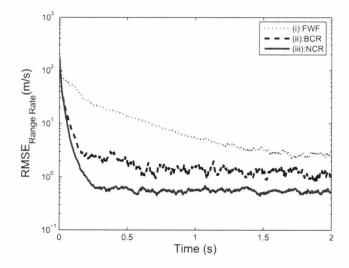
Figure 4.19: RMSE of target range-rate (Scenario C). (i) conventional radar equipped with fixed waveform (dotted line), (ii) basic cognitive radar (dashed line), and (iii) nested cognitive radar (solid line).
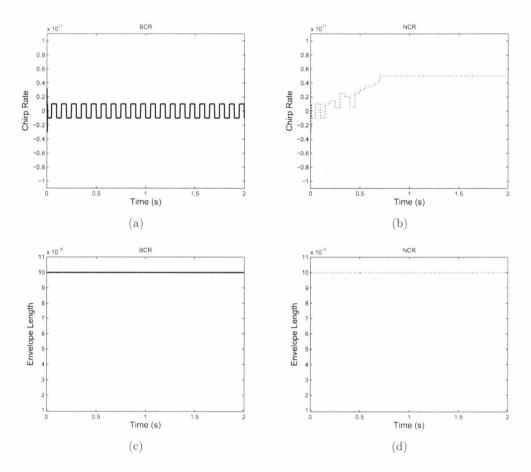
Figure 4.20: Waveform selection across time (Scenario C). (a) chirp rate for BCR, (b) chirp rate for NCR, (c) length of pulse envelope for BCR, (d) length of pulse envelope for NCR.

(a)

(b)

(c)
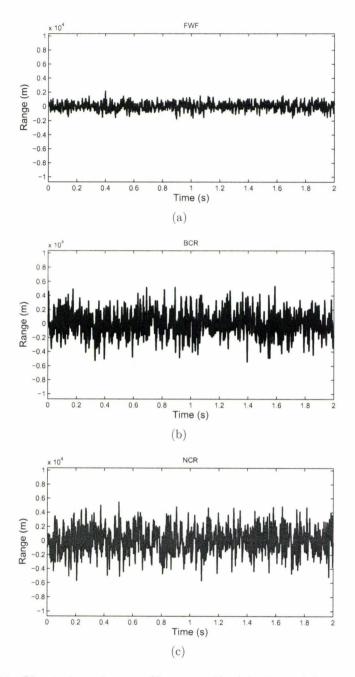
Figure 4.21: Chattering of range (Scenario C). (a) FWF, (b) BCR, (c) NCR.

(a)

(b)

(c)
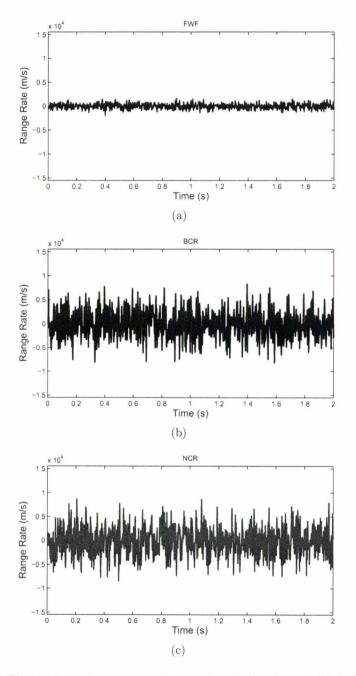
Figure 4.22: Chattering of range-rate (Scenario C). (a) FWF, (b) BCR, (c) NCR.

Observations from the Overall Simulation Results

Examining simulation results for Scenario A, B and C, we can make the following important observations:

- All simulations confirm that as the cognitive radar becomes more and more sophisticated, starting from the basic cognition to a fully cognition enabled by memory, the system performance becomes better and better.

- From Figures 4.1, 4.7, and 4.18, we can conclude that the performance enhancements are about in the order of 30 : 1, 25 : 1, and 7 : 1. These values explain the fact that as difficulties of the tasks increase, the performance enhancement a cognitive radar can make decreases.

- The waveform transition figures for all scenarios tends to suggest that for the scenarios employed in this thesis, the optimal waveform parameters are both the maximal values in the waveform library.

4.5 Summary

In this chapter, three scenarios were designed to challenge the capability of basic cognitive radar and nested cognitive radar. Computer simulations validated the improved performance of each member of the cognitive radar family by adding the essential components one by one:

- Global feedback from the receiver to the transmitter has provided basic computational intelligence to cognitive radar, which leads to a noticeable performance improvement of a cognitive radar compared to a traditional one.

- Furthermore, equipping the radar with three memories within the perception-action cycle has distinguished the nested cognitive radar from the basic cognitive radar. The three memories are perceptual memory in the receiver, executive memory in the transmitter, and coordinating perception-action memory that reciprocally couples the first two. The net result of having both the global feedback and three memory components is improved information processing power.

The first scenario considered a linear target tracking problem. The Kalman filter (KF) was employed in the radar tracker. A significant enhancement of radar resolution was obtained using the basic cognitive radar, and even more so when memory was incorporated into the perception-action cycle.

To go beyond the conventional Kalman filter, Scenario B selected to track a falling object in space. The cubature Kalman filter (CKF) was used as a radar tracker. Simulation results confirmed that the basic cognitive radar outperformed a conventional radar by an order of magnitude, and the nested cognitive radar enhanced the performance even further. Two cases of dynamic programming were considered, i.e. the special case, namely dynamic optimization for horizon-length $L = 1$, and dynamic programming with $L = 2$. A comparison between them demonstrated that increasing the length of horizon contributed positively to the performance enhancement of cognitive radar.

Scenario C was the most challenging one. A high-dimensional target tracking prob lem with continuous-discrete model was considered, based on which the continuou discrete cubature Kalman filter (CD-CKF) was employed. A surprisingly good pe formance was obtained with cognitive radars. Of course, the nested cognitive ra

performed even better than its basic counterpart.

In all three scenarios, an interesting phenomenon were observed, that is, the observables obtained by cognitive radar were generally much noisier than those obtained by conventional radar. This phenomenon is called the chattering effect in control systems. To inspire future research, an in-depth discussion of chatting effect is conducted in Chapter 5.

Chapter 5

Underlying Physical Phenomena in Cognitive Radar

Imagination is more important than knowledge. For knowledge is limited to all we now know and understand, while imagination embraces the entire world, and all there ever will be to know and understand.

Albert Einstein

In conducting the simulations in Chapter 4, an interesting phenomenon was observed: the noisy observables enable the performance enhancement of the cognitive radar systems. This phenomenon was called the chattering effect. Unlike in the study of control systems, the simulation results in Chapter 4 confirmed that the chattering effect played a positive role in increasing the resolution of a radar system. In this chapter, we will study this effect by looking into its underlying physical phenomenon.

5.1   Chattering Effect

For a cognitive radar system with system equation (2.4) and measurement equation (2.6), the main sources of uncertainty are:

- Imperfect knowledge of the system-equation model $\mathbf{f}(\cdot)$,

- Imperfect knowledge of the measurement-equation model $\mathbf{h}(\cdot)$, and

- Imperfect knowledge of the measurement noise $\mathbf{w}_k$, which acts as the *driving force*.

The uncertainties arising from the first two sources have been tackled by introducing the perceptual and executive memories into the perception-action cycle, where the system-equation model and measurement-equation model can be retrieved on-the-fly. The *driving force* then becomes the main challenge in optimally controlling the environment. In modern control theory, techniques of high-gain feedback and sliding-mode control are often applied to address the uncertainty of mathematical models [85, 86]. Sliding modes are the phenomena observed in a dynamic system, where the state changes discontinuously with the high-frequency switching of control actions [87]. For a cognitive radar *controlled* by the measurement noise, the control action, i.e. the waveform, is selected in a frequency that is much faster than a classic control system. Therefore, the fast dynamics of environmental-scene analyzer and actuator may cause an interesting phenomenon, namely the *chattering effect*, defined in the following:

Definition 5.1 (Chattering Effect). *The chattering effect is a physical phenomenon of the high-frequency and finite amplitude oscillations appearing in a control system, where the actions are taken discontinuously.*   □

Most of the research in chattering analysis concludes that the chattering effect is a harmful phenomenon since it leads to a low control accuracy and high heat losses in electrical circuits. Needless to say, this conclusion is very true for a dynamic system in which the control variable explicitly appears in the system equation. A cognitive system modeled by (2.6) avoids this harmful condition by having measurement noise $\mathbf{w}_k(\boldsymbol{\theta}_{k-1})$ as the control variable, where $\boldsymbol{\theta}_{k-1}$ is the radar waveform. As such, unlike the study of chattering in sliding-mode control focusing on the system state, in our study it is the chattering of measurements which result directly from the measurement noise.

5.1.1 Mathematical Definition of Chattering

The definition of chattering depends closely on the time and coordinate scales [88]. The chattering of a signal is defined with respect to a reference or nominal signal. While linear functions of time do not experience the chattering effect, any other nonlinear function experiences it to some extent, be it low or high. We can therefore define the reference signal at zero level of the chattering effect and study the difference between another signal and the reference signal

For the simplicity of exposition, let us consider a continuous real signal $s(t) \in \mathbb{R}$ with $t \in [t_1, t_2]$. Its reference signal is another continuous real signal $\bar{s}(t) \in \mathbb{R}$. The disturbance is assumed to be derivable, defined as

$$\Delta s(t) = s(t) - \bar{s}(t). \tag{5.1}$$

The disturbance $\Delta s(t)$ can be regarded as a *heat-release* process with a rate of $\Delta \dot{s}(t)$. Here $\Delta \dot{s}(t)$ is the derivative of the disturbance $\Delta \dot{s}(t)$. To elaborate the heat-release

process, consider a furnace of high temperature. The quantity of heat released by this furnace per second defines the heat-release rate. Obviously, the environment temperature defines the reference signal in this case. Note that the heat-release rate in this definition is not based on a normalized value compared to the terminology in thermodynamics. If we divide our heat-release rate by the total heat volume of the furnace, i.e., $\int_{t_1}^{t_2} s(t)dt$, we then obtain the normalized heat-release rate.

The $\mathcal{L}_1$-chattering of $s(t)$ is the $\mathcal{L}_1$ distance between $\dot{s}(t)$ and $\dot{\bar{s}}(t)$, defined as

$$\mathcal{L}_1\text{-chat}(s, \bar{s}, t_1, t_2) = \int_{t_1}^{t_2} |\dot{s}(t) - \dot{\bar{s}}(t)| \, dt. \tag{5.2}$$

The definition of Eq. (5.2) illustrates the physical resemblance of $\mathcal{L}_1$-chattering, that is, it defines the energy required to reduce the disturbance.

Quite often in practical applications, we also need to represent the chattering effect in an $\mathcal{L}_2$ or even $\mathcal{L}_p$ sense. We then have the $\mathcal{L}_2$-chattering and $\mathcal{L}_p$-chattering defined respectively as

$$\mathcal{L}_2\text{-chat}(s, \bar{s}, t_1, t_2) = \left[\int_{t_1}^{t_2} |\dot{s}(t) - \dot{\bar{s}}(t)|^2 \, dt \right]^{1/2} \tag{5.3}$$

and

$$\mathcal{L}_p\text{-chat}(s, \bar{s}, t_1, t_2) = \left[\int_{t_1}^{t_2} [\dot{s}(t) - \dot{\bar{s}}(t)]^p \, dt \right]^{1/p}. \tag{5.4}$$

Having the mathematical definitions presented in (5.2) to (5.4), we may discuss different categories of the chattering effect. In order to classify it, we follow Leveant's proposition in [88]. Define ε as the *chattering parameter* to measure the imperfections

of the model for which we write

$$\bar{s}(t) = \lim_{\varepsilon \to 0} s(t, \varepsilon) \tag{5.5}$$

for $t \in [t_1, t_2]$. For cognitive radar, we use ε to denote the interference or disturbance in the measurement model.

Let us take the $\mathcal{L}_p$-chattering as an example; it can be classified into three categories:

Definition 5.2 (Infinitesimal Chattering). *The $\mathcal{L}_p$-chattering of signal $s(t)$ is infinitesimal chattering if*

$$\lim_{\varepsilon \to 0} \mathcal{L}_p\text{-chat}(s, \bar{s}, t_1, t_2) = 0, \tag{5.6}$$

which means that the heat is completely released as the imperfections of signal model tends to zero.   □

Definition 5.3 (Bounded Chattering). *The $\mathcal{L}_p$-chattering of signal $s(t)$ is bounded chattering if*

$$\lim_{\varepsilon \to 0} \mathcal{L}_p\text{-chat}(s, \bar{s}, t_1, t_2) > 0, \tag{5.7}$$

which means that a fixed amount of heat is kept in the signal as the imperfections of signal model tends to zero.   □

Definition 5.4 (Unbounded Chattering). *The $\mathcal{L}_p$-chattering of signal $s(t)$ is unbounded chattering if*

$$\lim_{\varepsilon \to 0} \mathcal{L}_p\text{-chat}(s, \bar{s}, t_1, t_2) = \infty, \tag{5.8}$$

which means that the heat released is not bounded even if the signal model is perfectly known.   □

Using this definition and the measurement equation (2.6) and also assuming there is no external interference, we could define the $\mathcal{L}_p$-chattering of measurement as follows:

$$\mathcal{L}_p\text{-chat}(\mathbf{z}, \bar{\mathbf{z}}, t_1, t_2) = \left[\int_{t_1}^{t_2} \left[\dot{\mathbf{z}}(t) - \dot{\bar{\mathbf{z}}}(t) \right]^p dt \right]^{1/p} \tag{5.9}$$

for $t \in [t_1, t_2]$.

For the measurement obtained by a discrete sensor, we can further approximate the $\mathcal{L}_p$-chattering (5.9) as follows:

$$\mathcal{L}_p\text{-chat}(\mathbf{z}, \bar{\mathbf{z}}, t_1, t_2) \approx \left[\sum_{k=1}^{M} \dot{\mathbf{w}}_k^p(\boldsymbol{\theta}_{k-1}) T \right]^{1/p}, \tag{5.10}$$

where T is the sampling time and $M = (t_2 - t_1)/T$.

Two comments are made sequentially about this definition:

1. The value of $\mathcal{L}_p$-chattering reflects the total heat stored in the system within the duration of $[t_1, t_2]$. To compare the $\mathcal{L}_p$-chattering of two measurement systems $\mathcal{S}_1$ and $\mathcal{S}_2$, we offer the following scenarios:

   - If $\mathcal{L}_p\text{-chat}(\mathcal{S}_1) > \mathcal{L}_p\text{-chat}(\mathcal{S}_2)$, then the system $\mathcal{S}_1$ is said to be *warmer* than $\mathcal{S}_2$;

   - If $\mathcal{L}_p\text{-chat}(\mathcal{S}_1) = \mathcal{L}_p\text{-chat}(\mathcal{S}_2)$, then the system $\mathcal{S}_1$ is said to be *equally warm* with $\mathcal{S}_2$;

- If $\mathcal{L}_p$-chat$(\mathcal{S}_1) < \mathcal{L}_p$-chat$(\mathcal{S}_2)$, then the system $\mathcal{S}_1$ is said to be *cooler* than $\mathcal{S}_2$;

2. The approximation of (5.10) is valid under the assumption that the measurement noise is a zero-mean white Gaussian process.

For the measurement system, the unbounded chattering is obviously destructive. Furthermore, the infinitesimal chattering is not desirable for a cognitive radar system because the system relies on measurement noise to control the accuracy of the state estimation. We conclude that *the bounded chattering is the most realistic and also beneficial condition for cognitive radar.* As previously mentioned, the chattering effect can be regarded as the result of *heat release* process in the system; the bounded chattering can therefore guarantee that the system is *warm* enough to sustain the performance enhancement in the cognitive radar system.

5.1.2   Chattering Effect in Variable Structure Systems

As we have stated earlier in this chapter, the chattering effect in cognitive radar is due to uncertainty in the system model, specifically the measurement equation. At each time step, a measurement model is retrieved from the memory to reflect an updated knowledge about the target. These measurement models collectively define a *variable structure system* of the following form

$$\dot{\mathbf{z}}(t) = \dot{\mathbf{h}}(\mathbf{x}(t), \boldsymbol{\theta}, t), \tag{5.11}$$

where $\dot{\mathbf{h}}(\cdot) := \left[\dot{h}_1(\cdot), \dot{h}_2(\cdot), ..., \dot{h}_n(\cdot)\right]^T$ is a piecewise continuous function. The piecewise continuity property of these subsystems makes the system switch between different mathematical models stored in the executive memory, hence the name: *variable structure system* (VSS) [86]. As such, the method of controlling a variable structure system is referred to as variable structure control (VSC), which was first studied in early 1950's by Emelyanov and his coresearchers [89]. Currently, the main method used for VSC is sliding mode control [87], which is less sensitive to system-parameter uncertainty but highly possible of causing chattering problem in target state [90]. In the VSS framework of cognitive radar, the reduction of the chattering effect in the system equation requires an iterative filtering algorithm. Recently, a variable structure filter (VSF) has been proposed to accommodate model uncertainties [91], where the conventional Kalman filter gain is redesigned to reflect the noise uncertainty existing in a linear system. Revisiting the derivation of the cubature Kalman filter in Chapter 2 reveals a similar strategy in the nonlinear filtering algorithm, where the waveform $\boldsymbol{\theta}_{k-1}$ is incorporated into the time update step of the CKF. Therefore, we say that the CKF algorithm employed inside the perception-action cycle of the cognitive radar actually becomes a nonlinear variable structure filter. A question that we may ask is: *Is it possible to say that we also have a positive form of the chattering effect in the human brain?*

5.1.3 Chattering Effect in Cognitive Radar in Light of Experimental Results

Bearing the discussion of sources for the chattering effect in mind, we say that the objective of an optimal waveform control strategy for the variable structure system is

to reduce the target state chattering effect as much as possible, which is demonstrated by the root mean-squared errors (RMSEs) shown in Chapter 4. Generally speaking, the minimization of mean-squared error of target state is identical to the reduction of chattering. Since the state of the target is hidden from the observer, we are faced with an imperfect-state information problem. So we may estimate the state by having direct access to the measurements obtained by the radar receiver. As such, the chattering effect pertained to the measurements can help us gain insights into the mechanism of cognitive radar system. To ease our analysis in this chapter, we reproduce the chattering effects obtained in Chapter 4, shown in Figures 5.1, 5.2 and 5.3 for Scenario A, Scenario B and Scenario C, respectively.
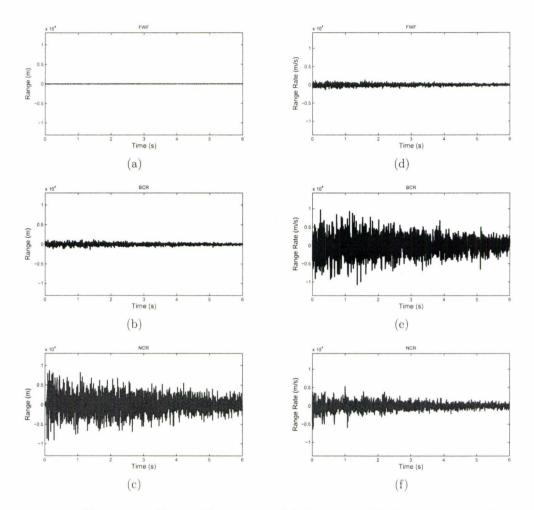
Figure 5.1: Chattering effect in Scenario A. (a)-(c) range, (d)-(f) range-rate. (Reproduced from Figures 4.4 and 4.5)
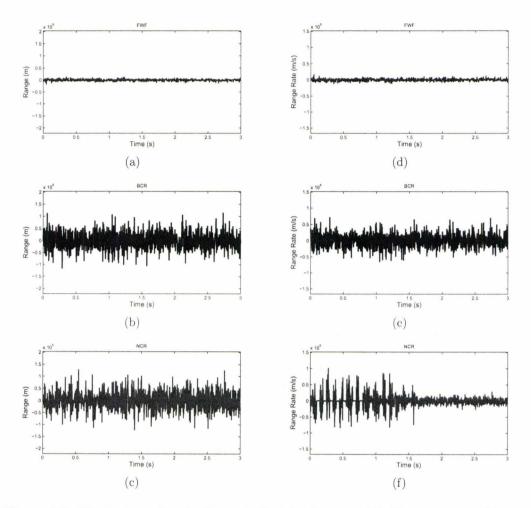
Figure 5.2: Chattering effect in Scenario B. (a)-(c) range, (d)-(f) range-rate. (Reproduced from Figures 4.11 and 4.12)
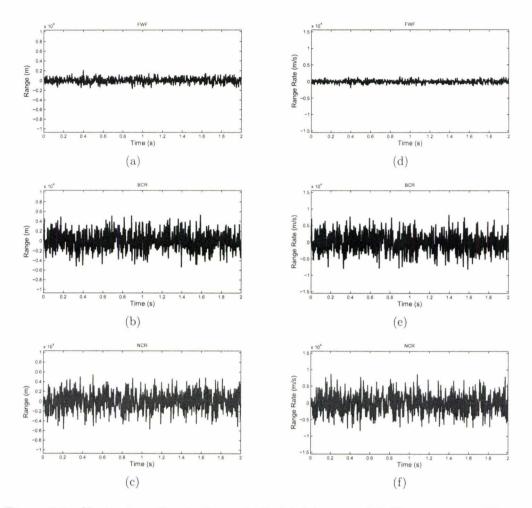
Figure 5.3: Chattering effect in Scenario C. (a)-(c) range, (d)-(f) range-rate. (Reproduced from Figures 4.21 and 4.22)

Observations from Simulation Results

A close observation of these results may remind us the following important aspects about the chattering effect:

1. All figures confirm that the bounded chattering in measurement space is the most realistic type. Hence cognitive radar is able to benefit from this bounded chattering.

2. Obviously, the chattering effects we observed in cognitive radar are much higher than those obtained in a conventional radar, which states that measurement noise acts as the driving force for reduction of state estimation error. Generally speaking, a *warm* chattering in measurement space is expected in cognitive radar.

3. As we can see from Figure 5.1, for a linear target tracking problem, the nested cognitive radar needs a *warmer* chattering to increase the range accuracy compared to its basic counterpart. Nevertheless, the nested cognitive radar needs a *cooler* chattering to increase the range-rate accuracy.

4. From Figure 5.2(f), we see that a strange chattering pattern happened in the range-rate. At the initial stage of the tracking: The nested cognitive radar makes use of a periodical *warm-cool* chattering to increase its resolution over the basic cognitive radar.

5.2 Behaviour of Cognitive Radar in the Presence of External Disturbance

Normally, the system equation should be provided for the two steps of the filtering algorithm employed in a radar tracker, be it cognitive or non-cognitive. For a conventional radar system and memoryless cognitive radar system, parameters of the system equation are assumed to be available at each time step deterministically. This process is not affected by the changes of the environment that the target resides in. However, for cognitive radar system enabled with the memory, neural networks are designed to store the features related to the system equation. The retrieval process at each time step is closely related to changes of the environment.

These claims about the difference between memoryless radar system and memory-enabled radar system are true provided that the assumption of reasonably *mild* white noise is satisfied. Take Scenario A, i.e. the linear target tracking problem, as an example, the white noise $\mathbf{v}_k$ in system equation (4.1) models all the noises that are added to the states of the target. Presumably, these noises include the wind, cloud and other climatic facts mostly. Obviously, the study of each factor can be a research topic of its own. To be more specific, the analysis of the wind-excited response of flying objects requires a careful modeling of the wind field, which is usually called turbulence [92]. All of these factors can be considered as the disturbance to the target trajectory, which we have denoted by $\mathbf{v}_k$ in all simulations. In Chapter 4, we focused on a relatively *stationary* environment, where the covariance of $\mathbf{v}_k$, i.e. $\mathbb{E}\{\mathbf{v}_k\mathbf{v}_k^T\} = \mathbf{Q}_k$, is fixed. We call this case the *single-mode disturbance*.

In practical applications, we may encounter another case where the target's trajectory is sharply affected by a strong disturbance for a short period of time. We call this problem target tracking in *multi-mode disturbance*. In this section, we offer an extended simulation of Scenario A presented in Chapter 4 to experimentally study the behaviour of cognitive radar system in this scenario. For simplicity in exposition, here we recompose the system equation (4.1) as follows:

$$\mathbf{x}_k = \mathbf{F}_k\mathbf{x}_{k-1} + \mathbf{v}_k + \mathbf{d}_k,$$

where $\mathbf{F}_k$ is the state transition model, $\mathbf{v}_k$ is a white Gaussian noise, and the disturbance $\mathbf{d}_k$ is assumed to be Gaussian attributed to turbulence. We further assume that $\mathbf{v}_k$ and $\mathbf{d}_k$ are jointly Gaussian; then the linear combination of $\mathbf{v}_k$ and $\mathbf{d}_k$ is also Gaussian [93]. Here, we define that $\mathbf{v}_k + \mathbf{d}_k$ has a covariance $\mathbb{E}\{(\mathbf{v}_k + \mathbf{d}_k)(\mathbf{v}_k + \mathbf{d}_k)^T\} = \mathbf{Q}_k$. Two system noise covariances are considered [94], as follows:

1. Constant-velocity (CV) noise

$$\mathbf{Q}_{\mathrm{CV}} = \sigma_{\mathbf{v}+\mathbf{d}}^2 \begin{bmatrix} T^3/3 & T^2/2 \\ T^2/2 & T \end{bmatrix}$$

2. Constant-acceleration (CA) noise

$$\mathbf{Q}_{\mathrm{ca}} = \sigma_{\mathbf{v}+\mathbf{d}}^2 \begin{bmatrix} T^4/4 & T^3/2 \\ T^3/2 & T^2 \end{bmatrix},$$

where $\sigma_{\mathbf{v}+\mathbf{d}}^2$ characterizes the level of disturbance.
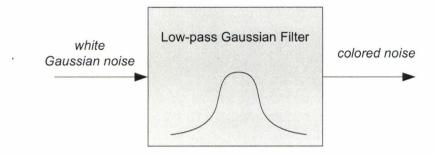
Figure 5.4: Block diagram of a low-pass Gaussian filter.

To configure the environment, it is assumed that the target travels toward the radar linearly from 3 km with speed 200 m/s. For the first 2 seconds, it encounters a *small enough* disturbance of $\sigma_{\mathbf{v+d}} = 0.7$. It then reaches to a moderately disturbing environment, where the noise $\sigma_{\mathbf{v+d}} = 4$. After another 2 seconds, the target gets out of the region with high disturbance and travels linearly along in a disturbance of 0.7. The radar is configured in the same way as Scenario A of Section 4.2.

In an effort to emulate the disturbance due to turbulence, the Gaussian noise is passed through a low-pass Gaussian filter before it is added to the system equation, demonstrated by Figure 5.4. The cut-off frequency is assumed to be 300 Hz. The frequency spectra for both the filtered Gaussian noise and white Gaussian noise are also depicted in Figure 5.5, where the spectra are based on a 1024-point fast Fourier transform (FFT).

The RMSE results are plotted in Figures 5.6, 5.7, 5.9 and 5.10, where Figures 5.6 and 5.7 depict the radar behaviour in constant-velocity disturbance, and Figures 5.9 and 5.10 depict the radar behaviour in constant-acceleration disturbance.

Recalling that the mathematical framework of the chattering effect has been developed in the first part of this chapter, it is also necessary to study the chattering effects that happen in the presence of a moderate disturbance. Figures 5.8 and 5.11 show the

135
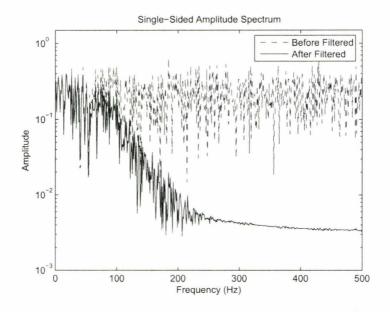
Figure 5.5: Single-sided amplitude spectrum for Gaussian noise before and after it is filtered by a Gaussian filter.

chattering effects under the constant-velocity disturbance and constant-acceleration disturbance, respectively. Referring to the NCR, we see a *warmer* chattering in the range domain, depicted by Figures 5.8(c) and 5.11(c), and a *cooler* chattering in the range-rate domain, depicted by Figures 5.8(f) and 5.11(f), comparing to the BCR. Interestingly, when the moderate disturbance appears in time duration $2 \sim 4$ seconds, we observe that both the BCR and NCR demonstrate a *calm* chattering behaviour. The explanation we may offer is that moderate turbulence appears only in the system equation. The turbulence has no direct influence on the measurements chattering.

Insofar as the level of the disturbance is concerned, the moderate disturbance poses a great challenge to traditional radar and even the basic cognitive radar. The nested cognitive radar can nevertheless mitigate this problem by having the memory component along with the basic perception-action cycle. To look into the behaviour of

cognitive radar in different level of disturbance, more simulations are also needed. To emulate low disturbances, we select $\sigma_{v+d} = 1$, based on which Figures 5.12 and 5.13 respectively depict the RMSE results for constant-velocity disturbance, and Figures 5.15 and 5.16 respectively depict the RMSE results for constant-acceleration disturbance. Similarly, to emulate high disturbances, we select $\sigma_{v+d} = 40$. Figures 5.18 and 5.19 respectively depict the RMSE results for high constant-velocity disturbance, and Figures 5.21 and 5.22 respectively depict the RMSE results for high constant-acceleration disturbance. Similar to the moderate disturbance, the chattering effects are also plotted in Figures 5.14 and 5.17 for low disturbance, and in Figures 5.20 and 5.23 for high disturbance, respectively.

Low Disturbance ($\sigma_{v+d} = 1$)		
EA-RMSE	Range (meters)	Range-rate (meters/second)
FWF	0.3465	1.2848
BCR	0.1469	0.6818
NCR	0.0591	0.1163
Moderate Disturbance ($\sigma_{v+d} = 4$)		
EA-RMSE	Range (meters)	Range-rate (meters/second)
FWF	0.3547	1.5244
BCR	0.1641	0.8915
NCR	0.0670	0.1377
High Disturbance ($\sigma_{v+d} = 40$)		
EA-RMSE	Range (meters)	Range-rate (meters/second)
FWF	0.4271	4.5346
BCR	0.3413	2.6280
NCR	0.1411	0.2568

Table 5.1: Ensemble-averaged RMSE for FWF, BCR and NCR with different level of constant-velocity disturbance: Scenario A

Low Turbulence ($\sigma_{v+d} = 1$)		
EA-RMSE	Range (meters)	Range-rate (meters/second)
FWF	0.3412	0.5075
BCR	0.1237	0.2068
NCR	0.0357	0.0402
Moderate Turbulence ($\sigma_{v+d} = 4$)		
EA-RMSE	Range (meters)	Range-rate (meters/second)
FWF	0.3393	0.5237
BCR	0.1244	0.2112
NCR	0.0406	0.0402
High Turbulence ($\sigma_{v+d} = 40$)		
EA-RMSE	Range (meters)	Range-rate (meters/second)
FWF	0.3483	0.5356
BCR	0.1249	0.2419
NCR	0.0499	0.0770

Table 5.2: Ensemble-averaged RMSE for FWF, BCR and NCR with different level of constant-acceleration turbulence: Scenario A

To summarize, the EA-RMSE results for different level of constant-velocity and constant-acceleration disturbances are listed in Table 5.1 and Table 5.2, respectively. All results show that a *warm* chattering in range and a *cool* chattering in range-rate are beneficial to nested cognitive radar, compared to basic cognitive radar.
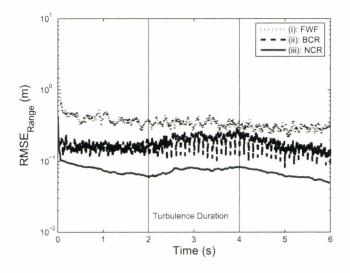
Figure 5.6: RMSE of target range for moderate constant-velocity disturbance. (i) conventional radar equipped with fixed waveform (dotted line), (ii) basic cognitive radar (dashed line), and (iii) nested cognitive radar (solid line).

Figure 5.7: RMSE of target range-rate for moderate constant-velocity disturbance. (i) conventional radar equipped with fixed waveform (dotted line), (ii) basic cognitive radar (dashed line), and (iii) nested cognitive radar (solid line).

Figure 5.8: Chattering of range and range-rate in moderate constant-velocity distur-bance. (a)-(c) range, (d)-(f) range-rate.

Figure 5.9: RMSE of target range for moderate constant-acceleration disturbance. (i) conventional radar equipped with fixed waveform (dotted line), (ii) basic cognitive radar (dashed line), and (iii) nested cognitive radar (solid line).
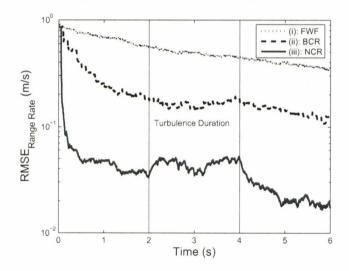
Figure 5.10: RMSE of target range-rate for moderate constant-acceleration distur- bance. (i) conventional radar equipped with fixed waveform (dotted line), (ii) basic cognitive radar (dashed line), and (iii) nested cognitive radar (solid line).
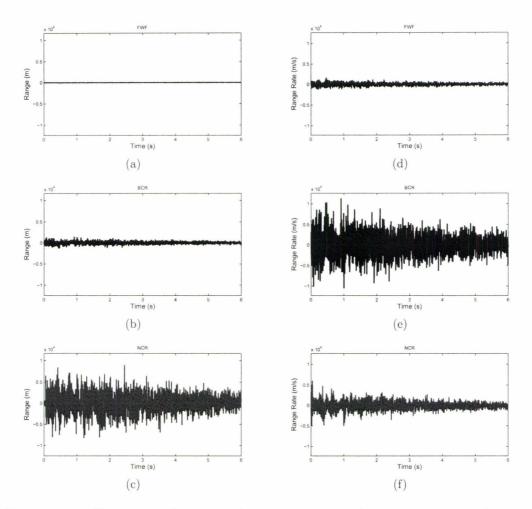
Figure 5.11: Chattering of range and range-rate in moderate constant-acceleration disturbance. (a)-(c) range, (d)-(f) range-rate.
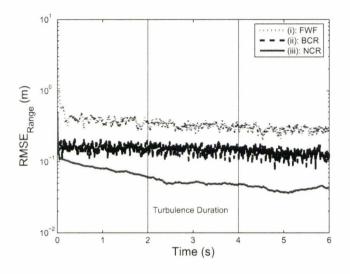
Figure 5.12: RMSE of target range for low constant-velocity disturbance. (i) conventional radar equipped with fixed waveform (dotted line), (ii) basic cognitive radar (dashed line), and (iii) nested cognitive radar (solid line).
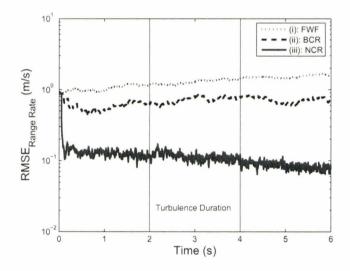
Figure 5.13: RMSE of target range-rate for low constant-velocity disturbance. (i) conventional radar equipped with fixed waveform (dotted line), (ii) basic cognitive radar (dashed line), and (iii) nested cognitive radar (solid line).
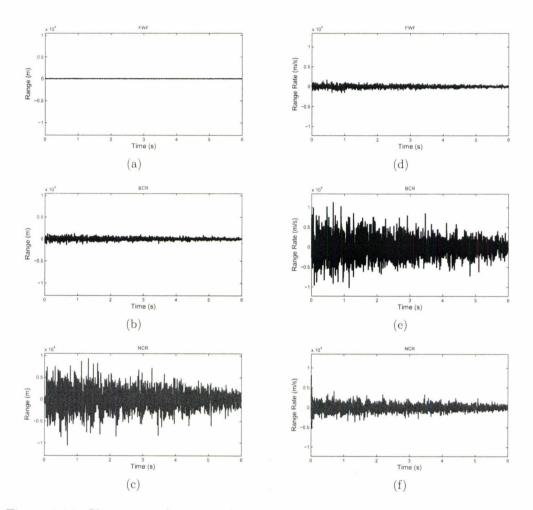
Figure 5.14: Chattering of range and range-rate in low constant-velocity disturbance. (a)-(c) range, (d)-(f) range-rate.
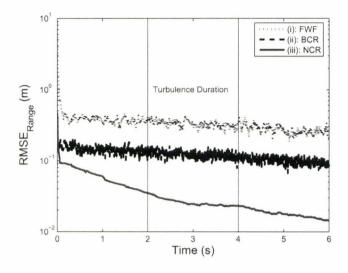
Figure 5.15: RMSE of target range for low constant-acceleration disturbance. (i) conventional radar equipped with fixed waveform (dotted line), (ii) basic cognitive radar (dashed line), and (iii) nested cognitive radar (solid line).
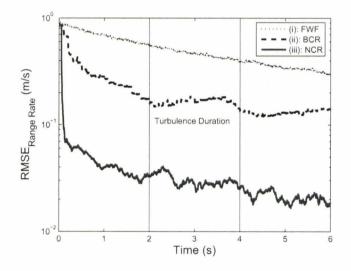
Figure 5.16: RMSE of target range-rate for low constant-acceleration disturbance. (i) conventional radar equipped with fixed waveform (dotted line), (ii) basic cognitive radar (dashed line), and (iii) nested cognitive radar (solid line).
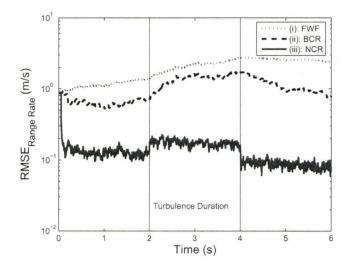
145
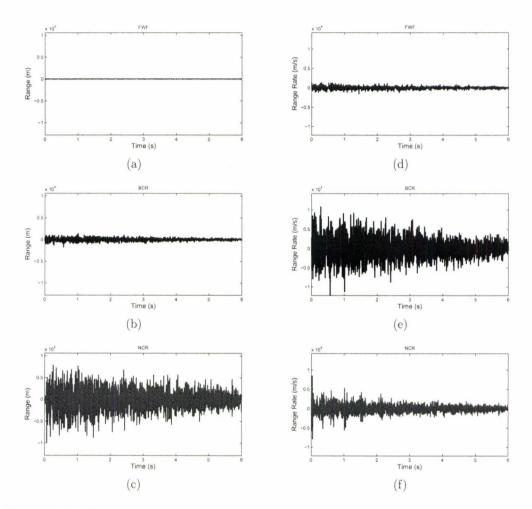
Figure 5.17: Chattering of range and range-rate in low constant-acceleration disturbance. (a)-(c) range, (d)-(f) range-rate.
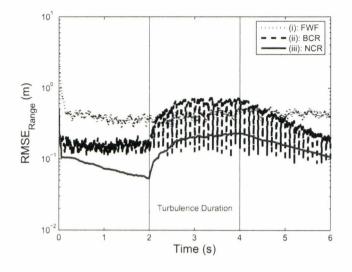
Figure 5.18: RMSE of target range for high constant-velocity disturbance. (i) conventional radar equipped with fixed waveform (dotted line), (ii) basic cognitive radar (dashed line), and (iii) nested cognitive radar (solid line).
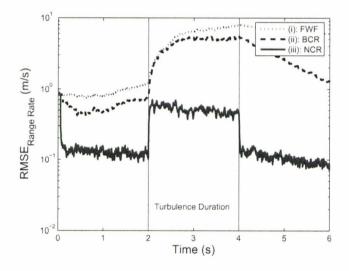
Figure 5.19: RMSE of target range-rate for high constant-velocity disturbance. (i) conventional radar equipped with fixed waveform (dotted line), (ii) basic cognitive radar (dashed line), and (iii) nested cognitive radar (solid line).
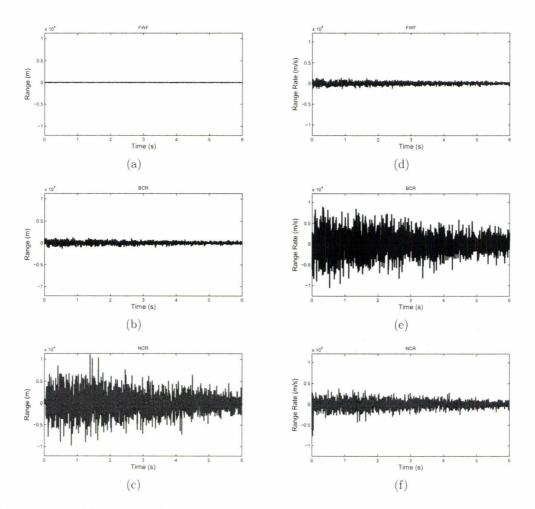
147
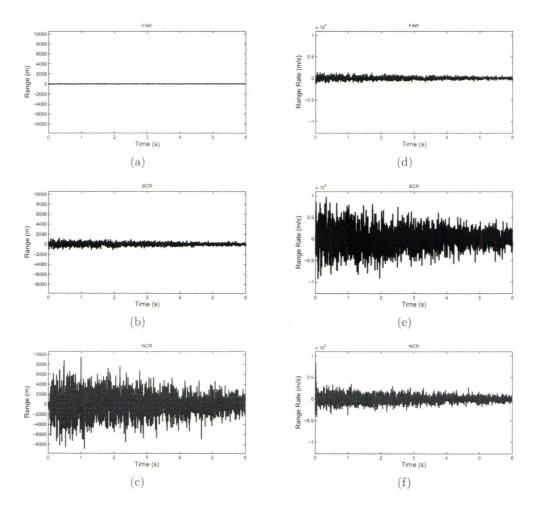
Figure 5.20: Chattering of range and range-rate in high constant-velocity disturbance. (a)-(c) range, (d)-(f) range-rate.
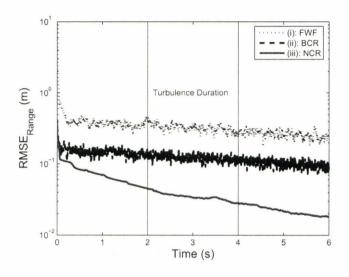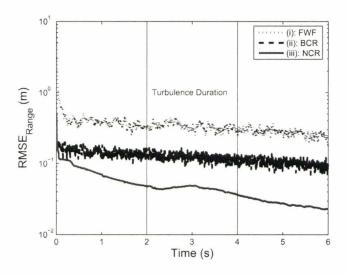
Figure 5.21: RMSE of target range for high constant-acceleration disturbance. (i) conventional radar equipped with fixed waveform (dotted line), (ii) basic cognitive radar (dashed line), and (iii) nested cognitive radar (solid line).
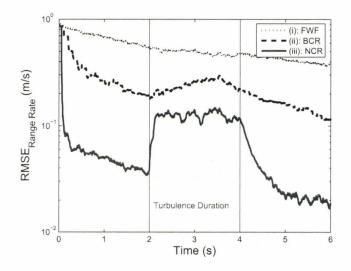
Figure 5.22: RMSE of target range-rate for high constant-acceleration disturbance. (i) conventional radar equipped with fixed waveform (dotted line), (ii) basic cognitive radar (dashed line), and (iii) nested cognitive radar (solid line).
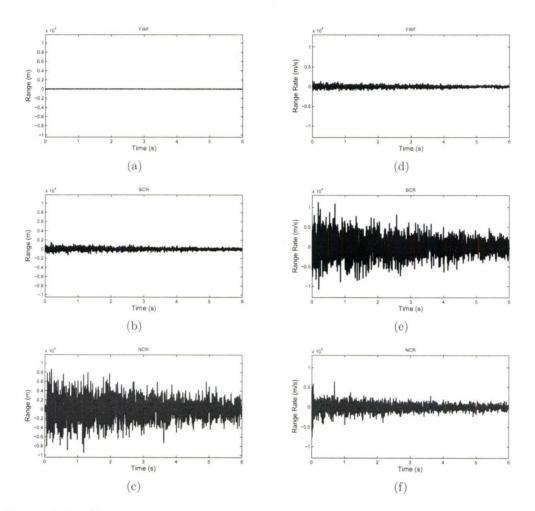
Figure 5.23: Chattering of range and range-rate in high constant-acceleration distur-bance. (a)-(c) range, (d)-(f) range-rate.

Observations from Simulation Results

Examining all the simulation results in this section, we have the following observations about the behaviour of cognitive radar in the presence of external disturbance:

1. From Figures 5.12, 5.6 and 5.18, we see that as the level of disturbance increases, it becomes more and more difficult for the BCR to provide a good performance. For the low disturbance, the BCR has a reasonable performance. As the disturbance reaches moderate level, the BCR struggles to mitigate the impact of disturbance on its performance. Furthermore, when the disturbance is high, the BCR breaks down into what appears to be an oscillatory behaviour. Interestingly enough, the NCR still performs well for all levels of disturbance. These results prove that feedback is indeed a double-edged sword. It will be detrimental if the feedback is not carefully designed. Obviously, the NCR can efficiently alleviate this problem thanks to the embedding of three memories within the basic perception-action cycle. In the NCR, the negative impact of disturbance is confined to its occurrence duration.

2. Comparing Figure 5.6 and Figure 5.9, we see that the range resolution of cognitive radar is more sensitive to the constant-velocity disturbance than the constant-acceleration disturbance. While Figures 5.7 and 5.10 show that the range-rate resolution is sensitive to both constant-velocity and constant-acceleration disturbances.

5.3   Summary

Two underlying physical phenomena were discussed in this chapter, namely the chattering effect and multi-mode disturbance. In an effort to analyze the chattering effect, a mathematical model of an $\mathcal{L}_p$-chattering was defined. Different from the role of the chattering effect in variable structure systems, we conclude that the chattering effect happening in the measurement space is very beneficial to the performance enhancement of cognitive radar. Generally speaking, the cognitive radar system encounters a higher-level chattering effect compared to conventional radar with fixed waveform. Furthermore, rather than merely increasing the chattering level, the nested cognitive radar increases the resolution by utilizing the chattering effect more efficiently.

To further study the behaviour of cognitive radar in the presence of different level of disturbance, we conducted extensive computer simulations. Simulation results proved that, for low disturbance, the basic cognitive radar can improve the resolution for both the constant-velocity disturbance and constant-acceleration disturbance, compared to conventional radar with fixed waveform. However, as the level of disturbance increases, the BCR exhibits a struggling behaviour. It almost breaks down for an intensively high disturbance. Interesting enough, the NCR enabled with memory performs well for all disturbance levels. Most importantly, it can adjust quickly to withstand the impact of disturbance.

Chapter 6

Conclusions and Future Research

The last part of an endeavor is the hardest to finish.

An ancient Chinese proverb

6.1 Concluding Remarks

For over six decades, the theory and design of radar systems have been dominated by probability theory and statistics, information theory, signal processing and control. However, the similar encoding-decoding property that exists between the visual brain and radar has been sadly overlooked in all radar systems. A lesson we have learned is that there is much that we can learn from the mammalian brain in an effort to build a new generation of radar systems.

In this thesis, we have presented the underlying theory of cognitive radar in a progressive way, starting from the basic cognitive radar that has only the perception-action cycle in the basic form to the nested cognitive radar equipped with memory. Extensive computer simulations were conducted to demonstrate the ability of this

new radar concept in significantly outperforming a traditional radar tracker. The following ideas have been exploited in the thesis:

Optimal Bayesian filter: A recently proposed nonlinear filter, namely the cubature Kalman filter (CKF), as well as the continuous-discrete CKF (CD-CKF), is employed in the receiver for perception of radar environment. This new filter is the best known approximation to optimal Bayesian filter under Gaussianity assumption.

Approximate dynamic programming algorithm: A new dynamic programming algorithm, namely dynamic optimization for length of horizon $L = 1$, is designed to control the waveform selection in the transmitter. This novel algorithm derives its information-processing power in two important ways:

- First, it is based on the notion of *imperfect-state information*, which gets around the fact that Bellman's dynamic programming requires perfect knowledge of the state, whereas in a real-world environment, the state is hidden from the radar.

- Second, cubature rule of third degree is used in the approximation of certain integrals involved in deriving the dynamic optimization algorithm.

Memory: The cognitive radar is equipped with perceptual memory in the receiver, executive memory in the transmitter, and the coordinating perception-action memory that reciprocally couples the two aforementioned memories. To distinguish all generations of the cognitive radar systems, we name the cognitive radar equipped with the basic perception-action cycle the *basic cognitive radar* and the one equipped with nested memory the *nested cognitive radar*.

Attention: To selectively allocate the available information-processing resources in the cognitive radar, we have also developed perceptual attention and executive attention in the nested and hierarchical cognitive radar systems. Using attention, the

feedback-information metric can be built to optimally allocate the resources pertaining to the cognitive radar system.

Intelligence: Among the four properties of cognitive radar, i.e. perception, memory, attention and intelligence, intelligence stands out as the most complex one due to the fact that the other three properties make contributions to intelligence in their own individual ways. Also, there is no separate structure of group of structures dedicated to intelligence as a separate functional block of the system. A comment that we can make here is that through the use of approximate dynamic programming, the cognitive radar becomes increasingly more intelligent as the feedback-information metric is progressively minimized, cycle after cycle.

6.2   Future Research Directions

In developing the underlying theory and system structure of cognitive radar, we found that there is still much future research that needs to be done in the application of cognition to radar systems. We summarize three future directions as follows:

New lower bound for cognitive radar: To assess the performance of an estimator, a lower bound is always desirable. The Cramér-Rao lower bound (CRLB) is a lower bound that is commonly used in time-invariant systems. It can be easily calculated as the inverse of Fisher information matrix. The CRLB represents the lowest possible mean squared error (MSE) for all unbiased estimators. For a dynamic system that is generally nonlinear, a similar version of the CRLB, namely the posterior Cramér-Rao lower bound (PCRB), was derived in [95]. To calculate it in an on-line manner, an iterative version of the PCRB was proposed in [96], where the posterior information matrix of the hidden state is decomposed for each discrete time instant

by virtue of the factorization of the joint probability density of the state variables. In this way, an iterative structure is obtained for the evolution of the information matrices.

Until now, utility of a lower bound has focused on traditional unbiased estimators, be it linear or nonlinear, continuous or discrete. For the cognitive radar system proposed in this thesis, we obviously have a feedback system, which means the estimator may be biased through continuous interactions between the system and the environment. Although the CRLB of an biased estimator is derived in [95], its calculation requires knowledge of the bias gradient matrix, which often does not exist. Hence, it is of limited practical value. In saying so, a new lower bound is needed for cognitive radar. Future research should be able to address this problem in the following manner:

- Under the framework of the basic cognitive radar, our first task is to develop a lower bound that uses available knowledge. Considering that a basic cognitive radar system is dynamic, the lower bound would have to be calculated iteratively. In a mathematical context, derivation of such a bound may well prove to be a challenging task.

- However, when we move onto the nested cognitive radar, the system becomes much more complicated because of the many feedback loops, global as well as local, that are distributed throughout the system and the fact that all three memory units in the system are nonlinear. In this new situation, we may have to be content with the use of Monte Carlo simulations to provide an assessment of overall system performance.

Chattering effect: Chattering effect has engaged a lot of control engineers' effort

in recent years. Although we have provided a mathematical analysis of chattering effect in cognitive radar, it is still in its primitive stage. Future research on the chattering effect will meet the following challenges:

- The benefits a cognitive radar can gain from chattering effect should be formulated quantitatively.

- The simulation results have also demonstrated another fact, which says the memory component in a nested cognitive radar is able to utilize the chattering effect more efficiently than a basic cognitive radar. More research is needed to discover the secret behind this fact.

External disturbance: Simulations conducted in Chapter 5 have shown that external disturbance is detrimental to the behavior of cognitive radar without memory. With the existence of external disturbance, basic cognitive radar exhibits difficulties in getting back to original operation. However, adding memory will confine the impact of disturbance to its minimum. Future research under this topic should follow the following directions:

- The reasons that basic cognitive radar fails and nested cognitive radar succeeds in the presence of external disturbance is an interesting topic that deserves attention.

- The capacity of nested cognitive radar to withstand external disturbance can be regarded as a joint research topic accompanied by the stability and lower bound study described earlier on in this section.

Appendix A

Cubature Kalman Filter (CKF)

The cubature Kalman filter is the closest known approximation to the Bayesian filter that could be designed in a nonlinear setting under the key assumption: The predictive density of the joint state-measurement random variable is Gaussian [56]. Under this assumption, the optimal Bayesian filter reduces to the problem of how to compute moment integrals whose integrands are of the following form:

$$\text{nonlinear function} \times \text{Gaussian.} \tag{A.1}$$

To numerically compute integrals whose integrands are of this form, we use a rule described next.

The Cubature Rule of Third Degree

Consider an example of the integrand described in Eq. (A.1), which consists of the nonlinear function $\mathbf{f}(\mathbf{x})$ multiplied by a multivariate Gaussian density denoted by

$\mathcal{N}(\mathbf{x}; \boldsymbol{\mu}, \boldsymbol{\Sigma})$, where $\boldsymbol{\mu}$ is the mean and $\boldsymbol{\Sigma}$ is the covariance. According to the third-degree cubature rule [97], the resulting integral may be approximated as follows:

$$\int_{\mathbb{R}^{N_x}} \mathbf{f}(\mathbf{x}) \mathcal{N}(\mathbf{x}; \boldsymbol{\mu}, \boldsymbol{\Sigma}) d\mathbf{x} \approx \frac{1}{2n} \sum_{i=1}^{2n} \mathbf{f}(\boldsymbol{\mu} + \sqrt{\boldsymbol{\Sigma}} \boldsymbol{\alpha}_i) \tag{A.2}$$

where N_x is the state-space dimension, and a square-root factor of the state-estimation error covariance $\boldsymbol{\Sigma}$ satisfies the factorization $\boldsymbol{\Sigma} = \sqrt{\boldsymbol{\Sigma}} \sqrt{\boldsymbol{\Sigma}}^T$; the set of $2n$ cubature points is given by

$$\boldsymbol{\alpha}_i = \begin{cases} \sqrt{n}\boldsymbol{e}_i, & i = 1, 2 \ldots n \\ -\sqrt{n}\boldsymbol{e}_{i-n}, & i = n+1, n+2 \ldots 2n. \end{cases} \tag{A.3}$$

with $\boldsymbol{e}_i \in \mathbb{R}^{N_x}$ denoting the i-th elementary column vector. The CKF specifically uses the third-degree cubature rule to numerically compute Gaussian weighted integrals [97]. This rule is exact for integrands being polynomials of degree up to three or any odd integer.

Next, we present the CKF's two-step update cycle, namely, the time update and the measurement update, as described next.

Time Update

In the time-update step, the CKF [56] computes the mean $\hat{\mathbf{x}}_{k|k-1}$ and the associated covariance $\mathbf{P}_{k|k-1}$ of the Gaussian predictive density numerically using cubature rules.

We write the predicted mean as follows

$$\hat{\mathbf{x}}_{k|k-1} = \mathbb{E}\left[\mathbf{x}_k | \mathbf{Z}_{k-1}\right], \tag{A.4}$$

where $\mathbb{E}\left[\cdot\right]$ is the statistical expectation operator; $\mathbf{Z}_k$ is the history of measurements available up to time k. Substituting the system equation (2.4) into Eq. (A.4) yields

$$\hat{\mathbf{x}}_{k|k-1} = \mathbb{E}\left[\mathbf{f}(\mathbf{x}_{k-1}) + \mathbf{v}_k | \mathbf{Z}_{k-1}\right]. \tag{A.5}$$

Because $\mathbf{v}_k$ is assumed to be zero-mean and uncorrelated with the measurement sequence, we get

$$
\begin{aligned}
\hat{\mathbf{x}}_{k|k-1} &= \mathbb{E}\left[\mathbf{f}(\mathbf{x}_{k-1}) | \mathbf{Z}_{k-1}\right] \\
&= \int_{\mathbb{R}^{N_x}} \mathbf{f}(\mathbf{x}_{k-1}) p(\mathbf{x}_{k-1} | \mathbf{Z}_{k-1}) d\mathbf{x}_{k-1} \\
&= \int_{\mathbb{R}^{N_x}} \mathbf{f}(\mathbf{x}_{k-1}) \mathcal{N}(\mathbf{x}_{k-1}; \hat{\mathbf{x}}_{k-1|k-1}, \mathbf{P}_{k-1|k-1}) d\mathbf{x}_{k-1},
\end{aligned} \tag{A.6}
$$

where, as before, $\mathcal{N}(.;.,.)$ is the conventional symbol for a Gaussian density. Similarly, we obtain the associated error covariance

$$
\begin{aligned}
\mathbf{P}_{k|k-1} &= \mathbb{E}[(\mathbf{x}_k - \hat{\mathbf{x}}_{k|k-1})(\mathbf{x}_k - \hat{\mathbf{x}}_{k|k-1})^T | \mathbf{Z}_{k-1}] \\
&= \int_{\mathbb{R}^{N_x}} \mathbf{f}(\mathbf{x}_{k-1})\mathbf{f}^T(\mathbf{x}_{k-1}) \mathcal{N}(\mathbf{x}_{k-1}; \hat{\mathbf{x}}_{k-1|k-1}, \mathbf{P}_{k-1|k-1}) d\mathbf{x}_{k-1} \\
&\quad - \hat{\mathbf{x}}_{k|k-1}\hat{\mathbf{x}}_{k|k-1}^T + \mathbf{Q}_{k-1},
\end{aligned} \tag{A.7}
$$

where $\mathbf{Q}_k$ is the covariance of system noise $\mathbf{v}_k$.

Measurement Update

Recognizing that the so-called innovation process is not only white but also zero-mean Gaussian when the additive measurement noise is Gaussian, the predicted measurement may be estimated in the least-square error sense. In this case, we write the predicted measurement density (also called the filter likelihood density) as follows

$$p(\mathbf{z}_k|\mathbf{Z}_{k-1}) = \mathcal{N}(\mathbf{z}_k; \hat{\mathbf{z}}_{k|k-1}, \mathbf{P}_{\mathbf{zz},k|k-1}), \tag{A.8}$$

where the predicted measurement itself and the associated covariance are respectively given by

$$\hat{\mathbf{z}}_{k|k-1} = \int_{\mathbb{R}^{N_x}} \mathbf{h}(\mathbf{x}_k)\mathcal{N}(\mathbf{x}_k; \hat{\mathbf{x}}_{k|k-1}, \mathbf{P}_{k|k-1})d\mathbf{x}_k \tag{A.9}$$

$$\mathbf{P}_{\mathbf{zz},k|k-1} = \int_{\mathbb{R}^{N_x}} \mathbf{h}(\mathbf{x}_k)\mathbf{h}^T(\mathbf{x}_k)\mathcal{N}(\mathbf{x}_k; \hat{\mathbf{x}}_{k|k-1}, \mathbf{P}_{k|k-1})d\mathbf{x}_k$$
$$-\hat{\mathbf{z}}_{k|k-1}\hat{\mathbf{z}}_{k|k-1}^T + \mathbf{R}_k(\boldsymbol{\theta}_{k-1}). \tag{A.10}$$

Accordingly, we may write the Gaussian conditional density of the joint state and measurement:

$$p\left([\mathbf{x}_k^T, \mathbf{z}_k^T]^T|\mathbf{Z}_{k-1}\right) = \mathcal{N}\left(\begin{bmatrix} \hat{\mathbf{x}}_{k|k-1} \\ \hat{\mathbf{z}}_{k|k-1} \end{bmatrix}, \begin{bmatrix} \mathbf{P}_{k|k-1} & \mathbf{P}_{\mathbf{xz},k|k-1} \\ \mathbf{P}_{\mathbf{xz},k|k-1}^T & \mathbf{P}_{\mathbf{zz},k|k-1} \end{bmatrix}\right), \tag{A.11}$$

where the cross-covariance is

$$\mathbf{P}_{\mathbf{xz},k|k-1} = \int_{\mathbb{R}^{N_x}} \mathbf{x}_k\mathbf{h}^T(\mathbf{x}_k)\mathcal{N}(\mathbf{x}_k; \hat{\mathbf{x}}_{k|k-1}, \mathbf{P}_{k|k-1})d\mathbf{x}_k - \hat{\mathbf{x}}_{k|k-1}\hat{\mathbf{z}}_{k|k-1}^T. \tag{A.12}$$

On the receipt of a new measurement $\mathbf{z}_k$, the CKF computes the posterior density $p(\mathbf{x}_k|\mathbf{Z}_k)$ from Eq. (A.11) yielding

$$p(\mathbf{x}_k|\mathbf{Z}_k) \;\; = \;\; \frac{p(\mathbf{x}_k, \mathbf{z}_k|\mathbf{Z}_{k-1})}{p(\mathbf{z}_k|\mathbf{Z}_{k-1})} = \mathcal{N}(\mathbf{x}_k; \hat{\mathbf{x}}_{k|k}, \mathbf{P}_{k|k}), \tag{A.13}$$

where

$$\hat{\mathbf{x}}_{k|k} \;\; = \;\; \hat{\mathbf{x}}_{k|k-1} + \mathbf{G}_k(\mathbf{z}_k - \hat{\mathbf{z}}_{k|k-1}) \tag{A.14}$$

$$\mathbf{P}_{k|k} \;\; = \;\; \mathbf{P}_{k|k-1} - \mathbf{G}_k \mathbf{P}_{\mathbf{zz},k|k-1} \mathbf{G}_k^T, \tag{A.15}$$

with the *Kalman gain* being defined by

$$\mathbf{G}_k \;\; = \;\; \mathbf{P}_{\mathbf{xz},k|k-1} \mathbf{P}_{\mathbf{zz},k|k-1}^{-1}. \tag{A.16}$$

In summary, the CKF numerically computes Gaussian weighted integrals that are present in Eqs. (A.6)-(A.7), (A.9)-(A.10) and (A.12) using cubature rules. From Eqs. (A.10) and (A.15) we notice that the error covariance matrix $\mathbf{P}_{k|k}$ indeed relies on the waveform parameter $\boldsymbol{\theta}_{k-1}$, on which the radar transmitter acts at time $k-1$. For simplification of presentation, when we use $\mathbf{P}_{k|k}$ in the rest of the thesis, its full expression is $\mathbf{P}_{k|k}(\boldsymbol{\theta}_{k-1})$.

Appendix B

Continuous-Discrete Cubature

Kalman Filter (CD-CKF)

In this appendix, we describe the two steps of continuous-discrete cubature Kalman filter (CD-CKF)[58].

Time Update

With the Itô-Taylor expansion of order 1.5, we can now update the posterior density of the state before the next observable is available. Let us denote $\mathbf{x}_k^m$ as the intermediate state at time $t = kT + m\delta$, where $m = 1, ..., T/\delta$. Since $\mathbf{x}_k$ follows the Gaussian distribution, i.e., $\mathbf{x}_k \sim \mathcal{N}(\hat{\mathbf{x}}_{k|k}, \mathbf{P}_{k|k})$, we may express the m-th predicted state estimate as

$$
\hat{\mathbf{x}}_{k|k}^m = \mathbb{E}\left[\mathbf{x}_k^m | \mathbf{Z}_k\right] \tag{B.17}
$$

$$
= \mathbb{E}\left[\mathbf{f}_d(\mathbf{x}_k, kT) + \sqrt{\mathbf{Q}}\boldsymbol{\omega} + (\mathbb{L}\mathbf{f}(\mathbf{x}_k, kT))\boldsymbol{\psi} | \mathbf{Z}_k\right], \tag{B.18}
$$

where $\boldsymbol{\omega}$ and $\boldsymbol{\psi}$ are both independent Gaussian processes with $\boldsymbol{\omega} \sim \mathcal{N}(\mathbf{0}, \delta\mathbf{I}_{N_x})$, $\boldsymbol{\psi} \sim \mathcal{N}(\mathbf{0}, \frac{1}{3}\delta^3\mathbf{I}_{N_x})$ and $\mathbb{E}\left[\boldsymbol{\omega}\boldsymbol{\psi}^T\right] = \frac{1}{2}\delta^2\mathbf{I}_{N_x}$. We now simplify Eq. (B.18) to

$$\hat{\mathbf{x}}_{k|k}^m = \mathbb{E}\left[\mathbf{f}_d(\mathbf{x}_k, kT)|\mathbf{Z}_k\right] \tag{B.19}$$

$$= \int_{\mathbb{R}^{N_x}} \mathbf{f}_d(\mathbf{x}_k, kT)\mathcal{N}(\mathbf{x}_k; \hat{\mathbf{x}}_{k|k}, \mathbf{P}_{k|k})d\mathbf{x}_k. \tag{B.20}$$

Using the same strategy, we may also simplify the state-error covariance matrix

$$\mathbf{P}_{k|k}^m = \mathbb{E}\left[(\mathbf{x}_k^m - \hat{\mathbf{x}}_{k|k}^m)(\mathbf{x}_k^m - \hat{\mathbf{x}}_{k|k}^m)^T|\mathbf{Z}_k\right] \tag{B.21}$$

$$= \int_{\mathbb{R}^{N_x}} \mathbf{f}_d(\mathbf{x}_k, kT)\mathbf{f}_d^T(\mathbf{x}_k, kT)\mathcal{N}(\mathbf{x}_k; \hat{\mathbf{x}}_{k|k}, \mathbf{P}_{k|k})d\mathbf{x}_k +$$

$$\frac{\delta^3}{3}\int_{\mathbb{R}^{N_x}} (\mathbb{L}\mathbf{f}(\mathbf{x}_k, kT))(\mathbb{L}\mathbf{f}(\mathbf{x}_k, kT))^T\mathcal{N}(\mathbf{x}_k; \hat{\mathbf{x}}_{k|k}, \mathbf{P}_{k|k})d\mathbf{x}_k +$$

$$\frac{\delta^2}{2}\left[\sqrt{\mathbf{Q}}(\hat{\tilde{\mathbf{x}}}_{k|k}^m)^T + (\hat{\tilde{\mathbf{x}}}_{k|k}^m)\sqrt{\mathbf{Q}}^T\right] + (\hat{\mathbf{x}}_{k|k}^m)(\hat{\mathbf{x}}_{k|k}^m)^T + \delta\mathbf{Q}, \tag{B.22}$$

where $\hat{\tilde{\mathbf{x}}}_{k|k}^m = \int_{\mathbb{R}^{N_x}} \mathbb{L}\mathbf{f}(\mathbf{x}_k, kT)\mathcal{N}(\mathbf{x}_k; \hat{\mathbf{x}}_{k|k}, \mathbf{P}_{k|k})d\mathbf{x}_k$.

For a system equation with *mild* nonlinearities, we could approximate its differentials at time k by replacing $\mathbf{x}_k$ with its filtered estimate $\hat{\mathbf{x}}_{k|k}$. This assumption will eliminate the necessity to evaluate integrals for the higher-order expansion in Eq. (B.22) and yields

$$\mathbf{P}_{k|k}^m \approx \int_{\mathbb{R}^{N_x}} \mathbf{f}_d(\mathbf{x}_k, kT)\mathbf{f}_d^T(\mathbf{x}_k, kT)\mathcal{N}(\mathbf{x}_k; \hat{\mathbf{x}}_k, \mathbf{P}_{k|k})d\mathbf{x}_k +$$

$$\frac{\delta^3}{3}(\mathbb{L}\mathbf{f}(\hat{\mathbf{x}}_{k|k}, kT))(\mathbb{L}\mathbf{f}(\hat{\mathbf{x}}_{k|k}, kT))^T +$$

$$\frac{\delta^2}{2}\left[\sqrt{\mathbf{Q}}(\mathbb{L}\mathbf{f}(\hat{\mathbf{x}}_{k|k}, kT))^T + (\mathbb{L}\mathbf{f}(\hat{\mathbf{x}}_{k|k}, kT))\sqrt{\mathbf{Q}}^T\right] -$$

$$(\hat{\mathbf{x}}_{k|k}^m)(\hat{\mathbf{x}}_{k|k}^m)^T + \delta\mathbf{Q}. \tag{B.23}$$

Using the third-order cubature rule to calculate the integrals numerically, we obtain the state and error covariance as follows:

$$\hat{\mathbf{x}}_{k|k}^m \approx \frac{1}{2n} \sum_{i=1}^{2n} X_{i,k|k}^{*(m)} \tag{B.24}$$

$$\mathbf{P}_{k|k}^m \approx (\mathcal{X}_{k|k}^{*(m)})(\mathcal{X}_{k|k}^{*(m)})^T + \frac{\delta^3}{3}(\mathbb{L}\mathbf{f}(\hat{\mathbf{x}}_{k|k}, kT))(\mathbb{L}\mathbf{f}(\hat{\mathbf{x}}_{k|k}, kT))^T +$$
$$\frac{\delta^2}{2}\left[\sqrt{\mathbf{Q}}(\mathbb{L}\mathbf{f}(\hat{\mathbf{x}}_{k|k}, kT))^T + (\mathbb{L}\mathbf{f}(\hat{\mathbf{x}}_{k|k}, kT))\sqrt{\mathbf{Q}}^T\right] + \delta\mathbf{Q}, \tag{B.25}$$

where

$$X_{i,k|k}^{*(m)} = \mathbf{f}_d(\hat{\mathbf{x}}_{k|k} + \mathbf{P}_{k|k}^{1/2}\boldsymbol{\alpha}_i, kT) \tag{B.26}$$

$$\mathcal{X}_{k|k}^{*(m)} = \frac{1}{\sqrt{2n}}\left[X_{1,k|k}^{*(m)} - \hat{\mathbf{x}}_{k|k}^m \quad X_{2,k|k}^{*(m)} - \hat{\mathbf{x}}_{k|k}^m \quad \cdots \quad X_{2n,k|k}^{*(m)} - \hat{\mathbf{x}}_{k|k}^m \right], \tag{B.27}$$

where the cubature points $\boldsymbol{\alpha}_i$ are defined in accordance to Eq. (A.3), with $2n$ denoting the number of cubature points.

Eqs. (B.24) and (B.25) are computed for m consecutive loops until we end up with the time update and obtain $(\hat{\mathbf{x}}_{k|k}^m, \mathbf{P}_{k|k}^m)$, which is used as the predicted state and its corresponding error covariance, i.e., $(\hat{\mathbf{x}}_{k+1|k}, \mathbf{P}_{k+1|k})$. The state and its error covariance are updated upon receiving a new measurement at time $t_{k+1} = kT + m\delta$.

Measurement Update

For the CD-CKF, the discrete measurement equation is same as that of the CKF. Therefore, for any new measurement $\mathbf{z}_k$, we can use the same update strategy. The measurement update starts with the propagation of the cubature points to predict

the measurement and its associated covariance, expressed as

$$\hat{\mathbf{z}}_{k|k-1} \;=\; \frac{1}{2n}\sum_{i=1}^{2n} Z_{i,k|k-1} \tag{B.28}$$

$$\mathbf{P}_{\mathbf{zz},k|k-1} \;=\; \frac{1}{2n}\sum_{i=1}^{2n} Z_{i,k|k-1}Z_{i,k|k-1}^{T} - \hat{\mathbf{z}}_{k|k-1}\hat{\mathbf{z}}_{k|k-1}^{T} + \mathbf{R}_k(\boldsymbol{\theta}_{k-1}), \tag{B.29}$$

where $2n$ is the number of cubature points, and $Z_{i,k|k-1}$ is the i-th propagated cubature point originating from $X_{i,k|k-1}$, as given by

$$X_{i,k|k-1} \;=\; \mathbf{P}_{k|k-1}^{1/2}\boldsymbol{\alpha}_i + \hat{\mathbf{x}}_{k|k-1} \tag{B.30}$$

$$Z_{i,k|k-1} \;=\; \mathbf{h}(X_{i,k|k-1}). \tag{B.31}$$

Similarly, the cross-covariance between the state and the measurement can be written as

$$\mathbf{P}_{\mathbf{xz},k|k-1} \;=\; \frac{1}{2n}\sum_{i=1}^{2n} X_{i,k|k-1}Z_{i,k|k-1}^{T} - \hat{\mathbf{x}}_{k|k-1}\hat{\mathbf{z}}_{k|k-1}^{T}. \tag{B.32}$$

The new measurement $\mathbf{z}_k$ is then incorporated into the update of the state and its covariance, is given by:

$$\hat{\mathbf{x}}_{k|k} \;=\; \hat{\mathbf{x}}_{k|k-1} + \mathbf{G}_k(\mathbf{z}_k - \hat{\mathbf{z}}_{k|k-1}) \tag{B.33}$$

$$\mathbf{P}_{k|k} \;=\; \mathbf{P}_{k|k-1} - \mathbf{G}_k\mathbf{P}_{\mathbf{zz},k|k-1}\mathbf{G}_k^{T}, \tag{B.34}$$

with the *Kalman gain* being defined by

$$\mathbf{G}_k \;=\; \mathbf{P}_{\mathbf{xz},k|k-1}\mathbf{P}_{\mathbf{zz},k|k-1}^{-1}. \tag{B.35}$$

Appendix C

Approximate Dynamic Programming for Waveform Selection

At any discrete time k, the waveform-selection algorithm seeks to find the set of best waveform parameters by minimizing a cost-to-go function for a rolling horizon of L steps, that is, to minimize the cost incurred in steps $k : k + L - 1$. Denoting the control policy for the next L steps by $\pi_k = \{\mu_k, ..., \mu_{k+L-1}\}$ with the policy function $\mu(\mathbf{I}_k) = \boldsymbol{\theta}_k \in \mathcal{P}_k$ mapping the information vector into an action in the waveform library $\mathcal{P}_k$, we wish to find a policy π_k at time k corresponding to the solution of the following minimization:

$$\min_{\pi_k} \mathbb{E}\left[\sum_{i=k}^{k+L-1} g(\mathbf{x}_i, \boldsymbol{\theta}_i)\right]. \tag{C.36}$$

The cost function $g(\cdot, \cdot)$ inside the summation is defined in (2.26). Obviously, for an L-step dynamic programming algorithm, we need to predict L-steps ahead, which

also means that accurate performance of the predictor in the receiver is of crucial importance to the cognitive tracking radar.

Algorithm Description

As a general case of dynamic optimization algorithm described in Chapter 2, the recursive dynamic programming (DP) algorithm at time k is made up of two parts: Terminal point:

$$\mathcal{J}(\mathbf{I}_{k+L-1}) = \min_{\boldsymbol{\theta}_{k+L-1} \in \mathcal{P}_{k+L-1}} g(\mathbf{x}_{k+L-1}, \boldsymbol{\theta}_{k+L-1}) \tag{C.37}$$

Intermediate points:

$$\mathcal{J}(\mathbf{I}_p) = \min_{\boldsymbol{\theta}_p \in \mathcal{P}_p} \left[g(\mathbf{x}_p, \boldsymbol{\theta}_p) + \mathbb{E}_{\mathbf{x}_{p+1}, \mathbf{z}_{p+1} | \mathbf{I}_p, \boldsymbol{\theta}_p} \left[\mathcal{J}_{p+1} \right] \right] \tag{C.38}$$

for $p = k, ..., k + L - 2$, where $\mathcal{J}_{p+1} = \mathcal{J}(\mathbf{I}_p, \mathbf{z}_{p+1}, \boldsymbol{\theta}_p)$ and $\mathcal{P}_k$ is the waveform library at time k. With Eq. (C.37) pertaining to the terminal point, Eq. (C.38) pertains to the intermediate points that go backward from the terminal point in $(L - 1)$ steps. The optimal policy $\{\mu_k^*, ..., \mu_{k+L-1}^*\}$ is obtained in the following two-step manner:

1. We first minimize the terminal point (C.37) for every possible value of the information vector $\mathbf{I}_{k+L-1}$ to obtain μ_{k+L-1}^*. Meanwhile, $\mathcal{J}_{k+L-1}$ is also computed;

2. Then, $\mathcal{J}_{k+L-1}$ is substituted into the calculation of the intermediate points (C.38) to obtain μ_{k+L-2}^* over every possible value of $\mathbf{I}_{k+L-2}$. This step is repeated until we reach the initial point with μ_k^*.

Measurement Space Approximation

The measurement space is an infinite dimensional continuous-valued space. Moreover, the dimension of this space grows exponentially with depth of the optimization horizon L. In fact, at each step of the optimization, we need to examine an infinite number of possibilities that the perfect state information vector $\mathbf{I}_k$ can evolve to the next step in time. To simplify this computation, we use the same approximation technique used in development of the CKF in Section 2.3 by approximating the expectation in Eq. (2.26) using the third-degree cubature-rule. According to CKF, the predicted measurement $\mathbf{z}_{k+1}$ is Gaussian-distributed with mean $\hat{\mathbf{z}}_{k+1|k}$ as in Eq. (A.9) and covariance $\mathbf{P}_{\mathbf{zz},k+1|k}$ in Eq. (A.10). Therefore the expectation term in Eq. (2.26) may now be written as

$$
\begin{aligned}
\mathbb{E}_{\mathbf{x}_{k+1},\mathbf{z}_{k+1}|\mathbf{I}_k,\boldsymbol{\theta}_k} \left[\mathrm{Tr}(\mathbf{P}_{k+1|k+1}) \right] &= \mathrm{Tr}\left(\mathbb{E}_{\mathbf{x}_{k+1},\mathbf{z}_{k+1}|\mathbf{I}_k,\boldsymbol{\theta}_k} \left[\mathbf{P}_{k+1|k+1} \right] \right) \\
&= \mathrm{Tr}\left(\int_{\mathbb{R}^{N_z}} \mathbf{P}_{k+1|k+1} p(\mathbf{z}_{k+1}|\mathbf{I}_k,\mathbf{x}_{k+1},\boldsymbol{\theta}_k) d\mathbf{z}_{k+1} \right) \\
&= \mathrm{Tr}\left(\int_{\mathbb{R}^{N_z}} \mathbf{P}_{k+1|k+1} \mathcal{N}(\hat{\mathbf{z}}_{k+1|k},\mathbf{P}_{\mathbf{zz},k+1|k}) d\mathbf{z}_{k+1} \right).
\end{aligned}
$$

$$(C.39)$$

Using the cubature-rule of (A.2) to approximate the integral in (C.39) , we obtain

$$
\mathbb{E}_{\mathbf{x}_{k+1},\mathbf{z}_{k+1}|\mathbf{I}_k,\boldsymbol{\theta}_k} \left[\mathrm{Tr}(\mathbf{P}_{k+1|k+1}) \right] \approx \mathrm{Tr}\left(\frac{1}{2n_z} \sum_{i=1}^{2n_z} \mathbf{P}_{k+1|k+1} \left(\hat{\mathbf{z}}_{k+1|k} + \mathbf{P}_{\mathbf{zz},k+1|k}^{1/2} \boldsymbol{\alpha}_i \right) \right),
$$

$$(C.40)$$

where $\mathbf{P}_{k+1|k+1}$ is expressed as a function of $(\hat{\mathbf{z}}_{k+1|k} + \mathbf{P}_{\mathbf{zz},k+1|k}^{1/2} \boldsymbol{\alpha}_i)$, and $\mathbf{P}_{\mathbf{zz},k+1|k}^{1/2}$ is the square root of the covariance matrix $\mathbf{P}_{\mathbf{zz},k+1|k}$ and the cubature points $\boldsymbol{\alpha}_i$ are defined

in accordance to Eq. (A.3), with $2n_z$ denoting the number of cubature points.

Thus, using the approximation of Eq. (C.40), the DP algorithm is simplified into the following pair of equations:

Terminal point:

$$\mathcal{J}(\mathbf{I}_{k+L-1}) \;\;=\;\; \min_{\boldsymbol{\theta}_{k+L-1}\in\mathcal{P}_{k+L-1}} \mathrm{Tr}(\mathbf{P}_{k+L|k+L}) \tag{C.41}$$

Intermediate points:

$$\mathcal{J}(\mathbf{I}_p) \;\;=\;\; \min_{\boldsymbol{\theta}_p\in\mathcal{P}_p} \mathrm{Tr}\left(\mathbf{P}_{p+1|p+1} + \frac{1}{2n_z}\sum_{i=1}^{2n_z}\mathbf{P}_{p+1|p+1}\left(\hat{\mathbf{z}}_{p+1|p} + \mathbf{P}_{\mathbf{zz},p+1|p}^{1/2}\boldsymbol{\alpha}_i\right)\right) \tag{C.42}$$

for $p = k, ..., k + L - 2$. In other words, the terminal point (C.41) computes the cost-to-go function looking L cycles into the future, where L is the prescribed depth of horizon. Then, starting with the computed cost $\mathcal{J}(\mathbf{I}_{k+L-1})$, the DP algorithm (C.42) computes the sequence of cost-to-go functions by going backward from the terminal point step-by-step till we arrive at the present cycle time k. We need to mention that intermediate points (C.42) collapse to terminal point (C.41) if and only if $L = 1$.

The DP algorithm of Eqs. (C.41) and (C.42) includes dynamic optimization of the CTR as a special case. For the case when there is no provision of a horizon looking into the future of $L \geq 2$, the terminal point in (C.41) defines the dynamic optimization algorithm. Then, there is a single cost-to-go function to be optimized as shown by

$$\mathcal{J}(\mathbf{I}_k) \;\;=\;\; \min_{\boldsymbol{\theta}_k\in\mathcal{P}_k} \mathrm{Tr}(\mathbf{P}_{k+1|k+1}). \tag{C.43}$$

Curse of Dimensionality

Unfortunately, when we include a horizon depth of L time-steps into the future in the DP algorithm, which is a highly desirable thing to do, we may run into Bellman's curse-of-dimensionality problem. To explain this important practical issue, we define the following parameters:

- N_z: the measurement-space dimension

- N_x: the state-space dimension

- N_g: the waveform-parameter grid size

- L: dynamic-programming horizon-depth

In general, the complexity of the dynamic-programming algorithm for waveform selection is of the order of

$$\mathcal{O}(N_s^3 (2N_z N_g)^L) \tag{C.44}$$

where $N_s = \max(N_z, N_x)$, the term N_s^3 is for the matrix inversions in computing the expected error covariance matrix, and the term $2N_z$ is for the number of cubature points for computation of the expectation operators in computing the measurements of Eq. (C.42). For this general case, it is assumed that all individual optimizations in each stage of the DP are performed over the complete set of waveform-library grid. For the special case of dynamic optimization, it boils down to minimize the terminal point of (C.41).

We see from Eq. (C.44) that a main source of complexity in the DP algorithm is due to the exponential growth of computations arising from the horizon depth L. More specifically, at each stage or depth of DP and for each cubature point in Eq.

171

(C.44) a new search in the waveform library needs to be performed. We refer to such a complete search of the waveform library as the *global search*. As L increases, the level of computation becomes unsustainable.

To mitigate the curse-of-dimensionality problem, we may try to perform the optimization by searching a *local* neighbourhood of the current cubature point. In other words, we consider the use of an *explore-exploit strategy* for waveform selection by constraining the DP algorithm to be in a locality of the current cubature point as well as a limited-size neighbourhood in the wave-parameter grid. The exploration-exploitation strategy is discussed in [98] and [99].

Appendix D

Derivation of the Approximation Formula in Eq. (2.31)

To the best of our knowledge, the approximation described in Eq. (2.31) appeared for the first time in [22]; therein, however, no derivation was presented for the approximation. This appendix is intended to fill this gap. For brevity in notation, henceforth, we omit explicit representation of the dependence of $\hat{\mathbf{x}}_{k+1|k+1}$ on $(\mathbf{I}_k, \mathbf{x}_{k+1}, \mathbf{z}_{k+1}, \boldsymbol{\theta}_k)$, and also write $\bar{\mathbf{x}}_{k+1} = \mathbf{x}_{k+1} - \hat{\mathbf{x}}_{k+1|k+1}$, that is, we focus on Eq. (2.26) and thus write

$$g(\mathbf{x}_k, \boldsymbol{\theta}_k) = \mathbb{E}_{\mathbf{x}_{k+1}, \mathbf{z}_{k+1}|\mathbf{I}_k, \boldsymbol{\theta}_k} \left[\bar{\mathbf{x}}_{k+1}^T \bar{\mathbf{x}}_{k+1} \right] \tag{D.45}$$

$$= \mathbb{E}_{\mathbf{z}_{k+1}|\mathbf{I}_k, \mathbf{x}_{k+1}, \boldsymbol{\theta}_k} \mathbb{E}_{\mathbf{x}_{k+1}|\mathbf{I}_k, \boldsymbol{\theta}_k} \left[\bar{\mathbf{x}}_{k+1}^T \bar{\mathbf{x}}_{k+1} \right] \tag{D.46}$$

where in Eq. (D.46), we used the definition of conditional expectation.

The expectation in Eq. (D.46) is over the distribution $p(\mathbf{z}_{k+1}|\mathbf{I}_k, \mathbf{x}_{k+1}, \boldsymbol{\theta}_k)$. Observe that within the measurement prediction and update cycles of the CKF discussed

in Section 2.3, the measurements are functions of $\boldsymbol{\theta}_k$ solely through the noise covariance $\mathbf{R}(\boldsymbol{\theta}_k)$ defined in Eq. (2.21). Recognizing that the parameter vector $\boldsymbol{\theta}_k$ is irrelevant once the measurement $\mathbf{z}_{k+1}$ is available to the receiver, we are justified to approximate the distribution $p(\mathbf{z}_{k+1}|\mathbf{I}_k, \mathbf{x}_{k+1}, \boldsymbol{\theta}_k)$ by the predicted measurement distribution $p(\mathbf{z}_{k+1}|\mathbf{I}_k, \boldsymbol{\theta}_k)$. In other words, we may set $\mathbb{E}_{\mathbf{z}_{k+1}|\mathbf{I}_k, \mathbf{x}_{k+1}, \boldsymbol{\theta}_k}(\cdot) \approx \mathbb{E}_{\mathbf{z}_{k+1}|\mathbf{I}_k, \boldsymbol{\theta}_k}(\cdot)$ and therefore write

$$g(\mathbf{x}_k, \boldsymbol{\theta}_k) \quad \approx \quad \mathbb{E}_{\mathbf{z}_{k+1}|\mathbf{I}_k, \boldsymbol{\theta}_k} \mathbb{E}_{\mathbf{x}_{k+1}|\mathbf{I}_k, \boldsymbol{\theta}_k} \left[\bar{\mathbf{x}}_{k+1}^T \bar{\mathbf{x}}_{k+1} \right]. \tag{D.47}$$

Next, using the identity $\mathbf{x}^T \mathbf{y} = \mathrm{Tr}\left(\mathbf{y}\mathbf{x}^T\right)$ and the fact that order of the expectation and the trace are interchangeable, we may go on to write

$$g(\mathbf{x}_k, \boldsymbol{\theta}_k) \quad \approx \quad \mathbb{E}_{\mathbf{z}_{k+1}|\mathbf{I}_k, \boldsymbol{\theta}_k} \left[\mathrm{Tr}\left(\mathbb{E}_{\mathbf{x}_{k+1}|\mathbf{I}_k, \boldsymbol{\theta}_k} \left[\bar{\mathbf{x}}_{k+1} \bar{\mathbf{x}}_{k+1}^T \right] \right) \right]. \tag{D.48}$$

By definition, the expression of $\mathrm{Tr}(\cdot)$ in Eq. (D.48) is the state-estimation error covariance $\mathbf{P}_{k+1|k+1}$; hence,

$$g(\mathbf{I}_k, \boldsymbol{\theta}_k) \quad \approx \quad \mathbb{E}_{\mathbf{z}_{k+1}|\mathbf{I}_k, \boldsymbol{\theta}_k} \left[\mathrm{Tr}\left(\mathbf{P}_{k+1|k+1} \right) \right]. \tag{D.49}$$

Finally noting that in deriving the CKF, $\mathbf{P}_{k+1|k+1}$ is independent of the measurement $\mathbf{z}_{k+1}$, we now arrive at

$$\begin{aligned} g(\mathbf{I}_k, \boldsymbol{\theta}_k) \quad &\approx \quad \mathbb{E}_{\mathbf{z}_{k+1}|\mathbf{I}_k, \boldsymbol{\theta}_k} \left[\mathrm{Tr}\left(\mathbf{P}_{k+1|k+1} \right) \right] \\ &= \quad \mathrm{Tr}\left(\mathbf{P}_{k+1|k+1} \right), \end{aligned} \tag{D.50}$$

which is the desired approximation reported in Eq. (2.31).

174

Bibliography

[1] S. Haykin, *Adaptive Radar Signal Processing*. Wiley Interscience, 2007.

[2] M. I. Skolnik, Ed., *Radar Handbook*, 3rd ed. McGraw-Hill, 2008.

[3] F. E. Nathanson, J. P. Reilly, and M. N. Cohen, *Radar Design Principles*, 2nd ed. McGraw-Hill, 1991.

[4] F. E. Nathanson, *Radar Design Principles*, 1st ed. McGraw-Hill, 1969.

[5] [Online]. Available: http://www.radarworld.org/huelsmeyer.html

[6] C. Speidemann, Y. Chen, and W. S. Geisler, *The Cognitive Neurosciences*, 4th ed., M. S. Gazzaniga, Ed. MIT Press, 2009.

[7] S. Haykin, "Keynote lecture on cognitive dynamic systems," in *NIPS 2009*, Whistler, BC, Canada, 2009.

[8] [Online]. Available: http://histru.bournemouth.ac.uk/Oral_History/Talking_About_Technology/radar_research/the_magnetron.html

[9] J. R. Klauder, A. C. Price, S. Darlington, and W. J. Albersheim, "The theory and design of chirp radars," *Bell Syst. Tech. J.*, vol. 39, pp. 745–808, 1960.

[10] A. A. Oliner and G. H. Knittel, *Phased Array Antennas*.   Artech House, 1972.

[11] J. A. Thomas, C. F. Moss, and M. Vater, *Echolocation in Bats and Dolphins*. The University of Chicago Press, 2004.

[12] Z. W. Pylyshyn, *Computation and Cognition*.   MIT Press, 1984.

[13] J. M. Fuster, *Cortex and Mind: Unifying Cognition*.   Oxford University Press, 2003.

[14] S. Haykin, "Cognitive radar: a way of the future," *IEEE Signal Processing Magazine*, vol. 23, pp. 30–40, 2006.

[15] P. M. Woodward, *Probability and Information Theory, with Applications to Radar*.   Pergamon, 1953.

[16] H. L. V. Trees, *Detection, Estimation and Modulation Theory, Part III*.   Wiley Press, 1971.

[17] D. F. Delong and E. M. Hofstetter, "On the design of optimum radar waveforms for clutter rejection," *IEEE Trans. on Information Theory*, vol. 13, no. 3, pp. 454–463, 1967.

[18] ——, "The design of clutter-resistant radar waveform with limited dynamic range," *IEEE Trans. on Information Theory*, vol. 15, no. 3, pp. 376–385, 1969.

[19] S. Boyd and L. Vandeberghe, *Convex Optimization*.   Cambridge University Press, 2004.

[20] S. Haykin, T. Kirubarajan, and B. Currie, "Adaptive radar for improved small target detection in a maritime environment," Adaptive Systems Laboratory, McMaster University," ASL Report 03-01, 2003.

[21] M. Athans and F. C. Schweppe, "Optimal waveform design via control theoretic principles," *Information and Control*, vol. 10, pp. 335–377, April 1967.

[22] D. J. Kershaw and R. J. Evans, "Optimal waveform selection for tracking systems," *IEEE Trans. on Information Theory*, vol. 40, pp. 1536–1550, 1994.

[23] ——, "Waveform selective probabilistic data association," *IEEE Trans. Aerosp. Electron. Syst.*, vol. 33, pp. 1180–1188, 1997.

[24] H. W. Sorenson, Ed., *Kalman filtering: Theory and application.* IEEE Press, 1985.

[25] S. J. Julier and J. K. Uhlmann, "A new extension of the Kalman filter to nonlinear systems," *Proc. of AeroSense: The 11th Int. Symp. on Aerospace/Defence Sensing, Simulation and Controls*, April 1997.

[26] N. J. Gordon, D. J. Salmond, and A. F. M. Smith, "Novel approach to nonlinear/non-Gaussian Bayesian state estimation," *IEE Proc-F*, vol. 140, no. 2, pp. 107–113, 1993.

[27] S. P. Sira, A. P. Suppappola, and D. Morrell, "Dynamic configuration of time-varying waveforms for agile sensing and tracking in clutter," *IEEE Trans. on Signal Processing*, vol. 55, pp. 3207–3217, 2007.

[28] S. Suvorova and S. D. Howard, "Waveform libraries for radar tracking applications: Maneuvering targets," in *Proceedings of 2006 Conference on Information Sciences and Systems*, 2006, pp. 1424–1428.

[29] P. M. Woodward, "Information theory and the design of radar receivers," *Proc. IRE*, vol. 39, pp. 1521–1524, December 1951.

[30] P. M. Woodward and I. L. Davis, "A theory of radar information," *Phil. Mag.*, vol. 41, pp. 1101–1117, October 1951.

[31] M. R. Bell, "Information theory and radar: Mutual information and the design and analysis of radar waveforms and systems," Ph.D. dissertation, California Institute of Technology, 1988.

[32] ——, "Information theory and radar waveform," *IEEE Trans. on Infor. Theo.*, vol. 39, no. 5, pp. 1578–1597, September 1993.

[33] A. Leshem, O. Naparstek, and A. Nehorai, "Information theoretic adaptive radar waveform design for multiple extended targets," *IEEE Journal on Selected Topics in Signal Processing*, vol. 1, no. 1, pp. 42–55, 2007.

[34] T. M. Cover and J. A. Thomas, *Elements of Information Theory.* NY: Wiley-Interscience, 1991.

[35] S. Haykin, Y. Xue, and T. N. Davidson, "Optimal waveform design for cognitive radar," *42nd Asilomar Conference on Signals, Systems and Computers*, pp. 3–7, October 2008.

[36] N. A. Goodman, P. R. Vaenkata, and M. A. Neifeld, "Adaptive waveform design and sequential hypothesis testing for target recognition with active sensors,"

IEEE Journal of Selected Topics in Signal Processing, vol. 1, pp. 105–113, June 2007.

[37] A. Newell, *Unified Theories of Cognition.*   Harvard University Press, 1990.

[38] F. Rosenblatt, "A probabilistic model for information storage and organization in the brain," *Psychological Review*, vol. 65, no. 6, pp. 386–408, 1958.

[39] M. L. Minsky and S. A. Papert, *Perceptrons.*   Cambridge, MA: MIT Press, 1969.

[40] D. S. Broomhead and D. Lowe, "Multivariable functional interpolation and adaptive networks," *Complex Systems*, vol. 2, pp. 321–335, 1988.

[41] T. Poggio and F. Girosi, "Networks for approximation and learning," *Proceedings of the IEEE*, vol. 78, pp. 1481–1497, 1990.

[42] V. N. Vapnik, *Statistical Learning Theory.*   Wiley Press, 1998.

[43] H. Jaeger, "Harnessing nonlinearity: Predicting chaotic systems and saving energy in wireless communication," *Science*, vol. 304, pp. 18–80, April 2004.

[44] Y. Xue, L. Yang, and S. Haykin, "Decoupled echo state networks with lateral inhibition," *Neural Networks*, vol. 20, no. 3, pp. 365–376, April 2007.

[45] C. E. Shannon, "A mathematical theory of communication," *The Bell System Technical Journal*, vol. 27, pp. 379–423,623–656, July, October 1948.

[46] S. Haykin, A. Zia, Y. Xue, and I. Arasaratnam, "Cognitive tracking radar: Theory and simulations," *Digital Signal Processing*, pp. under review DSP–10–65, 2010.

[47] S. Haykin, "Cognitive dynamic systems," *Proceedings of the IEEE*, vol. 94, no. 11, pp. 1910–1911, November 2006.

[48] Y. C. Ho and R. C. K. Lee, "A Bayesian approach to problems in stochastic estimation and control," *IEEE Trans. Automatic Control*, vol. 9, pp. 333–339, 1964.

[49] R. Bellman, *Dynamic Programming*. Princeton University Press, 1957.

[50] S. Haykin, *Communication Systems*. Wiley Press, 2000.

[51] D. P. Bertsekas, *Dynamic Programming and Optimal Control*, third, Ed. Athena Scientific, 2005.

[52] A. H. Jazwinski, *Stochastic Processes and Filtering Theory*. NY: Academic, 1970.

[53] P. E. Kloeden and E. Platen, *Numerical Solution of Stochastic Differential Equations*. Springer: Berlin, 1999.

[54] A. P. Sage and J. L. Melsa, *System Identification*. Academic Press, 1971.

[55] F. Daum, "Nonlinear filter: Beyond the Kalman filter," *IEEE A&E Systems Magazine*, vol. 20, no. 8, pp. 57–69, August 2005.

[56] I. Arasaratnam and S. Haykin, "Cubature Kalman filters," *IEEE Trans. Automatic Control*, vol. 54, pp. 1254–1269, June 2009.

[57] A. H. Stroud, *Approximate Calculation of Multiple Integrals*. Prentice Hall, 1971.

[58] I. Arasaratnam, S. Haykin, and T. R. Hurd, "Cubature Kalman filter for continuous-discrete systems: Theory and simulations," *IEEE Trans. on Signal Processing*, p. under review, 2010.

[59] S. Sarkka, "On unscented Kalman filtering for state estimation of continuos-time nonlinear systems," *IEEE Trans. on Automatic Control*, vol. 52, no. 9, pp. 1631–1641, September 2007.

[60] C. Uller, *The Evolution of Cognition: The Case of Number*, ser. Computation, Cognition, and Pylyshyn, D. Dedrick and L. Trick, Eds.   The MIT Press, 2009.

[61] S. Haykin and Y. Xue, "New generation of radar systems enabled with cognition," US Patent US serial 61/331,977, 2010.

[62] S. Haykin, "New generation of radar systems enabled with cognition," in *2010 IEEE Radar Conference*, Arlington, VA, USA, May 2010.

[63] W. James, *Principles of Psychology*, 1890.

[64] J. Bryant and D. Miron, "Excitation-transfer theory," in *Communication and emotion: Essays in honor of Dolf Zillmann*, J. Bryant, D. Roskos-Ewoldsen, and J. Cantor, Eds.   NJ: Erlbaum: Mahwah, 2003, pp. 31–59.

[65] E. I. Knudsen, "Fundamental components of attention," *Annu. Rev. Neurosci.*, vol. 30, pp. 57–78, 2007.

[66] A. D. Braddeley, *Essentials of Human Memory*.   Psychology Press Ltd, 1999.

[67] A. S. Reber, *Penguin Dictionary of Psychology*.   Penguin Reference, 1995.

[68] S. Legg and M. Hutter, "A collection of defintions of intelligence," in *Advances in Artifical General Intelligence: Concepts Architectures and Algorithms*, B. Goertzel and P. Wang, Eds. IOS Press, 2007, pp. 17–24.

[69] M. A. Fishchler and O. Firschein, *Intelligence: The Eye, the Brain, and the Computer.* Addison-Wesley Publishing Company Inc., 1987.

[70] W. Baldygo, M. Wicks, R. Brown, P. Antonik, G. Capraro, and L. Hennington, "Artificial intelligence applications to constant false alarm rate (CFAR) processing," *Proc. IEEE 1993 Nat. Radar Conf.*, pp. 275–280, April 1993.

[71] G. T. Capraro, A. Farina, H. Griffiths, and M. C. Wicks, "Knowledge-based radar signal and data processing: A tutorial overview," *IEEE Signal Processing Magazine*, vol. 23, no. 1, pp. 18–29, 2006.

[72] F. Gini and M. Rangaswamy, Eds., *Knowledge Based Radar Detection, Tracking and Classification.* Wiley Interscience, 2008.

[73] S. Haykin, *Neural Networks and Learning Machines.* Prentice hall, 2009.

[74] P. J. Werbos, "Beyond regression: New tools for prediction and analysis in the behavioral sciences," Ph.D. dissertation, Harvard University, 1974.

[75] ——, "Backpropagation through time: What it does and how to do it," *Proceedings of IEEE*, vol. 78, pp. 1550–1560, 1990.

[76] D. O. Hebb, *The Organization of Behavior: A Neuropsychological Theory.* Wiley Press, 1949.

[77] T. D. Sanger, "Optimal unsupervised learning in a single-layer feedforward neural network," *Neural Networks*, vol. 2, pp. 459–473, 1989.

[78] B. R. Mahafza, *Radar Systems Analysis and Design Using Matlab.* Chapman & Hall/CRC, 2000.

[79] Y. Bar-Shalom and X. Li, *Estimation and Tracking: Principles, Techniques and Software.* Artech House, 1993.

[80] M. Athans, R. P. Wishner, and A. Bertolini, "Suboptimal state estimation for continuous-time nonlinear systems from discrete noise measurements," *IEEE Trans. Automatic Control*, vol. 13, pp. 504–514, 1968.

[81] S. Haykin, A. Zia, Y. Xue, and I. Arasaratnam, "Cognitive tracking radar," Canada and US Patent US Application Serial No. 12/588,346. Can Application No. 2,682,428, 2009.

[82] X. Li and V. P. Jilkov, "Survey of maneuvering target tarcking Part I: Dynamic models," *IEEE Trans. on Aerospace and Electronic Systems*, vol. 39, no. 4, pp. 1333–1364, October 2003.

[83] M. Mallick, T. Kirubarajan, and S. Arulampalam, "Comparison of nonlinear filtering algorithms in ground target indicator (GMTI) tracking," in *Proceedings of the 4th International Conference on Information Fusion*, Montreal, Canada, 2001.

[84] M. Mahendra and L. S. Barbara, "Comparison of single-point and two-point difference track initition algorithms using position measurements," *ACTA Automatica Sinica*, vol. 34, pp. 258–265, March 2008.

[85] J. J. E. Slotine and W. Li, *Applied Nonlinear Control*. London: Prentice-Hall Inc., 1991.

[86] V. I. Utkin, *Sliding Modes in Control and Optimization*. Springer-Verlag, 1992.

[87] V. I. Utkin, J. Guldner, and J. Shi, *Sliding Mode Control in Electro-Mechanical Systems*, 2nd ed. CRC Press, 2009.

[88] A. Levant, "Chattering analysis," in *European Control Conference*, Kos, Greece, 2007.

[89] H. K. Khalil, *Nonlinear Systems*, 3rd ed. Upper Saddle River, NJ: Prentice Hall, 2002.

[90] [Online]. Available: http://en.wikipedia.org/wiki/Variable_structure_control

[91] S. R. Habibi and R. Burton, "The variable structure filter," *Journal of Dynamic Systems, Measurement and Control*, vol. 125, no. 3, pp. 287–293, 2003.

[92] G. Solari and F. Tubino, "A turbulence model based on principal components," *Probabilistic Engineering Machanics*, vol. 17, pp. 327–335, 2002.

[93] M. Masonson, "On the Gaussian sum of Gaussian variates, the non-Gaussian sum of Gaussian variates, and the Gaussian sum of non-Gaussian variates," *Proceedings of the IEEE*, vol. 55, no. 9, p. 1661, 1967.

[94] Y. Bar-Shalom, X. R. Li, and T. Kirubarajan, *Estimation with Applications to Tracking and Navigation*. Wiley Interscience, 2001.

[95] H. L. V. Trees, *Detection, Estimation and Modulation Theory, Part I*. Wiley Press, 1968.

[96] C. H. M. Petr Tichavsky and A. Nehorai, "Poseterior Cramér-Rao bounds for discrete-time nonlinear filtering," *IEEE Trans. on Signal Processing*, vol. 46, pp. 1386–1396, 1998.

[97] R. Cools, "Constructing cubature formulas: The science behind the art," *Acta Numerica*, vol. 6, pp. 1–54, 1997.

[98] S. Thrun, W. Burgard, and D. Fox, *Probabilistic Robotics*. MIT Press, 2005.

[99] W. B. Powell, *Approximate Dynamic Programming*. Wiley-Interscience, 2007.